

Spectral and Spatial Indices based Specific Class Identification from Airborne Hyperspectral Data

AKHIL KALLEPALLI

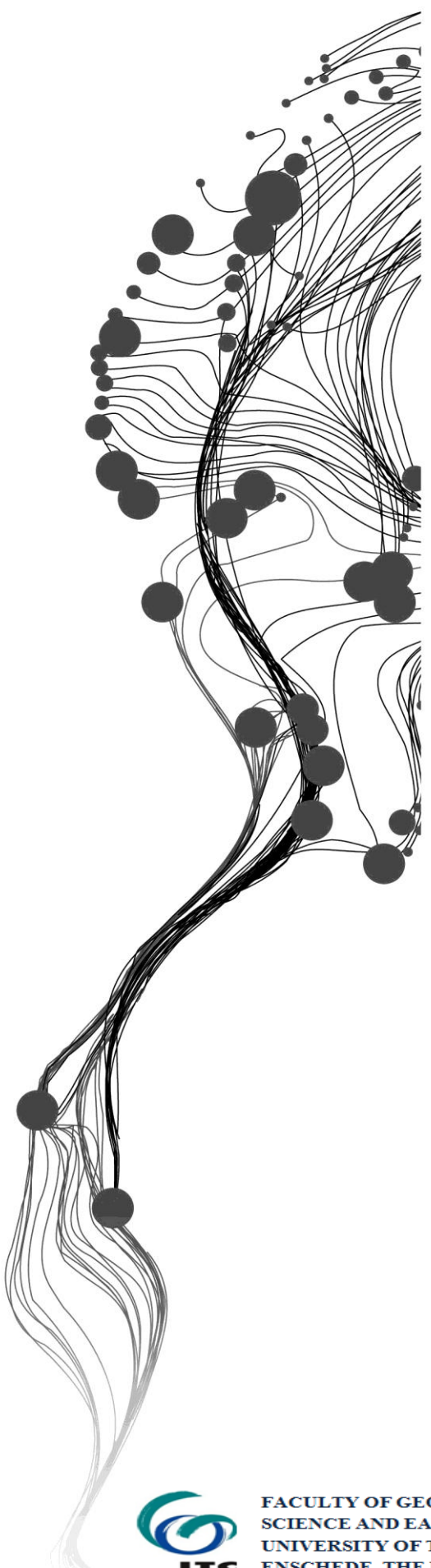
March, 2014

IIRS SUPERVISOR

Dr. Anil Kumar

ITC SUPERVISOR

Dr. Kourosh Khoshelham



Spectral and Spatial Indices based Specific Class Identification from Airborne Hyperspectral Data

AKHIL KALLEPALLI

Enschede, The Netherlands [March, 2014]

Thesis submitted to the Faculty of Geo-information Science and Earth Observation (ITC) of the University of Twente in partial fulfilment of the requirements for the degree of Master of Science in Geo-information Science and Earth Observation.

Specialization: Geoinformatics

THESIS ASSESSMENT BOARD:

Chair	: Prof. Dr. Ir. A. Stein
ITC Professor	: Prof. Dr. Ir. M. G. Vosselman
External Examiner	: Prof. Dr. P. K. Garg (IIT, Roorkee)
IIRS Supervisor	: Dr. Anil Kumar
ITC Supervisor	: Dr. Kourosh Khoshelham

OBSERVERS:

IIRS Observer	: Dr. S. K. Srivastav
ITC Observer	: Dr. N. A. S. Hamm



FACULTY OF GEO-INFORMATION
SCIENCE AND EARTH OBSERVATION,
UNIVERSITY OF TWENTE,
ENSCHDE, THE NETHERLANDS



INDIAN INSTITUTE OF REMOTE SENSING
Indian Space Research Organisation
Department of Space, Government of India

DISCLAIMER

This document describes work undertaken as part of a programme of study at the Faculty of Geo-information Science and Earth Observation (ITC), University of Twente, The Netherlands. All views and opinions expressed therein remain the sole responsibility of the author, and do not necessarily represent those of the Institute.

Dedicated to Mom, Dad and Asha

ABSTRACT

Hyperspectral remote sensing has emerged as one of the most versatile and information rich source of data. Hyperspectral data finds applications in various domains, like specific land use land cover identification and hence, has emerged as one of the most significant research areas. Hyperspectral data has many advantages, but the major limiting disadvantage to its applicability is that of its dimensionality. Known as the “Hughes Phenomenon”, traditional classification and image processing approaches fail to process data along many contiguous bands due to inadequate training samples. Another aspect of classification is to deal with the real world scenario of mixed pixels i.e. presence of more than one class within a single pixel. An attempt has been made to deal with the problems of dimensionality and mixed pixel, with an objective to improve the accuracy of class identification.

The present research intends to use an indices based approach to deal with the dimensionality of the Airborne Prism EXperiment (APEX) hyperspectral dataset and improve the classification accuracy using Possibilistic ϵ -Means (PCM) algorithm. APEX Open Science Dataset (OSD) was acquired over Baden, Switzerland and consists of 285 bands at 1.8 m resolution, allowing formulation of spectral and spatial indices to describe the information in the dataset in a lesser dimensionality. This reduced dimensionality is used for classification, attempting to improve the accuracy of determination of specific class of interest, in the context of a number of classes. Spectral indices are derived from the features of the dataset and spatial indices have been defined using texture analysis over defined neighbourhoods. The classifications of 20 classes of varying spatial distributions were considered in order to evaluate the applicability of spectral and spatial indices in extraction of specific class information.

The proposed approach to dimensionality reduction aims to assess the results of classification, relative to a traditional dimensionality reduction approach i.e. PCA in this research. In order to understand the effect of indices on classification, spectral and a combination of spectral and spatial indices were individually assessed and studied. Improvements in specific class determination were assessed by certainty measures of entropy and correctness measures of user’s and producer’s accuracies. Besides reduction of entropy for classes while considering a spectral-spatial indices approach, an overall classification accuracy of 80.50% was obtained for the same, against 65% (spectral indices) and 59.50% (optimally determined principal components).

Utilizing the high dimensionality and fine resolution of the airborne hyperspectral dataset, the spectral knowledge-based approach to feature selection, extraction and reduction of dimensionality has been researched. An improvement in accuracy of class determination supports the motivation of the research, concluding that the application of indices using their spectral-spatial properties can indeed improve in identification of land use/land cover.

Keywords: Airborne hyperspectral remote sensing, Hughes Phenomenon, Spectral indices, Textural analysis, Possibilistic ϵ -Means (PCM), Entropy

ACKNOWLEDGEMENTS

“Appreciation is the highest form of prayer, for it acknowledges the presence of good wherever you shine the light of your thankful thoughts” – Alan Cohen

I am very grateful to Dr. Anil Kumar, my supervisor through the course of this research work. His support and encouragement have been pivotal in the successful completion of this work. His constant presence and involvement have made the monumental task of this MSc research achievable. He has always been available for vital suggestions, clarifications and assistance throughout and beyond this research work. I will always consider him a strong motivation in my career ahead. I will be ever thankful and owe him for this.

I would like to express my sincere gratitude to Dr. Kourosh Khoshelham for co-supervising this research work. Interactions with him throughout the proposal duration while at ITC were excellent and very thought provoking. He has always been available for critical evaluation, key suggestions and guidance throughout the research. I thank him for urging me to develop a critical outlook towards my research and in my future endeavours. Without the divide of distance, Dr. Khoshelham has always been available for reviews and Skype meetings to discuss various aspects of the research and played an instrumental part in its successful completion.

I would like to take this opportunity to thank Dr. Andreas Hueni and all the people associated with the Airborne Prism EXperiment (APEX) program for providing the excellent data and assistance at various stages of the research work. Dr. Hueni was involved quite influentially in the process of understanding the dataset and obtaining ground truth knowledge for the study. I would also like to thank Dr. Prasad Thenkabail, Dr. Pablo J. Zarco-Tejada and Dr. Josep Peñuelas for their clarifications and literature support.

I also thank Dr. Nicholas Hamm for his assistance and support during the entire duration of the MSc program and ensuring that our stay at ITC memorable and comfortable.

A special note of gratitude to Dr. Y. V. N. Krishna Murthy (Director, IIRS), Mr. P. L. N. Raju (Group Head, RSGG) and Dr. S. K. Srivastav (Head, Geoinformatics Department) for the available infrastructure and guidance through the duration of the MSc program at IIRS, Dehradun. I would also like to take this opportunity to thank all the faculty members for sharing their knowledge in the course modules. I thank the CMA department for their timely technical support.

I thank God for this wonderful life and parents, to whom I owe and dedicate this achievement. They have been a source of inspiration to me. They have always encouraged every endeavour and supported me through every second of my life, success or failure immaterial. I will always be at a loss of adequate words to describe their love and appreciation for their support in my life. I also dedicate this success to a very special person. Asha, without your unconditional support and encouragement, none of this would have been possible.

Friends at IIRS and ITC have been a very special part of my MSc journey. I thank each and every person I have met and known over the past few months. The long haul of research would not have been possible without the company of my classmates and friends – Tanya (thank you for tolerating my “jokes”), Apoorva, Aravind, Sapna, Juna Akka, Vanya, Siddhi, Neha, Guru and all MSc and M. Tech. course mates. I will always owe you for the encouragement at every moment over the last year and a half. Without the presence of such wonderful friends in the labs and classrooms, this journey would not have been perfect. A special thank you to my long time buddies, Abhishek and Raghudeep for being there for me at every stage, as friends and critics. I would also like to thank my seniors Vishnu, Shankar, Bharadwaj, Pavan and Bhavya whose advice has been very helpful.

Akhil Kallepalli

TABLE OF CONTENTS

Abstract.....	i
Acknowledgements.....	ii
List of Figures.....	vi
List of Tables	viii
1. Introduction	1
1.1. Background and Motivation	1
1.1.1. Hyperspectral Remote Sensing (Imaging Spectroscopy).....	1
1.1.2. Curse of Dimensionality.....	2
1.1.3. Spectral Indices	3
1.1.1. Spatial Information.....	3
1.2. Problem Statement.....	4
1.3. Research Objectives.....	5
1.3.1. Sub – objectives	5
1.4. Research Questions.....	5
1.5. Innovation	5
1.6. Structure of Thesis	6
2. Literature Review.....	7
2.1. Hyperspectral Remote Sensing.....	7
2.2. Dimensionality Reduction.....	9
2.3. Pixel based Spectral Indices	11
2.4. Texture based Spatial Indices	15
2.5. Classifiers and Classification.....	16
2.6. Entropy and Accuracy Assessment	18
3. Dataset and Study Area	21
4. Methodology	25
4.1. Data Processing and Identification of Classes	26
4.2. Classifier and Classification.....	30
4.3. Principal Components database and Baseline Classification	31

4.4. Exploring Spectral Indices.....	33
4.5. Spatial Information through Textural Analysis	37
4.6. Entropy analysis and Defuzzification	39
5. Results and Discussion	41
5.1. Determination of Optimal PCs input database.....	41
5.2. Entropy and Accuracy Assessment Comparison	43
5.3. Classification using PCA based database.....	46
5.4. Classification using Indices based database	53
5.5. Proposed Approach of Spectral and Spatial Indices database for Classification	58
6. Conclusions and Recommendations	67
References.....	71
Appendix – A	81
Appendix – B	83
Appendix – C	85
Appendix – D.....	91
Appendix – E	95
Appendix – F	99

LIST OF FIGURES

Figure 1-1: Spectral reflectance curves of Kaolinite in LANDSAT TM, AVIRIS sensors and a field spectrometer. Source - [5]	1
Figure 1-2: Typical Spectral Reflectance Curve for Vegetation. Source - [6].....	2
Figure 1-3: Ordering of elements of visual photo-interpretation. Source - [33]	4
Figure 3-1: Illustration of at-sensor data acquisition by APEX. Source - [45]	21
Figure 3-2: True Colour Composite of APEX Open Science Dataset.....	22
Figure 4-1: Adopted Methodology for Present Research	25
Figure 4-2: Mixed Deciduous vs. Mixed Coniferous Forest (Reflectance Curves).....	26
Figure 4-3: Clay Soil vs. Grass vs. Stressed Grass vs. Vineyard (Reflectance Curves).....	26
Figure 4-4: Different Sports Surfaces (Reflectance Curves).....	27
Figure 4-5: Depiction of object classes in the study area	27
Figure 4-6: Reflectance curve of stressed grass	28
Figure 4-7: REP analysis for Stressed Grass using first derivative method	29
Figure 4-8: Reflectance curve of grass.....	29
Figure 4-9: REP analysis for Grass using first derivative method	29
Figure 4-10: Percentage depiction of gain in variance with increase in PCs.....	32
Figure 4-11: Graphical depiction of reduction of variance with increasing PCs.....	33
Figure 4-12: Spectral curve of Artificial Turf vs. Roofs	36
Figure 4-13: Illustration of class differentiation from soft outputs	39
Figure 5-1: Graphical illustration of entropy of classes identified with respective to PCs	42
Figure 5-2: Entropy of classes with respective to 7 and 8 PCs	42
Figure 5-3: Optimal PC input-classification – Clay Soil.....	46
Figure 5-4: Optimal PC input-classification – Red Roof.....	47
Figure 5-5: Optimal PC input-classification – Roads	48
Figure 5-6: Optimal PC input-classification – Sand.....	48
Figure 5-7: Optimal PC input-classification – Mixed Coniferous Forest.....	49
Figure 5-8: Optimal PC input-classification – Red Synthetic Ground (A); Vineyard (B).....	50
Figure 5-9: Optimal PC input-classification – Lawn Tennis Court (A); Buildings (B)	51
Figure 5-10: Defuzzified optimal PCs classification output (i – iii).....	52
Figure 5-11: Spectral indices input-classification – Artificial Turf (A); Clay Soil (B)	53
Figure 5-12: Spectral indices input-classification – Mixed Coniferous (A) and Deciduous (B) Forests	54
Figure 5-13: Spectral indices input-classification – Pasture (A); Roofs (B).....	55
Figure 5-14: Spectral indices input-classification – Stressed Grass (A); Vineyard (B).....	55
Figure 5-15: Spectral indices input-classification – Water (A); Yellow Tartan (B)	56
Figure 5-16: Defuzzified spectral indices input database classification output (i – iii).....	57

Figure 5-17: Spectral-Spatial indices classification – Artificial Turf (A); Building (B)	59
Figure 5-18: Spectral-Spatial indices database-classification – Clay Soil (A); Grass (B)	60
Figure 5-19: Spectral-Spatial indices classification – Lawn Tennis Court (A); Pasture (B)	60
Figure 5-20: Spectral-Spatial indices classification – Mixed Coniferous (A); Deciduous (B) Forests	61
Figure 5-21: Spectral-Spatial indices classification – Red Roof (A); Red Synthetic Ground (B).....	62
Figure 5-22: Spectral-Spatial indices classification – Road (A); Synthetic Sports Surface (B)	63
Figure 5-23: Spectral-Spatial indices classification – Stressed Grass (A); Vineyards (B)	63
Figure 5-24: Spectral-Spatial indices classification – Water (A); Yellow Tartan (B).....	64
Figure 5-25: Defuzzified spectral-spatial indices input database classification output (i – iii).....	65
Figure C-1: Optimal PC input-classification – Artificial Turf (A); Black Roof (B)	85
Figure C-2: Optimal PC input-classification – Grass (A); Mixed Deciduous Forest (B)	86
Figure C-3: Optimal PC input-classification – Pasture (A); Stressed Grass (B).....	86
Figure C-4: Optimal PC input-classification – Railway (A); Roof (B)	87
Figure C-5: Optimal PC input-classification – Synthetic Sports Surface (A); Water (B).....	88
Figure C-6: Optimal PC input-classification – Yellow Tartan	89
Figure D-1: Spectral indices input-classification – Black Roof (A); Buildings (B)	91
Figure D-2: Spectral indices input-classification – Grass (A); Lawn Tennis Court (B).....	92
Figure D-3: Spectral indices input-classification – Railway (A); Red Roof (B)	92
Figure D-4: Spectral indices input-classification – Red Synthetic Ground (A); Road (B).....	93
Figure D-5: Spectral indices input-classification – Sand (A); Synthetic Sports Surface (B)	94
Figure E-1: Spectral-spatial index for “Roofs” class	95
Figure E-2: Spectral-Spatial indices database-classification – Black Roof (A); Railway (B).....	96
Figure E-3: Spectral-Spatial indices database-classification – Roofs (A); Sand (B)	96

LIST OF TABLES

Table 4-1: Wavelengths and Significance. Source - [125].....	34
Table 4-2: Spectral indices for indices database as input for classification	35
Table 4-3: Depiction of index intended class and additional classes identified.....	37
Table 4-4: Spatial indices (texture analysis) added to input database of spectral indices	38
Table 5-1: PC and Indices input database – Entropy and Accuracy Assessment.....	43
Table 5-2: Spectral-spatial indices – Entropy and Accuracy Assessment (1).....	44
Table 5-3: Spectral-spatial indices – Entropy and Accuracy Assessment (2).....	45
Table A-1: APEX Selected Performances. Source - [45]	81

1. INTRODUCTION

1.1. Background and Motivation

“Remote sensing is the science and art of obtaining information about an object, area, or phenomenon through the analysis of data acquired by a device that is not in contact with the object, area, or phenomenon under investigation” [1]. As the definition suggests, the data acquisition is achieved without the requirement of any physical contact with the region being ‘remotely sensed’. This is achieved with the detection of electromagnetic radiation (EMR) [1]. A significant advantage of remote sensing is its ability to acquire information in inaccessible regions. Visible and infrared regions of the EMR spectrum are utilized in passive remote sensing, may it be multispectral or hyperspectral remote sensing.

1.1.1. Hyperspectral Remote Sensing (Imaging Spectroscopy)

Of the various types of remote sensing, hyperspectral imaging (or remote sensing) has become one of the most active areas of research [2]. Hyperspectral sensors, both airborne and spaceborne (also referred to as imaging spectrometers) acquire data in “many, very, narrow contiguous spectral bands through visible to thermal IR portions of spectrum” [1], [3]. The word *hyper* means ‘beyond’, and thus, in need of better fitting terminology, hyperspectral remote sensing is alternatively called *imaging spectroscopy* [4] by some researchers. Thus, hyperspectral remote sensing and imaging spectroscopy are considered synonymous in this literature.

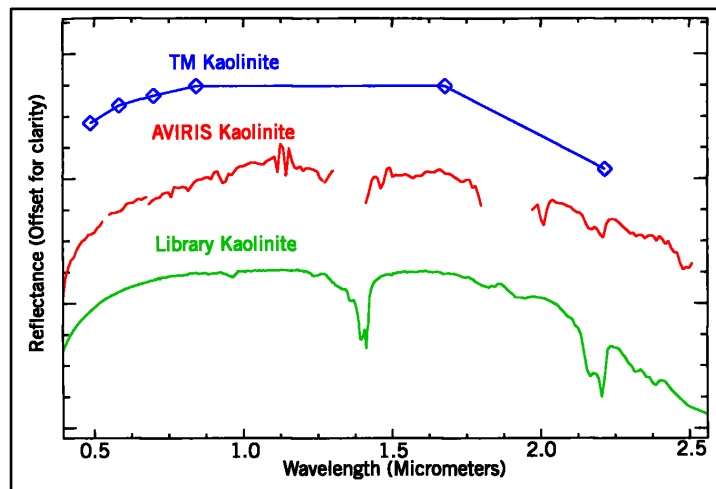


Figure 1-1: Spectral reflectance curves of Kaolinite in LANDSAT TM, AVIRIS sensors and a field spectrometer.
Source - [5]

The major advantage of imaging spectroscopy is data acquisition across contiguous spectral bands. Analysis of these contiguous response curves assists in studying specific properties of the objects on the ground. These spectral bands result in a continuous spectral reflectance

curve for any sample that is sensed from a spectrometer. Figure 1-1 illustrates a comparison of the multispectral sensor, LANDSAT Thematic Mapper (TM), Airborne Visible/Infrared Imaging Spectrometer (AVIRIS) and a field spectrometer. AVIRIS acquires images in 224 contiguous bands in comparison to TM's 6 bands. The resultant spectral curve of AVIRIS is much more continuous, making intricate details visible. The gaps in the curves are due to atmospheric absorptions, which are absent in the case of the library Kaolinite curve, acquired from a field spectrometer without any influence from the atmosphere.

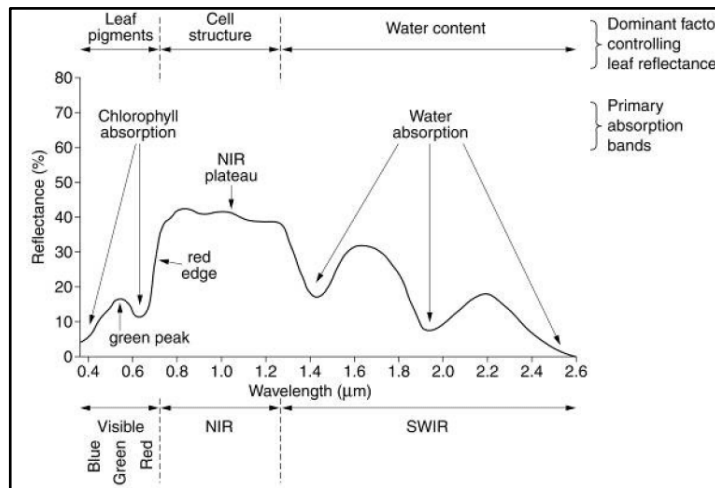


Figure 1-2: Typical Spectral Reflectance Curve for Vegetation. Source - [6]

As illustrated in the Figure 1-2, leaf pigments, cell structure and water content have discernable characteristics on the spectral curve. Similar analysis is possible for many objects that are 'remotely sensed', i.e. from detailed analysis of spectral curves. These advantages govern the choice of high resolution hyperspectral data for this study.

1.1.2. Curse of Dimensionality

Hyperspectral remote sensing enables identification of greater detail of spectral variation of targets [7] when compared to multi-spectral image acquisition. But, this higher spectral detail comes at the price of classification accuracy and high computational requirements, creating the problem of dimensionality. This dimensionality handling problem revolves around the presence of many bands in the acquired data cube while the colour composite image can only accommodate three components (R, G and B) [4]. Many methods have been developed to curb the impacts of high dimensionality on information extraction like Principal Component Analysis (PCA) [8], Minimum Noise Fraction (MNF) [9], etc.

The dimensionality problem affects the classification of raw hyperspectral bands and known as the "Hughes Phenomenon" [10]. Hughes describes this "peaking paradox" in relation to statistical recognition accuracy reaching an optimal value with a subset of the bands and then declining with increasing dimensionality due to inadequate training samples. Besides classification accuracy, the reduction of dimensionality also greatly reduces the computational effort [7]. Successful studies have been carried out to reduce the dimensionality of hyperspectral data [2], [7], [11], [12] for further processing. Although indices have been applied

for extraction of various properties of vegetation [13]–[17], their direct relation to classification of respective classes, many besides vegetation, provides an avenue for research.

1.1.3. Spectral Indices

Spectral indices have been extensively researched with their applications in emphasizing certain classes while subduing others. The most commonly known index is the Normalized Difference Vegetation Index (NDVI) [18]. First implemented by Rouse *et al.*, 1973 [19], this index is a numerical indicator that uses the near infrared and red bands of the EMR spectrum for identifying live vegetation against the previously used simple ratio methods [20]. However, disadvantages of NDVI in terms of high correlation to multiple vegetation parameters and influence of soil reflectance [21], makes separation of different vegetation classes amongst themselves highly unlikely. Therefore, various indices were developed for identification of chlorophyll content [22]–[24], Leaf Area Index (LAI) [15], [25], [26], water content [27], etc. Many other indices have been formulated for the identification of vegetation [15], [16]. Besides vegetation, spectral indices have been attempted to be formulated for other classes. Zha *et al.*, 2003 [28] attempted the utility of Normalized Difference Built-Up Index (NDBI), Gao (1996) [27] attempted to formulate a Normalized Difference Water Index (NDWI) using infrared bands and other indices like Normalized Difference Snow Index (NDSI) have been formulated and researched [28], [29]. The definition of indices depends on the identification of unique spectral curve properties/behaviour which can be used to emphasize a specific object class. As the remote sensing technologies advance, emphasis is shifting from multi-spectral to hyper-spectral image analysis. Hyperspectral images provide a much greater amount of spectral detail in images, enabling the identification of specific signatures of different vegetation and other object classes [17] – [19].

With the multitude of indices formulated for various object classes, the choice of optimal indices depends on the study area, nature of dataset and various other parameters. However, the advantage of spectral indices in extracting information from data is very significant. Understanding the priority of extracting spectral information (Figure 1-3), indices act as a valued method against other transformations.

1.1.1. Spatial Information

Colloquially used, spatial indices are interpreted in many ways [31]. In the present context, spatial information (through indices) is defined by influence of neighbour pixels and the distribution of objects in satellite data.

In defining characteristics for obtaining information from imagery, we look towards the types of characteristics that human beings use in interpretation of the same [32]. In this regard, the most important pattern elements are spectral, textural and contextual features [32]. Estes *et al.*, 1983 [33] supports this viewpoint of analysis, considering the tone/colour variations to be the primary element of visual image interpretation (Figure 1-3). Many researchers have analyzed the applicability of textural information, to support the above principle, for identifying objects or regions of interest in an image [32].

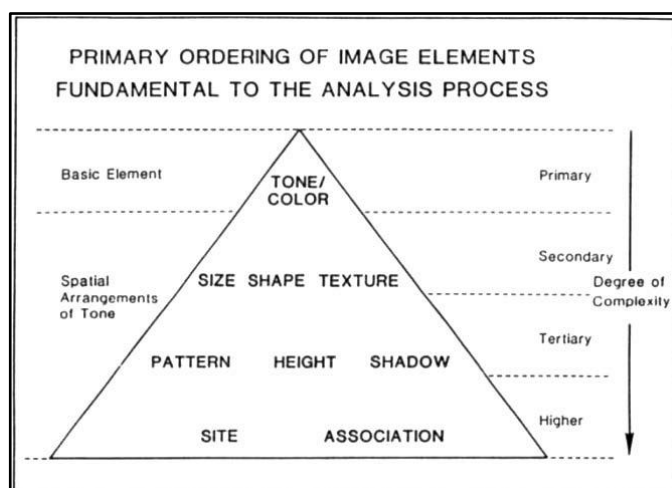


Figure 1-3: Ordering of elements of visual photo-interpretation. Source - [33]

A variety of research was performed before Haralick *et al.*, 1973 [32], but none tried to define or model texture. Combining textural analysis with spatial metrics (statistics derived from urban land use regions) [34], research has shown that textures as a feature in the input dataset improve the extraction of land use information from high resolution satellite imagery.

Research, therefore, proves that textures can perform as quantitative discriminators [34] for extracting spatial information from datasets. This research is an attempt to realise the significance of spatial information when combined with spectral indices, with focus on identification of a class of interest.

1.2. Problem Statement

Research is necessary to understand the applications of indices, as features, for identification of classes in a dataset. Existing methods of classification deal with reducing the dimensionality as the first step, with subsequent classification [2], [7], [11], [12], [35], [36]. The problem that this work intends to address is the appropriate integration of spatial indices with spectral indices for high dimensional and fine resolution data for improving classification, while achieving a knowledge-based dimensionality reduction approach. This research is an attempt at understanding the combined nature of these two aspects.

Indices application to datasets for identification of class of interest has been extensively attempted and is still under thorough research [15], [16], [37]. Through spectral indices (Section 1.1.3), average tonal variations in various bands are described, while texture illustrates the spatial distribution of tonal variations in one band [32], thus accommodating for both spectral and spatial information of the object class.

Their implications on classification are to be studied. Relying on both spatial and spectral properties, through indices, could facilitate in identification of classes that have similar spectral properties and contrasting spatial characteristics or vice versa. This creates a possibility of better extraction of class information, improving dimensionality reduction and subsequent optimal scene classification.

1.3. Research Objectives

The primary objective of this research is to establish and formulate a tested and acceptable methodology to extract a specific object class (like river, sand, soil, stressed grass, healthy grass, artificial grass, mixed forests, pastures, vineyards, roads, railways, houses, roofs, lawn tennis courts, sports surfaces, concrete, etc.) from the study area, using airborne hyperspectral data, feature extraction and dimensionality reduction (through class based indices) and classification algorithms.

1.3.1. Sub – objectives

- To establish a database of indices (spatial and spectral).
- To study spectral response curves of the ground truth data in order to identify keys, which would help identify indices or assist in formulation of indices for classes that do not have strict rules/indices.
- To study and analyze the applicability of pixel based classification approaches, specific to nature and properties of object classes.
- To study the applicability of a single classification technique for all types of object classes in the imagery.
- To establish a baseline classification method for comparison of results with the proposed methodology.

1.4. Research Questions

- Which object classes require formulation of indices in terms of airborne hyperspectral data?
- Which bands are relevant for the definition of indices?
- Which characteristics would be selected as spatial indices of the object classes?
- Which classifier is appropriate for the baseline classification, and subsequent classifications, and why?
- What is a suitable method to combine data from multiple bands in a single index?

1.5. Innovation

The innovation aimed at through this research for the award of Master of Science is an attempt to combine spectral and spatial information through indices database for feature extraction from airborne hyperspectral data and to study the implications of this method of dimensionality reduction on accuracy of classification of object classes from the image. The study area is a combination of manmade and natural object classes. Spectral indices would assist in extracting objects of similar spectral reflectance, while spatial indices would account for spatial distributions and behavior. Through this research, it is intended to innovatively combine these characteristics to improve the accuracy of classification of object classes from high resolution airborne hyperspectral data.

1.6. Structure of Thesis

This thesis is divided into 6 Chapters. The first Chapter provides a background of this research work, introducing the topic, and the motivation involved, problem statement, research objectives and questions. The second Chapter provides a detailed overview of the literature surveyed for gaining and providing a better understanding of the topics and concepts of the research. The third Chapter provides detailed information regarding the APEX sensor, data and the study area. The fourth Chapter describes the methodology followed during this research. A step-by-step description of procedures and analysis performed is presented in this chapter, ordered with respect to the overall workflow. Obtained results and their analysis is detailed in the fifth Chapter and Chapter six concludes the research work with answers to the research questions, simultaneously providing recommendations for future research. References to literature and appendices containing additional results referred to in the thesis follow.

2. LITERATURE REVIEW

This chapter provides a detailed review of the relevant literature reviewed for this research. The following sections justify the use of hyperspectral data, understanding of its dimensionality problem, indices for spectral information, textures for incorporating spatial information, choice of classifier and subsequent background of the certainty and correctness measures applied in this research.

2.1. Hyperspectral Remote Sensing

Vane and Goetz (1988) [38] published a comprehensive analysis of imaging spectroscopy, emerging as a new approach of Earth remote sensing. Through this work, they provide a viewpoint on the then emerging technology of imaging spectroscopy, review literature and discuss the Airborne Imaging Spectrometer (AIS). First images of AIS, were acquired in 1982, raised concerns of information handling and extraction about this new class of data [39]. There arose a need to define algorithms and develop softwares that could handle this data. Importance of acquired reflected solar spectrum in 200 contiguous, inherently registered spectral images was identified, as it could allow diagnostic narrow band spectral features, which could help uniquely identify on-ground materials [38]. Since the advent of this approach to Earth remote sensing, advancements of sensor technology and associated research have introduced systems like AVIRIS [40], [41], Compact Airborne Spectrographic Imager (CASI) [42], Digital Airborne Imaging Spectrometer (DIAS) [43] and the present sensor and data in focus, Airborne Prism Experiment (APEX) [44], [45].

A review of multi-spectral and hyperspectral remote sensing is given by Govender *et al.*, 2007 [3], with a focus on use of hyperspectral imagery in water resources and vegetation applications. Further, a review of the applications of hyperspectral data in flood detection and monitoring, detection of water quality, wetland mapping and measures of physiology and structure, etc. are also discussed. The strength of hyperspectral imaging spectrometers, their capability to image beyond the visible spectrum and obtaining information through contiguous response curves, is illustrated by Barott *et al.*, 2009 [37]. Although a different domain of research, this work was able to illustrate the applicability of spectroscopy at a coral reef organism's interaction scale. This research was able to illustrate that hyperspectral imagery could capture changes in the interaction zone, and the diagnostic narrow bands [38] can differentiate between organisms at this zone [37], which cannot be achieved by multi-spectral imaging.

Further advancements in sensor technology enabled a change of platforms from spaceborne to airborne. A comparative study of AVIRIS and Hyperion was performed by Kruse *et al.*, 2003 [46] in the research area of mineral mapping. Identifying the unique capability of combining spatially contiguous spectra and spectrally contiguous images [39], the authors describe the comprehensive methodology, from pre-processing to spatial mapping and abundance estimates, through endmember spectra extraction. The research rallies its key point to be that of reducing the data, both spatially and spectrally, to "locate, characterize and identify a few key spectra

(endmembers)” that would be used to map the rest of the hyperspectral data. This method illustrates the importance of integration of spectral and spatial information in extracting information from hyperspectral data. A concluding understanding showed that comparison of accuracies of both datasets resulted in identification of up to 60% of unclassified pixels in Hyperion, as compared to AVIRIS (varying with specific mineral), indicating the latter to be a better input to mineral mapping. This research showed both the strengths of airborne hyperspectral remote sensing and its data applicability to specific class (minerals, in this study) mapping. Similarly, Kratt *et al.*, 2009 [47] explored the applicability of hyperspectral remote sensing for mapping geothermal indicator minerals. Herold and Roberts (2005) [48] combined ground and imaging spectroscopy with in-situ pavement conditions for asphalt road assessment. A transition of hydrocarbon dominated roads to mineral dominated roads is an indication of aging and deterioration, a phenomenon that was found to have spectral evidence. This illustrates yet another application of hyperspectral remote sensing.

As previously illustrated in Figure 1-2, the continuous spectra of vegetation presents an excellent opportunity to analyze biophysical parameters of vegetation [49]. Zhang *et al.*, 2008 [49] illustrated a method for extracting leaf chlorophyll content from airborne hyperspectral imagery wherein, extensive field work and laboratory experiments were used to determine the input parameters for the PROSPECT [50] model. A geometrical-optical model 4-scale was combined with a modified PROSPECT model to estimate chlorophyll content from CASI [42] imagery to obtain results having good agreement between inverted and measured leaf reflectance.

Disturbances in the riverbed ecosystems had led to the application of hyperspectral imaging for mapping the probability of invasive species in Japan. Lu *et al.*, 2012 [51] applied binary logistic regression, using two variables of original reflectance bands and MNF (Minimum Noise Fraction) for detecting the invasive species of weeping love grass (*Eragrostis curvula*) on the riverbed of the Kinu River. The research not only strengthens the ability of hyperspectral imagery being applicable to differentiate species, but also shows that dimensionality reduction (MNF) improves the accuracy of detection of the invasive species.

Phenological or plant age classification allows for improving accuracy for species discrimination, improve in understanding the spatial variation of plant growth, amongst other advantages [52]. Knox *et al.*, 2013 [52] investigated the applicability of five vegetation indices for phenological studies and proposed a phenological index (PhIX). PhIX was found to produce the best phenological classification accuracy. Although discrimination between seedling and dormant age classes and adult and flowering classes was problematic, PhIX could still be considered an essential index to map spatial variation and monitor plant growth in savannah and grassland ecosystems [52].

Nakazawa *et al.*, 2012 [53] attempted to use hyperspectral remote sensing techniques for detecting illegal poppy fields amongst other crops. Identifying a possible improvement to previous technique of poppy field detection through IKONOS based change detection methods [54]; the authors applied the spectral difference of poppy against wheat crop. Amongst linear discriminant analysis using two bands, red edge position (REP) and partial least square

discriminant analysis (PLSDA), red edge analysis was found valid for differentiating wheat and poppy, while PLSDA was found appropriate when poppy crop was found in agricultural area with various crops.

Vegetation stress is another possible application to hyperspectral remote sensing. Pontius *et al.*, 2007 [55] mapped the stress in Ash, due to infestation by emerald ash borer (EAB). The study also examines the capabilities of SpecTIR VNIR spectrometer to map ash decline due to infestation.

2.2. Dimensionality Reduction

Most hyperspectral imagery processing must achieve two fundamental goals: 1) to detect and classify every pixel in the scene; 2) reduce the data volume/dimensionality without loss of critical information [11]. Conventional classification methods may not be useful without dimensionality reduction, which is mostly done by applying linear transformations [11], like PCA [36], MNF [9], etc. This is primarily due to ‘curse’ of dimensionality. Hughes (1968) [10] first described the problem of dimensionality for statistical pattern recognition. Results showed that recognition accuracy first increases as the number of measurements made on a pattern increase, but decay of the same occurs after the complexity crosses an optimal value. Interpreted for classification with hyperspectral data, the ‘Hughes phenomenon’ translates into increase in accuracy when a subset of the data is considered, but increase in dimensionality of the data causes a decay of accuracy measure. Stating this to be an ‘apparent paradox’, further research by Van Campenhout (1978) [56], amongst others, criticize the approach of Hughes as “making improper comparisons of models that are partially but not totally ordered.” However, even with criticism to the methodology adopted by Hughes, the phenomenon of curse of dimensionality stands as a complication of high spectral resolution of hyperspectral data.

A commonly used and highly accepted method of dimensionality reduction is that of Principal Component Analysis [8]. Rodarmel and Shan (2002) [36] provided a detailed explanation of this method of dimensionality reduction of hyperspectral data. The authors analyze PCA as a pre-processing technique for classification. Besides establishing the applicability of PCA, the study showed that after the first 10 components, the data would contain only noise [36] i.e. no valuable amount of information. A comparison of computational duration was also done, along with the accuracy assessment. This provides adequate proof that classification after pre-processing with PCA reduces the computational effort required to perform classification of data. PCA calculates orthogonal projections that maximize variance in data, yielding data in a new uncorrelated coordinate system [12]. However, hyperspectral data might not always match such projections [57]. This led to further research in the methods of dimensionality reduction.

Typical techniques of data reduction, like PCA, employ linear transformations to produce a new set of uncorrelated images in terms of decreasing information [58]. This reduced dimensionality is called “intrinsic dimensionality” [59]. Most approaches, up until that of Harsanyi and Chang (1994) [11], do not emphasize individual spectral classes or signatures of interest. The authors attempted to simultaneously reduce the dimensionality and classify the dataset, applicable for

both pure and mixed pixels. Each pixel vector is projected into a subspace orthogonal to that of the undesired signature. Once the undesired signals are removed, the residual is projected onto the signature of interest maximizes the signal-to-noise ratio and results in a single component image that represents the classification of the signature of interest.

Plaza *et al.*, 2005 [12] describes a sequence of extended morphological transformations for filtering and classification of high dimensionality remotely sensed hyperspectral datasets. Generalization of mathematical morphology transformations are performed by simultaneously considering spectral and spatial information from the dataset and applied to urban and agricultural classification problems. The proposed technique was well suited for separating slightly different spectral features that have distinct spatial properties. Yet another nonlinear dimensionality reduction approach was proposed by Qian and Chen (2007) [2]. The authors propose a method of combining Locally Linear Embedding (LLE) [60], [61], which preserves local topological structures, with Laplacian Eigenmaps, which preserve locality characteristics in terms of distance between data points [62]. The results showed that the new method can locate as many endmembers as PCA and LLE, but accuracy in terms of the endmember location is better.

Feature selection refers to algorithms that output a subset of the input feature set, while methods that create new features based on transformations or combinations of the original feature set are called feature extraction algorithms [63]. The procedures not only reduce the cost of recognition by reducing the number of features needed, but in some cases provide better classification accuracy due to finite sample size effects [64]. The paper clarifies the difference between feature selection and extraction procedures applied on high dimensional data. Providing a brief bibliographic review of all dimensionality reduction methods, Silva *et al.*, 2008 [7] provide a new method of feature selection using Genetic Algorithm, a search technique inspired by the natural evolutionary process. This research and the following couple of papers provide an overview of feature selection and extraction techniques, as a prelude to the present research of extracting indices from airborne hyperspectral data.

Jain and Zongker (1997) [63] research the various algorithms of feature subset selection. A large dataset is created by pooling together features from four different texture models, to classify SAR data. Feature selection of this dataset illustrates: 1) the existence of curse of dimensionality; and 2) combining features from different texture models improves classification accuracy against using only one of the models. Of the two outputs, the one that gains significance in the present context is the curse of dimensionality and the importance of feature subset selection algorithms. The research shows the various advantages of feature subset selection algorithms. The work also details the implications on feature selection, when training data is limited. Jain *et al.*, 2000 [65] provides a comprehensive review of statistical pattern recognition techniques.

Further feature subset selection research can be found in Kohavi and John (1997) [66]. Introducing the methods of filter based and wrapper based approaches of feature subset selection, the work compares both methods of feature subset selection, showing significant improvement in accuracies.

Dimensionality reduction procedures (feature selection and extraction) have found applications beyond that of hyperspectral datasets. Khoshelham and Elberink (2012) [67] illustrate the advantages of the dimensionality reduction in classification of damaged building roofs in airborne laser scanning data through a segment based approach. Experimental results showed that classification accuracy improves even for less complex classifiers when number of training samples in proportion with the input features, is small. Considering only two classes of intact and damaged roofs in this literature leaves a future research scope for extending the methodology with more classes.

Research for dimensionality reduction (both feature selection and extraction) has been described. However, amount of scientific literature is aplenty; therefore, a brief comparison of classification accuracy achieved with wrappers, filters and PCA approaches was researched by Janecek and Gansterer (2008) [68]. Describing the three types of feature selection approaches; filters, wrappers and embedded approaches, the literature, although not applied to spatial remote sensing data, provides an in-depth description of PCA and feature selection techniques.

2.3. Pixel based Spectral Indices

Jensen (1983) [69] reviewed the progress of remote sensing of fundamental biophysical variables. Introducing the colour and spectral signature of features through a human perspective of interpretation [32], [33], [70], the author determines the possibility of extracting spectral signatures that could uniquely identify an object or a characteristic. This signature provides quantitative information on how the electromagnetic radiation interacts with materials at various wavelengths. The work also discusses the interpretation of surface roughness and texture, stating the quality of a remote sensor to record these characteristics as a frequency of change and arrangement of tones in the image [33], [70].

The formulation of spectral indices began with the early research oriented around Simple Ratio (SR) of bands. Jordan (1969) [20] was able to illustrate the application of a simple ratio of infrared and red reflectance to estimate the Leaf Area Index (LAI). The ratio is based on the principle that leaves absorb relatively higher amounts of red when compared to infrared light due to selective absorption by leaf pigments. To maximize this ratio, the highest reflectance in infrared region around 800 μm and maximum absorption in 675 μm are considered.

One of the most applied and accepted index for vegetation is the Normalized Difference Vegetation Index (NDVI). Proposed by Rouse *et al.*, 1974 [19], the index utilizes reflectance of the infrared and red regions to highlight vegetation in the study area. The study was done using Earth Resources Technology Satellite (Landsat 1) MSS data, while formulating a Band Ratio parameter which was found to be highly correlated with above ground biomass and vegetation moisture content [19]. The extensive research conducted in the Great Plains Corridor of USA proposed a modified version of the previous SR index. $\text{NDVI} = (\text{Band } 7 - \text{Band } 5) / (\text{Band } 7 + \text{Band } 5)$ was majorly proposed for vegetation mapping and reducing the propagation of errors. To avoid working with negative values of the above mentioned vegetation index, a transformed vegetation index was also proposed, i.e. $\text{TVI} = \sqrt{(\text{R} + 0.5)}$. It has found a multitude of

applications in various vegetation studies [71], [72]. Besides the obvious applications of a vegetation index, it has been used in studies to map urban regions, using the NDVI result for exclusion of vegetation from study area [28]. Many variations to NDVI formulation have been attempted [73]–[78]. Although popular, NDVI has its pitfalls. Studies revealed that NDVI cannot overcome the influence of soil reflectance [21]. Derived from NDVI, another index was defined for remote sensing of liquid water from space. This index was named Normalized Difference Water Index (NDWI) and utilized the reflectance at 0.86 μm and 1.24 μm , i.e. $\text{NDWI} = (R_{0.86} - R_{1.24}) / (R_{0.86} + R_{1.24})$; where R denotes the reflectance.

Research on SR and NDVI had triggered a research in spectral indices for mapping vegetation. These indices were found to be highly correlated with various vegetation parameters like green leaf area, biomass, percent green cover, etc. [21]. Research by Huete (1988) [21] attempted to develop an index that would remove the limitations of atmospheric influence and soil substrate differences. Identifying a significant influence of soil on the results of vegetation indices of intermediate levels of vegetation cover, soil-vegetation spectral behaviour is modelled graphically through adjustment of the NIR-red wavelength space. Finally, the index is defined in Eq. (2-1):

$$\text{SAVI} = \frac{(\text{NIR} - \text{Red})}{(\text{NIR} + \text{Red} + L)} \times (1 + L) \quad \text{Eq. (2-1)}$$

In the given SAVI formulation, L defines prior knowledge of the study area, in terms of density of vegetation covers, i.e. low vegetation cover ($L=1$), intermediate vegetation cover ($L=0.5$) and high density cover ($L=0.25$). Single adjustment factor ($L=0.5$) has been found to reduce soil noise through all vegetation densities, but there could be no ideal factor. As an improvement to the SAVI, Qi *et al.*, 1994 [79] formulated an index that required no prior knowledge, thereby eliminating the “L” factor in Eq. (2-1). The defined MSAVI index in Eq. (2-2):

$$\text{MSAVI} = 0.5(2R_{\text{NIR}} + 1 - \sqrt{(2R_{\text{NIR}} + 1)^2 - 8(R_{\text{NIR}} - R_{\text{Red}})}) \quad \text{Eq. (2-2)}$$

The transformed SAVI index does not require any prior knowledge of the vegetation cover density.

Elvidge and Chen (1995) [80] detailed the implications and applications of narrow band technology in their work. The authors evaluated the ‘power’ of narrow band against broad band indices using AVHRR, TM and MSS data against their capability to estimate LAI and percent green cover. Gaining the basic understanding of indices being formulated from contrasting intense chlorophyll absorptions in red and high reflectance in NIR regions [81], the authors use previously formulated vegetation indices, and also formulate three indices of their own, 1DL_DVGI, 1DZ_DGVI and 2DZ_DGVI, each being a derivative green vegetation index. Results showed that NDVI and Ratio Vegetation Index were influenced by background effects, while PVI and SAVI reduced the same. Also, slightly better accuracy was obtained when using the narrow band data for index formulation. Background measures were minimized using the derivative based indices, formulated in this study, which applied the chlorophyll red edge

amplitude. This study illustrates both applicability of indices and the advantages of narrow band data acquisition.

Broge and Leblanc (2000) [25] studied the prediction power of previously formulated indices with respect to green LAI and canopy chlorophyll density (CCD) and their sensitivity analysis was accomplished. Indices studied were SR [20], NDVI [19], perpendicular vegetation index (PVI) [82], SAVI [21], TSAVI [83], etc. and the proposed triangular vegetation index (TVI). The proposed index, TVI, describes the energy absorbed by the pigments as a function of relative difference between red and NIR reflectance in conjunction with the maximum amount of reflectance in green [25]. The paper concludes that SAVI2 is the least affected by background reflectance and is the best predictor of LAI. RVI is the best estimator of both LAI and CCD for low vegetation canopy densities, while the new proposed indices were best suited for medium range vegetation densities.

MCARI (Eq. 2-3), a modification of Chlorophyll Absorption in Reflectance Index (CARI), was used by Daughtry *et al.*, 2000 [26] for estimating the chlorophyll content in corn leaves from leaf and canopy reflectance. CARI, the original index, was defined by Kim (1994) [84] to minimize the effect of non-photosynthetic materials on spectral calculations of photosynthetically active radiation. The proposed MCARI adds the depth of the absorption at 0.67 μm relative to that at 0.55 μm and 0.7 μm . Although proposed for calculation of chlorophyll variation, it was found that LAI, chlorophyll and chlorophyll LAI interaction accounted for 60%, 27% and 13% respectively, of MCARI variations [15], [26] as in Eq. (2-3):

$$MCARI = [(R_{700} - R_{670}) - 0.2(R_{700} - R_{550})] \times \left(\frac{R_{700}}{R_{670}}\right) \quad \text{Eq. (2-3)}$$

Research for LAI estimations was forwarded by the work of Haboudane *et al.*, 2004 [15]. The research identified the scope to determine the effect of leaf chlorophyll variations on LAI-vegetation index relationships. The main purpose was to formulate a vegetation index that is suitable to accurately determine the LAI of crop canopies, that is less susceptible to variations of leaf chlorophyll. Modelling was done using the PROSPECT [50] and SAILH [85] radiative transfer models. The work provides the following new indices; MCARI1 (Eq. (2-4)) and MTVI1 (Eq. (2-5)); and MCARI2 (Eq. (2-6)) and MTVI2 (Eq. (2-7)).

$$MCARI1 = 1.2[2.5(R_{800} - R_{670}) - 1.3(R_{800} - R_{550})] \quad \text{Eq. (2-4)}$$

$$MTVI1 = 1.2[1.2(R_{800} - R_{550}) - 2.5(R_{670} - R_{550})] \quad \text{Eq. (2-5)}$$

$$MCARI2 = \frac{1.5[2.5(R_{800} - R_{670}) - 1.3(R_{800} - R_{550})]}{\sqrt{(2R_{800} + 1)^2 - (6R_{800} - 5\sqrt{R_{670}}) - 0.5}} \quad \text{Eq. (2-6)}$$

$$MTVI2 = \frac{1.5[1.2(R_{800} - R_{550}) - 2.5(R_{670} - R_{550})]}{\sqrt{(2R_{800} + 1)^2 - (6R_{800} - 5\sqrt{R_{670}}) - 0.5}} \quad \text{Eq. (2-7)}$$

The extensive work by Haboudane *et al.*, 2004 [15] points out the applicability of the new formulated indices through estimations of LAI using simulated data of PROSPECT [50] and

SAILH [85] radiative models and linearity analysis using real world CASI hyperspectral data. Results showed that MCARI2 (Eq. (2-6)) and MTVI2 (Eq. (2-7)) were the most robust indices to estimate green LAI. New modelling algorithms are developed using the PROSPECT-SAILH model and then tested with CASI data, leading to highly positive results.

Zarco-Tejada *et al.*, 2001 [86] researched the applicability of optical narrow band indices for chlorophyll estimation. This study is yet another proof of applicability of indices for intrinsic hyperspectral data related applications. The study is an attempt to understand the link between leaf reflectance and transmittance and canopy hyperspectral data for chlorophyll content estimation. CASI data is used, along with canopy reflectance models of SAILH [85] and MCRM, coupled with the leaf radiative transfer model of PROSPECT [50]. Listing the various indices formulated to estimate the above mentioned properties, results of the research show that red edge indices are the best suited for C_{ab} estimation at canopy level. Extending this research with further investigations of combined indices like MCARI, TCARI and OSAVI, Zarco-Tejada *et al.*, 2004 [13] yielded reasonable results of C_{ab} estimation in open-canopy tree crops.

Zarco-Tejada *et al.*, 2005 [14] attempted to estimate and devise methods of monitoring physiological condition and chlorosis detection in *Vitis vinifera* L. (vineyard) through C_{ab} estimations at leaf and canopy levels. Gaining information from an extensive study of viticulture applications of remote sensing by Hall *et al.*, 2002 [87] and understanding the need for research in precision viticulture using remote sensing, the authors identified that the best indicators C_{ab} estimation were narrow band indices, but with poor performances from traditional indices, like NDVI. Using field dimensional data and the PROSPECT model of inversion, it was found that a combination index of TCARI (Transformed Chlorophyll Absorption in Reflectance Index) [88] and OSAVI (Optimized Soil-Adjusted Vegetation Index) [89] in form of TCARI/OSAVI was the most consistent for estimating C_{ab} [14].

Many indices have been formulated since NDVI was first applied by Rouse *et al.*, 1974 [19] and Simple Ratio [20]; like SAVI [21], PRI (Physiological Reflectance Index) [75], NPQI [74], VOG (Vogelmann Indices) [23], MSAVI [79], NPCI (Normalized Pigment Chlorophyll ratio Index) [76], SRPI (Simple Ration Pigment Index) [78], RDVI (Renormalized Difference Vegetation Index) [73], OSAVI (Optimized SAVI) [89], CTR (Carter Indices) [22], [90], LIC (Lichtenthaler Indices) [77], MSR (Modified Simple Ratio) [91], GM (Gitelson and Merzlyak) [24], MCARI [26], TVI [25], ZM (Zarco and Miller) [86], CRI (Carotenoid Reflectance Index) [92], MTVI1, MTVI2, MCARI1 and MCARI2 [15]. Each of the mentioned indices was formulated to serve a specific purpose, possible due to the narrow band nature of data acquired by hyperspectral sensors. Properties like LAI, chlorophyll content, stress, etc. are possible only due to continuous spectra in which the data is acquired by these sensors. If not formulated for hyperspectral sensors, the indices have been modified to find better accuracies in application with narrow band data [80].

Recent studies have also applied indices, using hyperspectral data, for estimation of biomass production. Cho and Skidmore (2009) [93] attempted to create predictors that help in monitoring grass/herb biomass production on a yearly basis. Considering spectral indices and

linear regression models for prediction, the authors were able to establish that despite high correlation of vegetation indices with biomass, the prediction errors of modelling from indices data was inadequate when compared to identification and utilization of red edge position. In a related research, Cho *et al.*, 2008 [17] uses the estimation of red edge position as a possible method to discriminate species of vegetation using hyperspectral indices at leaf and canopy scales.

Amongst indices research, one work by Verstraete and Pinty (1996) [94] talks about designing optimal indices for remote sensing applications using red and NIR reflectance of AVHRR data, considering perturbing effects and formulating Global Environmental Monitoring Index (GEMI). Although in the multispectral domain, the work establishes an alternate way to formulate indices, that can optimally work for applications of vegetation indices, a subset of the class of spectral indices [94].

2.4. Texture based Spatial Indices

Spatial indices are defined or approached in many ways. While some interpreted it in terms of geo-spatial indices for measuring urban sprawl in Beijing using Area Index, Shape Index, etc. [95], others argued of using spatial elements to analyze segregation, i.e. spatial distribution of population groups [31]. Some research analyzed spatial metrics, in combination with remote sensing, to derive and model information of land use change. However, in the present research, texture illustrates the spatial distribution of tonal variations in a band [32]. Extensive information can be found in Haralick *et al.*, 1973 [32], Berberoglu and Curran (2004) [96].

When humans visually interpret remotely sensed imagery, they take into account context, edge, texture and tonal or colour variations [32], [33], [97]. Haralick *et al.*, 1973 [32] regard the most important identification elements to be spectral, textural and contextual features. As shown in Figure 1-3, Estes *et al.*, 1983 [33] supports this viewpoint, attributing colour/tone to be the primary/basic element of visual image interpretation, followed by size, shape and texture (all of which are spatial elements). Many a research has been attempted or are attempting to incorporate these human derived interpretation characteristics into digital image analysis and classification [32], [97]. While considering tone/colour, it is a set of pixels having the same or almost the same pixel value (brightness value) [97]. When a region of pixels has a “wide variation of discrete tonal features, the dominant property of that area is *texture*” [97]. Jensen (1996) [97] provides a basic understanding of textural analysis, the approaches to automatic texture analysis, etc.

Identifying “texture as one of the important characteristics used in identifying objects or regions of interest in an image” [32], Haralick *et al.*, 1973 researched the applicability of textures in classifying or identifying objects from image data. The texture analysis and its validity were tested on three types of image data: photo-micrographs, 1:20000 panchromatic aerial photographs and ERTS MSS imagery. Deriving information from the human perspective of visual image interpretation, the work highlights the significance of spectral, spatial and contextual information for identifying objects in the image data. Studies previously were limited

to developing algorithms for understanding coarseness and edges. All textures are derived from angular nearest neighbour grey-tone spatial dependence matrices or co-occurrence matrices [32], [34], considering the statistical nature of textures. Results showed an accuracy of 89%, 82% and 83% for object identification in photo-micrographs, aerial photographs and MSS image data, respectively.

Texture information has been used in many a research to spatially describe the objects in the image data. Spatial metrics are used widely in urban environments to describe the spatial distribution of population and housing [34]. However, Herold *et al.*, 2003 [34] use a combination of texture measures and spatial metrics as features for quantitatively describing urban spatial characteristics. The work uses the object oriented approach to classify the large urban areas. Homogeneity was identified as a GLCM texture that was most valuable in providing spatial information, contributing to the 76.40% overall accuracy of land use classification.

Research has been also carried in terms of interpreting SAR imagery using grey level co-occurrence texture statistics by Clausi (2002) [98]. The co-occurrence probabilities provide a second order method for generating texture features [32] were used for interpreting SAR sea-ice imagery. Fisher linear discriminant (FLD) was used for classification of the datasets, results showed that it might not be advisable to use all the texture analysis features collectively, but a few might add information sufficient to classify the object classes. The independent statistics of Contrast, Entropy and Correlation are found to be the best suited to be added as features.

2.5. Classifiers and Classification

Traditional methods of remote sensing supervised classification, training information and results are depicted in the one-pixel-one-class method [99]. As class mixing cannot be taken into consideration while training ‘hard’ classifiers, this limitation has reduced the classification accuracy. Wang (1990) [99] provides a fuzzy supervised classification technique applying the principles of fuzzy sets. The literature describes the method in two steps; 1) estimation of fuzzy parameters from fuzzy training data, and 2) fuzzy partition of spectral space. A theoretical description of fuzzy sets and fuzzy partition of spectral space is given [99], in addition to estimation of fuzzy parameters, training and membership functions of the classification algorithm. Encouraging results of 91.21% accuracy was achieved as a result of fuzzy classification against 86.10% accuracy of ‘hardened’ conventional classification. This research work supports the applicability of fuzzy based classification techniques against conventional “one-pixel-one-class” methods. The fundamental drawback of all such classification techniques is that most spectral information is lost in the process of transforming the remotely sensed data to generate a thematic map [100]. Foody *et al.*, 1992 [100] were able to successfully modify the Maximum Likelihood (ML) classifier to obtain membership probabilities.

Foody (2004) [101] talks in detail about sub-pixel methods in remote sensing. Understanding the classification methods, advantages and applicability of sub-pixel classification techniques is important to understand the significance of these methods in present context. Considering that

data is obtained in varying spectral and temporal resolutions, many accurate methods of classification have been researched and published. However, this doesn't change the fact that, in practice, absolute accurate classification of land cover is a difficult task [102]. It is important to note that use of fine spatial resolution data does not necessarily eliminate the problem of mixed pixels, as the class's constituent parts may carry importance and fine resolution data over large regions is impractical. Amongst the various approaches for sub-pixel scale information [103], two methods are discussed in this literature; spectral unmixing and soft classification. Usually, distribution of the classes is represented through fraction images, wherein each fraction image corresponds to one class, the grey level depicting the coverage of the class [101].

Spectral unmixing is a basic linear mixture model that bases the assumption on spectral responses of a pixel being a linear weighed sum of its component classes [104]. However, the use of least square error criterion makes the analysis prone to outliers and the assumption of linear mixing does not apply, for example, in cases of vegetation regions where radiation interactions are non-linear [101]. Also, detailed descriptions of four methods of soft classification were provided; 1) Maximum Likelihood classification, 2) Fuzzy c-means (FCM), 3) Possibilistic c-means (PCM) [105] and 4) Neural networks.

Certain assumptions need to be made in case of hard classification techniques, like [101]:

- All the pixels in the image data are pure.
- All the classes are discrete, mutually exclusive and exhaustively defined.

In this regard, the concepts of soft or fuzzy classification can provide a method of sub-pixel information extraction. In soft classification, pixels are not required to show membership to only one class. They could show multiple and partial class membership, "since a single class label is no longer to forced upon pixels" [101]. Outputs of soft classification are also derived similar to linear unmixing, i.e. a fraction image corresponding to each class [106].

Detailed statistics of ML classifier, FCM and PCM are detailed in the literature [101]. Introduced as a clustering (unsupervised) technique [101], the ML algorithm was modified so that classification is based on class centres that are provided by the user, making it a supervised classification technique. Although widely applied and accepted, the FCM algorithm, like the ML classifier has the constraint that the membership values will equate to 1 for each pixel [101], [107]. This translates into the requirement of the user exhaustively specifying the classes in the data. In situations where the user is unable to do so, the PCM algorithm is better than the previously mentioned algorithms as the membership values derived are "measures of the absolute strength of class membership" [101], [107]. Therefore, the membership values attained by the pixels classified using PCM are not affected by the presence of untrained classes, making PCM more feasible in cases where the classes may not be exhaustively identified [108]. Extensive information, insights and other information about Possibilistic c -Means algorithm can be found detailed in Krishnapuram and Keller (1993, 1996) [105], [107].

Bastin (1997) [109] comparatively evaluated three popular soft classification techniques. Through this particular research, the author compared the accuracy of classification using FCM, linear mixture model and ML classifier through probabilities or membership values generated.

The author analyzed the capabilities of both ‘hard’ and ‘soft’ classification techniques, stressing on the mixed pixel problems due to scales and resolutions. With extensively cited research literature and description of algorithms, the methods area applied to coarse images generated from 30m Thematic Mapper images through mean filtering and asymmetric filter kernel. Results showed that the FCM classifier made the best predictions of sub-pixel land cover types.

2.6. Entropy and Accuracy Assessment

Remote sensing process is completed in three steps; 1) data acquisition; 2) image processing; and 3) interpretation processes [110]. All the techniques applied in each of these stages are prone to uncertainty [110], [111]. Uncertainty may be imposed on classifiers design and implementation due to [110]:

- Problem of determination of number of land cover types;
- Existence of mixed pixels and classes;
- Limitation of number of training samples and Hughes phenomenon
- Use of improper classifier

Entropy provides a method to study and understand the variation of uncertainty in classification outputs. The measure of degree of uncertainty of the classification results assist in evaluating the classifier performance, thereby indirectly providing a measure of how accurately a pixel is assigned to its class label [106], [110]. If a pixel has maximum probability or membership value of belonging to a class, entropy value is minimum [112] along that pixel’s membership vector (Eq. 2-8). Since soft classification outputs explicitly carry a certain degree of uncertainty, measures of the same are adequately supported and researched, like entropy [113]. Note that uncertainty is distinctly different from error, as error indicates a certain amount of knowledge of the deviation from the truth [110].

Mathematically, entropy expresses the amount of statistical information of a system described by N discrete levels [112]. Entropy is evaluated from the membership vector of a pixel. The membership vector ($\mu(P/x)$) of a pixel is the membership value of a pixel in each of the classes’ fraction outputs.

$$\mu(P/x) = [\mu(p_1/x), \mu(p_2/x), \mu(p_3/x) \dots \mu(p_k/x) \dots \mu(p_C/x)] \quad \text{Eq. (2-8)}$$

Where $\mu(P/x)$ is the membership vector; of class “k” for pixel “x” for “C” classes.

Entropy is a criterion that summarizes the classification uncertainty in a single number, per pixel, per class or per image [110]. It calculated using Eq. 2-9:

$$Entropy = - \sum_{i=1}^C \mu(p_i/x) \log_2 \mu(p_i/x) \quad \text{Eq. (2-9)}$$

Maselli *et al.*, 1994 [112] discusses the applicability of entropy for estimation of accuracy of soft ML classification. The ML classifier using non-parametric priors yielded a high accuracy,

supported by low entropy values. Results support the assumption of low entropy relating to better classification accuracy.

There is a requirement of fuzzy ground data as compared to the traditionally used hard ground truth data to assess the accuracy of fuzzy classification [114]. Foody (1995) [114] addressed the need to identify a method of accuracy assessment that would apply to fuzzy classifications. The author identified and emphasized the need of fuzzy ground truth to accurately assess fuzzy/soft classification outputs. Considering fuzzy ground truth information and comparing it with hardened classification results and assessment, it was established that in the presence of fuzzy ground truth data, cross-entropy, a derivative of entropy, could be used to assess the accuracy of land cover mapping. Cross-entropy is calculated from the probability distributions of class memberships derived from the remotely sensed and ground data sets [114]. The author reflects that a pixel with low entropy is generally considered to represent an accurate classification, but a useful indicator when the ground truth data is “hard”, i.e. pixels are pure. Identifying the pitfalls of entropy and cross-entropy, in spite of their advantages, they are suggested to be accurate indicators of accuracy of classification when both ground and remotely sensed datasets are fuzzy. Conventional methods can still be applied; “hardening” of outputs and traditional methods of accuracy assessment are still suggested and supported as supplements to support entropy measures.

Entropy was used as a measure of uncertainty in the study applied to MSS data by Dehghan and Ghassemian (2006) [110]. The research evaluates two classifiers, MLC and ANN, in terms of correctness (Accuracy and Reliability) and certainty (Mean Relative Error (MRE), Root Mean Square Error (RMSE), Linear Correlation Coefficient (LCC) and Entropy) measures. Among the results of two independent experiments, the interpretation of the relation between accuracy and entropy (proposed) was made. It was evidently noticed that with an increase in accuracy, there is decrease in entropy values. This supports the claim that there is decrease in uncertainty with reduction of entropy values. Entropy was also used by Kumar and Dadhwal (2009) [106] as a parameter addition to Fuzzy c-Means classifier as a soft classification attempt to handle mixed pixels information.

3. DATASET AND STUDY AREA

European Space Agency ventured into the development of the Airborne Prism EXperiment (APEX) in 1993, after identifying the need of a flexible hyperspectral mission against overseas acquisition systems like CASI (Compact Airborne Spectrographic Imager), GERIS (Geophysical Environment Research Imaging Spectrometer) and DAIS (Digital Airborne Imaging Spectrometer) [44]. Co-funded by Switzerland and Belgium, APEX instrument, operating between 380 and 2500 nm in 313 freely configurable bands [44], [45], is designed to provide high quality spectroscopic data for scientific applications [45]. APEX sensor and its data acquisition are illustrated in Figure 3-1. The indicated yellow lines show the path of light. It can even operate in 534 bands in full spectral mode [44]. Spatial synchronization of VNIR and SWIR images [44], which is feature offered separately from other sensors. This synchronization has led to a design that offers low data uncertainty.

Detailed information regarding the ESA-APEX program, sensor characteristics and other information can be found in Schl pfer *et al.*, 2000 [115], Itten *et al.*, 2008 [44], and Hueni *et al.*, 2009 [116] and Jehle *et al.*, 2010 [45]. Appendix – A provides detailed information regarding the APEX sensor and pre-processing of the Open Science Dataset (OSD).

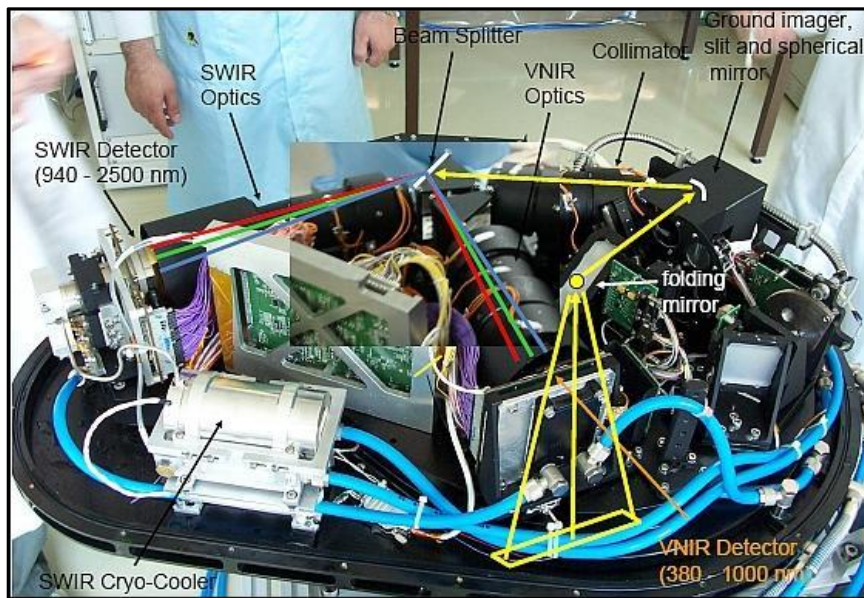


Figure 3-1: Illustration of at-sensor data acquisition by APEX. Source - [45]

Due to its high spectral, spatial and radiometric quality and the unprecedented performance requirements of the APEX mission [117], the instrument is expected to serve as a strong data source for a variety of applications. The various levels of processing [44] of the dataset, from acquisition and through the intermediary stages, indicate varying capabilities of the dataset. Information regarding these products can again be found described in Itten *et al.*, 2008 [44]. Each corresponding product has its own applicability and field of significance, ranging from

atmospheric sensing (aerosol retrieval) [118], geological applications, vegetation and ecological applications, etc [44].

The APEX OSD [44], [45] was acquired in June 2011. The dataset was processed from RAW state to Level1, relying on the calibration information [119]. The dataset was imaged in the vicinity of Baden, Switzerland on a clear day, with the sensor mounted on a Dornier DO-228 aircraft. Various methods of correction and calibration have been performed (details listed in the official APEX OSD Leaflet [119] and in Appendix – A). After extensive calibration and pre-processing of the raw data to Level1 processed data, the dataset is made available on the website, <http://www.apex-esa.org/content/free-data-cubes> [120], as Open Science Dataset with a spectral resolution of 285 bands and spatial resolution of 1.8 meters, in RAW (imaging geometry), ENVI cube format.



Figure 3-2: True Colour Composite of APEX Open Science Dataset.

Although the dataset is the priority in this case, an understanding of the study area is also important due the motivation of the present research. The dataset was acquired, as stated previously, in the vicinity of Baden, Switzerland. The study area (Figure 3-2) is on the banks of the Limmat River, and is an urban mixture of natural and manmade objects (vineyards, pastures, forested regions, buildings, railways, roads, highways, etc.) as shown above. A detailed identification of the object “classes” analyzed in this research will follow in Section 4.1. The APEX OSD data is provided along with ground truth information of 6 classes through a SPECCHIO spectral database [121] also assisted in the identification of classes.

It is very important to understand, at this point, about the ground truth information and its acquisition. Ground truth and knowledge of class sites plays an important part in the classification approach. This knowledge serves three purposes:

- i. Training the classifier;
- ii. Entropy calculations;
- iii. Testing the classification using these are testing sites.

The classes (Figure 4-5) were identified from interpretations from SwissTopo web portal [122]. Regions of Interest (ROIs) were collected, verified with the data providers and used for classification and accuracy analysis.

4. METHODOLOGY

This section provides an overview of the methodology adopted in this research, and depicted below in Figure 4-1. A broad division of the workflow into baseline classification and proposed approach of dimensionality reduction (DR) and classification (each segment is explained subsequently) is illustrated and discussed.

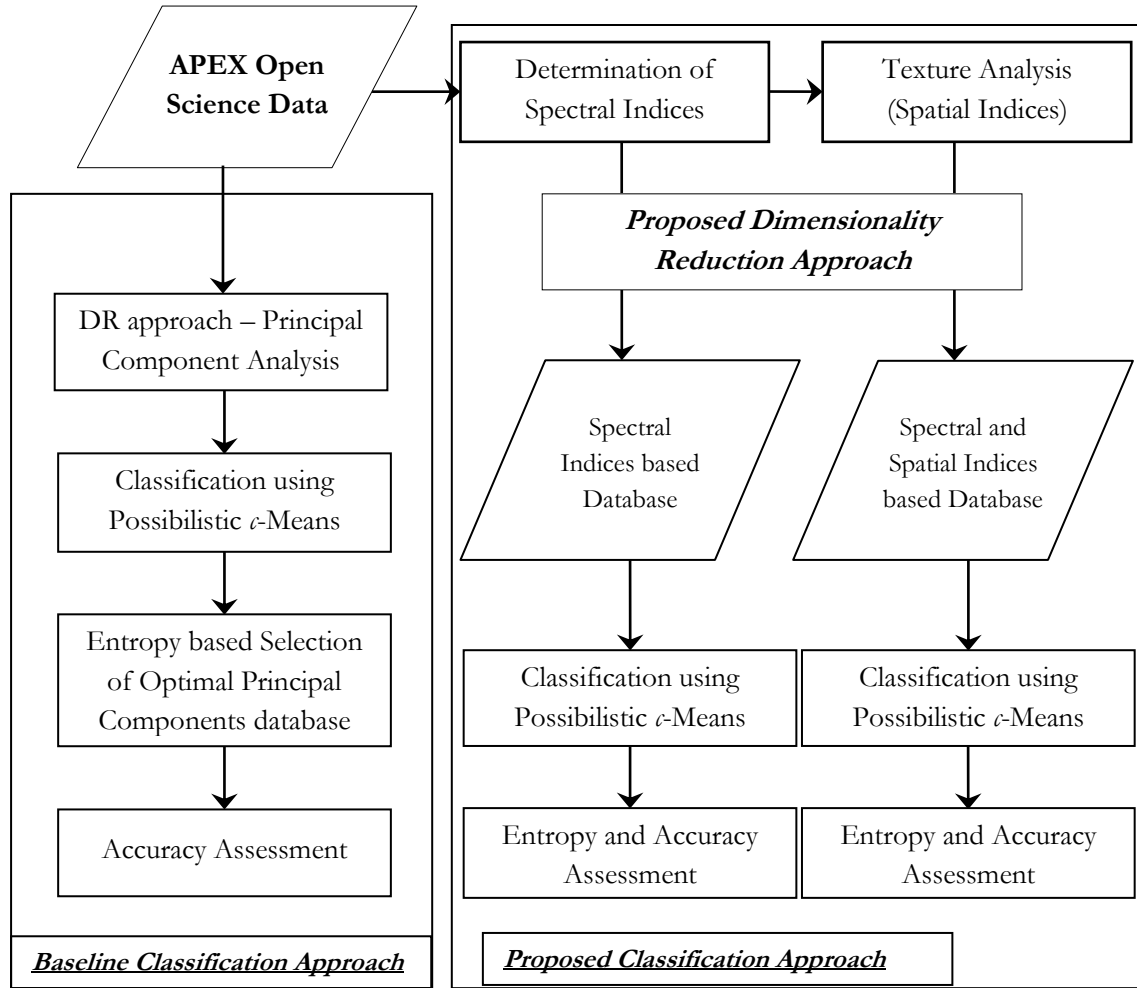


Figure 4-1: Adopted Methodology for Present Research

The research is broadly divided in two sections; 1) Baseline Classification Approach and 2) Proposed Classification Approach.

The baseline classification uses a traditional dimensionality reduction approach to reduce the number of features of the APEX dataset. A subsequent classification and accuracy assessment establishes a benchmark for comparison against the proposed dimensionality reduction and classification approach. The proposed classification approach uses a knowledge-based (understanding of the object classes, reflectance curves and indices formulations) approach of spectral and spatial descriptors (indices) to reduce the dimensionality of the dataset. Against previously used filter and wrapper dimensionality reduction approaches [66], the proposed

approach attempts to enhance the classification procedure by using indices, defined from knowledge of the object classes. A comparison of respective classes' accuracies provides an idea of overall accuracy and, if any, improvement of specific class identification.

4.1. Data Processing and Identification of Classes

The APEX OSD is made available after extensive pre-processing (Appendix – A). The data is interpreted in terms of classes constituted in the study area and identification of vital training and testing data sites. Due to the high spectral resolution of the hyperspectral dataset, very detailed spectral response curve analysis can be made of the classes (or object classes) on the ground. To exploit this advantage, classes were selected of different types of vegetation and of different health/stress conditions. Besides the high spectral resolution (of 285 bands), the dataset has a fine spatial resolution of 1.8 meters. An attempt is initiated at combining both these characteristics, through the indices database, for better identification of specific classes from the airborne hyperspectral data.

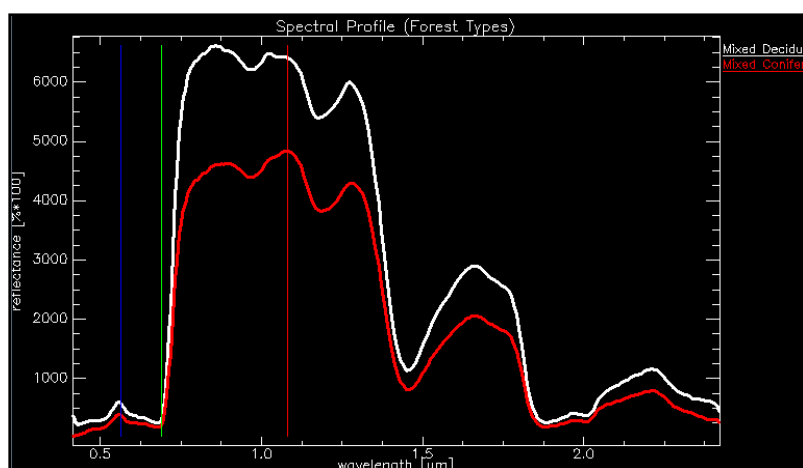


Figure 4-2: Mixed Deciduous vs. Mixed Coniferous Forest (Reflectance Curves)

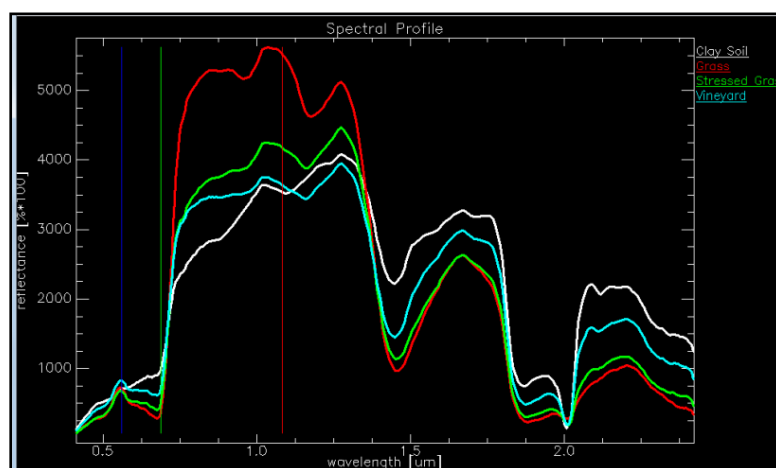


Figure 4-3: Clay Soil vs. Grass vs. Stressed Grass vs. Vineyard (Reflectance Curves)

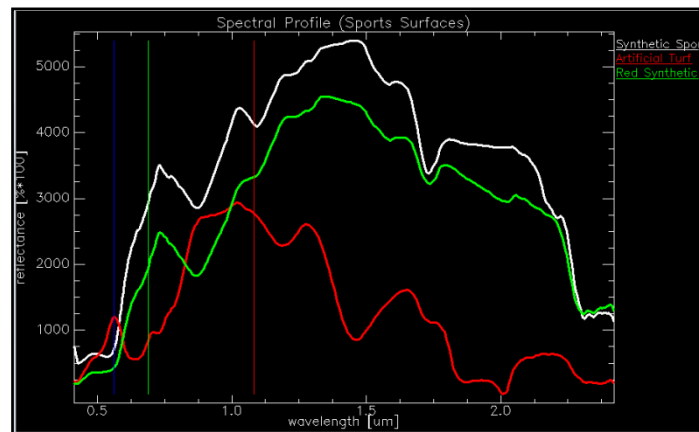


Figure 4-4: Different Sports Surfaces (Reflectance Curves)

Figures 4-2 to 4-4 illustrate the continuous spectra of the APEX data, specific to the indicated classes. The possibility of differentiating classes closely related and otherwise impossible to differentiate from multi-spectral data can be interpreted from the Figures (4-2 – 4-4). The reflectance curves are analyzed to differentiate object classes and, combined with interpretations from SwissTopo portal, identify pixels belonging to classes, to build training and testing set. Identified object classes from map sources, like the web portal [122], are denoted in Figure 4-5:

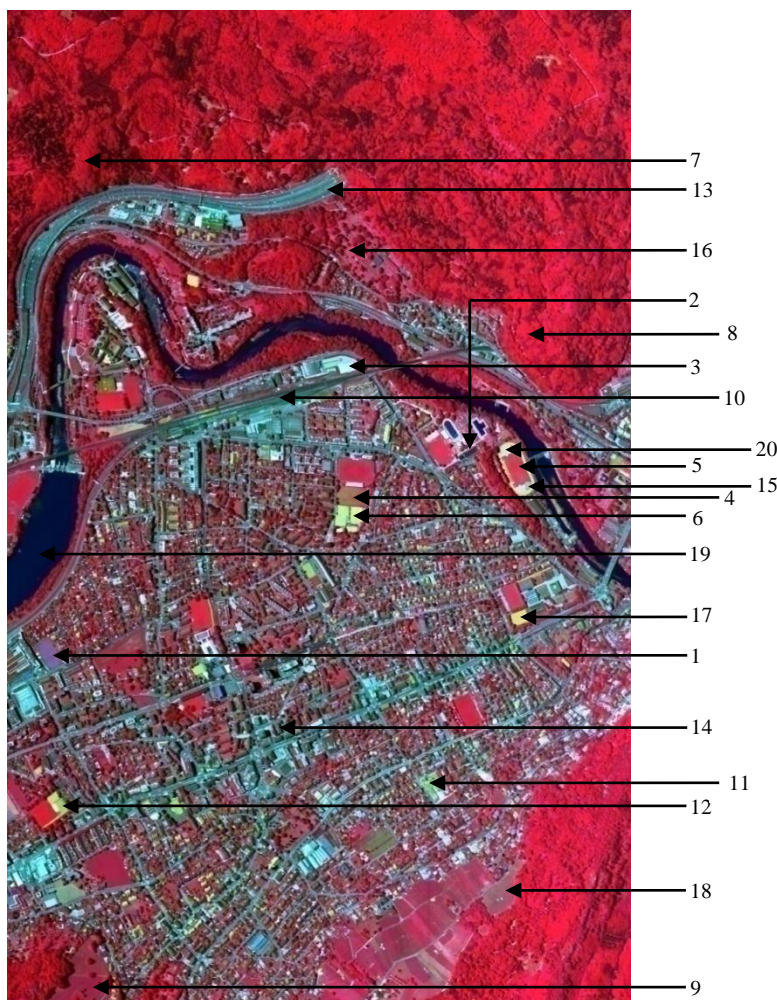


Figure 4-5: Depiction of object classes in the study area

The object classes (Figure 4-5) from the study area for this study are:

1. Artificial Turf (*Fig. 4-4*)
2. Black Roof
3. Building
4. Clay Soil (*Fig. 4-3*)
5. Grass (*Fig. 4-3*)
6. Lawn Tennis Court
7. Mixed Coniferous Forest (*Fig. 4-2*)
8. Mixed Deciduous Forest (*Fig. 4-2*)
9. Pasture
10. Railway
11. Red Roof
12. Red Synthetic Ground (*Fig. 4-4*)
13. Road
14. Roofs
15. Sand
16. Stressed Grass (*Fig. 4-3*)
17. Synthetic Sports Surface (*Fig. 4-4*)
18. Vineyard (*Fig. 4-3*)
19. Water
20. Yellow Tartan

Identifying object classes, like types of forests, stressed grass, etc. on the ground is a characteristic advantage of high resolution airborne hyperspectral imagery. Spectral curves were analyzed for 'keys'. Keys are bands which show distinct spectral curve response or behaviour that can assist in distinguishing the classes. An example of this differentiation was done by Zha *et al.*, 2003 [28] where differentiation of built up areas and vegetation was done using the decrease and increase of reflectance, respectively, from red to infrared wavelengths in the multi-spectral data. Similar identification of varying reflectance curve behaviour was done to identify and separate the classes.

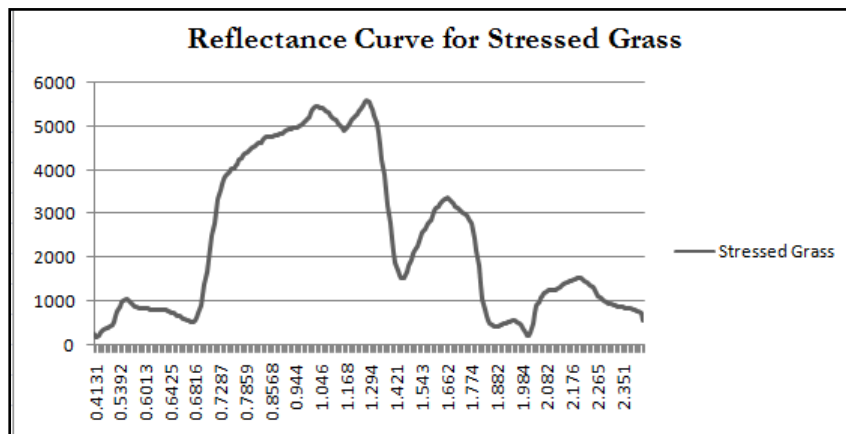


Figure 4-6: Reflectance curve of stressed grass

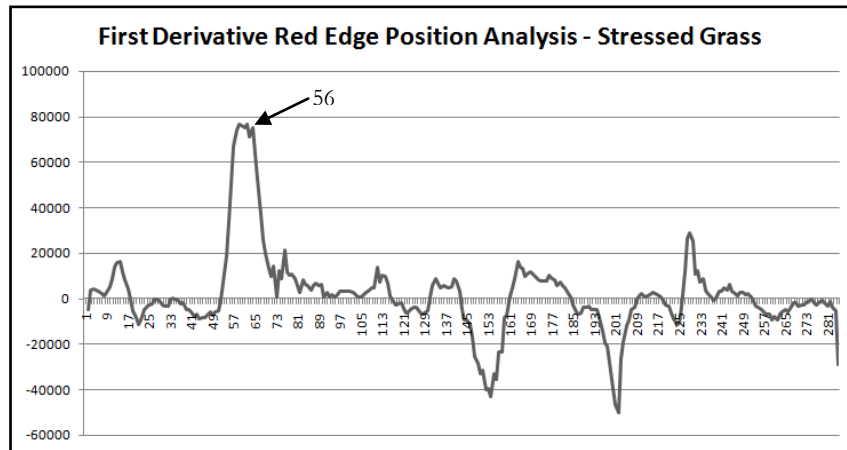


Figure 4-7: REP analysis for Stressed Grass using first derivative method

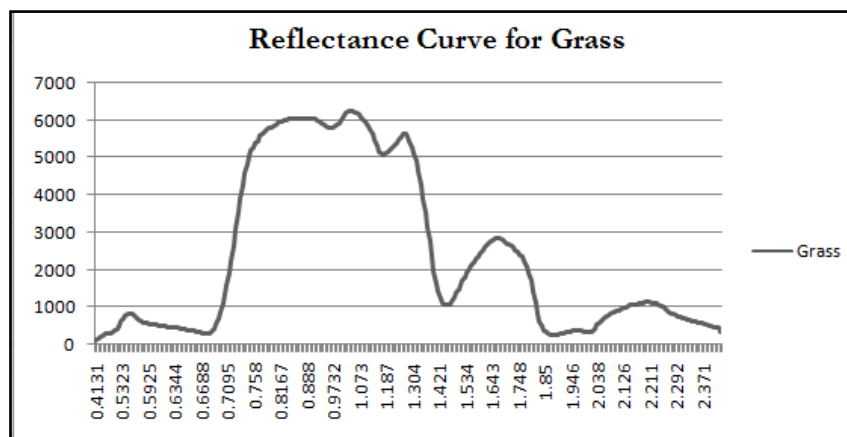


Figure 4-8: Reflectance curve of grass

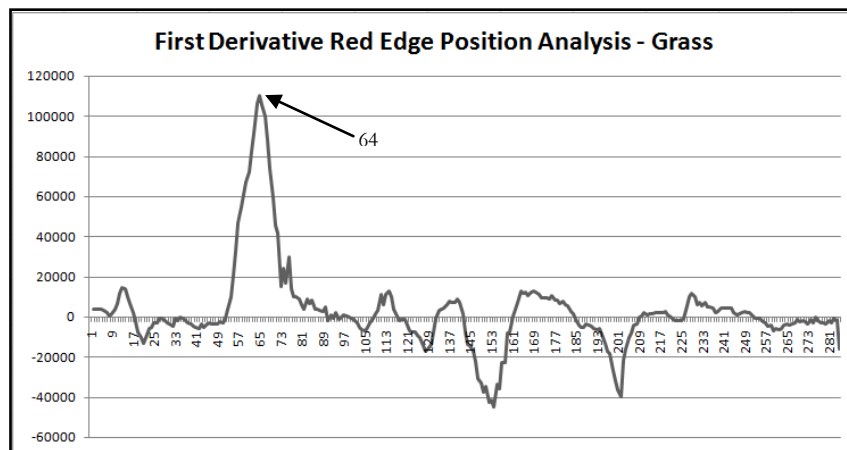


Figure 4-9: REP analysis for Grass using first derivative method

Distinguishing vegetation health/stress levels (Grass (Fig. 4-6) vs. Stressed Grass (Fig. 4-8)) can be checked using Red Edge Position (REP) analysis (discussed in Section 4.4). The first derivative method of the spectral curve helps identifying the REP (the point of maximum amount of reflectance per unit change in wavelength). It can be observed that REP shifts from the 64th band (for Grass; Fig. (4-9)) to 56th band (for Stressed Grass; Fig. (4-7)). This shift towards the red wavelengths is an indication of vegetation stress due to changes in chlorophyll content [123], which is responsible for maximum absorption in the red region of the spectra.

4.2. Classifier and Classification

Amongst the available techniques of classification, the high spatial and spectral resolutions of the airborne hyperspectral data prompted a classification approach that could solve problems of mixed pixels and exhaustive definition of object classes. Intending to exploit the advantages of fuzzy classification approaches, FCM and PCM classifiers were evaluated for the research. Although FCM has shown better classification accuracy [101] amongst the two, it is greatly hampered in the presence of unknown classes. FCM also fails when it is used in applications where membership values need to be a measure of typicality, instead of relative output membership values [105]. Therefore, Possibilistic c – Means algorithm is used for classification of the input datasets (due to the significant advantage of using the classes’ training data, without influence of classes that have not been identified).

Possibilistic c – Means algorithm was proposed by Krishnapuram and Keller (1993) [105] in order to overcome the probabilistic constraints of FCM and FCM derived classification algorithms. The memberships generated by FCM “do not always correspond to the intuitive concept of degree of belonging or compatibility” [105]. PCM classifies the data in terms of possibilistic divisions, wherein the output membership values are degree of possibility of the pixel belonging to a class. The algorithm overcomes the probabilistic constraint of previous algorithms and classifies the data as “measures of the absolute strength of class membership” [101], [105], [107].

The membership function constraints for PCM classification [101], [105] are shown below:

$$\begin{aligned} u_{ij} &\in [0,1] \text{ for all } i \text{ and } j; \\ 0 &< \sum_{j=1}^N u_{ij} \leq N \text{ for all } i; \text{ and} \\ \max_i u_{ij} &> 0 \text{ for all } j. \end{aligned}$$

In the above constraints of PCM algorithm,

- u_{ij} is the grade of membership value of pixel x_j belonging to class (or cluster) β_i ;
- N is total number of feature points (or pixels)

The only constraint that is placed on the membership value calculations is that it must lie in the interval (0, 1). The constraints above result in the distinct possibilistic partition of the feature space. The resulting membership values are possibilistic in nature and not “hard” in the case of a single class in the dataset. The constraints allow the membership function to calculate the values using the absolute strength of the trained classes, without the influence of untrained classes.

The FCM algorithm minimizes the objective function with the probabilistic constraint of all membership values to sum up to 1. The modified PCM objective function [101], [105] is shown in Eq. (4-1).

$$J_m(L, U) = \sum_{i=1}^C \sum_{j=1}^N (u_{ij})^m d_{ij}^2 + \sum_{i=1}^C \eta_i \sum_{j=1}^N (1 - u_{ij})^m \quad \text{Eq. (4-1)}$$

In the above objective function,

- $L = (\beta_1, \beta_2, \beta_3, \dots, \beta_C)$ where β_i is the i^{th} class.
- C is the number of classes;
- N is the total number of feature vectors;
- u_{ij} is the membership value of feature point x_j of β_i ;
- d_{ij}^2 is the distance of feature point x_j from signature feature of class β_i ;
- η_i is a parameter that specifies the distance (in the feature space) from the class centre when membership value is 0.5 ;
- $m \in [1, \infty)$ is the user defined weighing factor that defines the degree of fuzziness.

The first term minimizes the distance of the pixels from the feature vector and the second term maximizes the membership value (u_{ij}) [105]. The PCM algorithm membership function [101], [105] that calculates the membership values of the feature points (pixels) are shown in Eq. (4-2):

$$u_{ij} = \frac{1}{1 + \left(\frac{d_{ij}^2}{\eta_i}\right)^{\frac{1}{m-1}}} \quad \text{Eq. (4-2)}$$

A value of $m=1$ signifies conventional hard classification. Most studies use a value in the range $1.5 < m < 3.0$ [124]. The iterative process of determination of membership value is solely dependent on the distance of the feature point from the training feature vector of the respective class, with no relation to the locations of other classes. The classification procedure provides soft outputs, as many as number of classes. Each of the output layer is a grey-scale image, corresponding to each class, with values ranging from 0 (class completely absent) to 255 (class present with complete possibilistic membership).

The PCM classifier has been used for all the classification approaches through this research. The procedure for analysis, classifier, parameters, etc. has been constant for all approaches to evaluate the applicability and advantage of the principal components, spectral and spatial indices input databases.

4.3. Principal Components database and Baseline Classification

Two broad groups of reducing the dimensionality of data exist; 1) Feature Selection and 2) Feature Extraction [63]. Feature selection consists of algorithms that output a subset of the input feature set that performs the best under some classification system while feature

extraction algorithms create new features based on transformations of the original feature set [63].

Principal Component Analysis (PCA) is one the most important and widely used method of reducing the dimensionality of data. It produces new attributes/features through linear combinations of the original feature set, orthogonal to each other and quantifies the variation in the data [68]. These new features are called Principal Components (PCs). The four main properties/advantages of PCA [68] are:

- The features have 0 covariance;
- Output features are ordered in descending order with respect to variance or amount of data;
- First output feature contains the maximum amount of information (maximum variance of data);
- Each successive feature captures as much variance of data as possible (information).

In order to establish a baseline classification to compare results of spectral and spatial indices input database, a traditional method of dimensionality reduction, in PCA, and subsequent classification has been performed. The APEX data consists of 285 bands. Hughes phenomenon and training data constraints prevent classification without dimensionality reduction.

The principal components are generated, displaying the respective Eigen values and percentages of information contained in the respective components (Figure 4-10). Figure 4-11 graphically illustrates the reduction in gain of information with increasing PCs. Depending on the amount of information and lack of gain of variance in the increasing PCs, the initial intrinsic dimensionality is reduced to 8 components. However, the optimal components or PCs input database was determined from the results of the classification. The combination of optimal number of PCs is the considered database used as input for determining the baseline classification.

PC	Eigenvalue	Percent
1	159601775.4429	58.23%
2	96614615.8858	93.48%
3	9851259.1543	97.08%
4	3916676.3754	98.51%
5	2606432.8342	99.46%
6	546564.7847	99.66%
7	231126.5171	99.74%
8	190529.6382	99.81%
9	101521.6944	99.85%
10	88093.3343	99.88%
11	71342.5535	99.91%
12	49514.8198	99.93%
13	46252.1440	99.94%
14	32861.5641	99.95%
15	27799.2097	99.96%
16	14364.7275	99.97%
17	11934.5378	99.97%
18	11567.9244	99.98%
19	6852.9200	99.98%

Very small gain
of information

Figure 4-10: Percentage depiction of gain in variance with increase in PCs

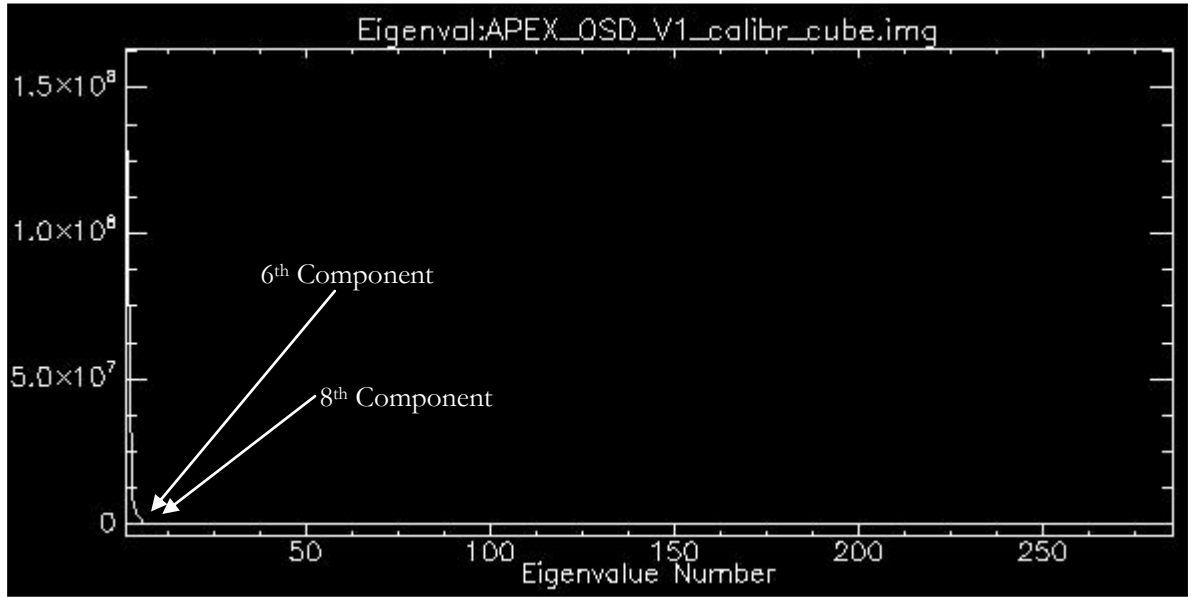


Figure 4-11: Graphical depiction of reduction of variance with increasing PCs

The inputs to the classifier considered are (PC_1) , $(PC_1 \text{ and } PC_2)$, $(PC_1, PC_2 \text{ and } PC_3)...$, $(PC_1, PC_2 \dots PC_8)$. The end result of adding one PC at a time to the input helps understand which database of PCs is an optimal choice for baseline classification, i.e. the reference classification.

An entropy analysis of the end result is done in order to select the optimal choice of PCs and the baseline classification values. The formula shown in Eq. (2-9) calculates the entropy of the membership vector. However, the constraint of entropy calculation ($\sum_{i=1}^C \mu_i = 1$) is the same as that of FCM. In application of the PCM classifier, where this constraint is not followed, the calculation of entropy is modified to Eq. (4-3) [110]:

$$Entropy = \frac{-\sum_{i=1}^C \mu(p_i/x) \log_2 \mu(p_i/x)}{\sum_{i=1}^C \mu(p_i/x)} \quad \text{Eq. (4-3)}$$

In the above equation, the denominator summation of membership values is applied to normalize the membership values calculated by the PCM algorithm.

4.4. Exploring Spectral Indices

Hyperspectral remote sensing acquires imagery in multiple bands, enabling contiguous reflectance curve. These reflectance curves serve as vital inputs to assess properties that cannot otherwise be identified from multi-spectral imagery. Spectral indices have been formulated to highlight certain object classes using the properties from their spectral curves.

Identification of specific 'keys' or distinguishing properties in the reflectance curve played a vital role in the definition of the indices input database. The spectral curves of the object classes listed in Section 4.1 were individually analyzed for identifiable changes in reflectance and then comparatively analyzed for differentiating reflectance behaviour. For example, reflectance curve of "Artificial Turf" for first analyzed for find the bands suitable for band ratio (a significant and

sudden increase in reflectance portion) and then comparatively analyzed with similar classes like “Synthetic Sports Surface” and “Red Synthetic Ground” to avoid conflict of index outputs. Parallel analysis was performed in combinations of all 20 classes, through vegetation and manmade classes, to build an input of indices database that identify a specific class or set of classes.

Note that dimensionality of the dataset is reduced as the feature selection of a subset of the original data is being done and an index formula transforms the choice of features into a single input feature that assists in classification of the class itself. Therefore, this approach towards dimensionality reduction can be considered to be a knowledge driven feature selection and extraction process as it combines the understanding of the reflectance curve with the selection of bands and subsequent transformation of the subset selected.

An understanding of the spectral curve behaviour and the properties associated with the curve are important. Table 4-1, adopted from Thenkabail *et al.*, 2002 [125], illustrates the properties that are associated with parts of the reflectance curves of vegetation. These properties play a vital role in identifying keys for definition of narrow band indices for vegetation classes, as classification of variations of stress and species is also an important part of the present research.

Table 4-1: Wavelengths and Significance. Source - [125]

Wavelength Portion Name	Wavelength (λ) in μm	Band Description and Significance
Blue	0.49	Sensitive to loss of chlorophyll, browning, ripening senescing and soil background effects [126]. Also sensitive to Carotenoid pigments
Green 1	0.52	Maximum “positive change in reflectance per unit variation in wavelength” of visible spectrum is seen around this green wavelength and is sensitive to pigment content.
Green 2	0.55	Green peak in the visible spectrum; strongly related to chlorophyll content
Green 3	0.575	Maximum “negative change in reflectance per unit variation in wavelength” of visible spectrum is seen around this green wavelength and is sensitive to pigment content.
Red 1	0.66	Chlorophyll absorption pre-maxima (reflectance minima – 1)
Red 2	0.675	Chlorophyll absorption maxima. Greatest soil – crop contrast seen at this wavelength.
Red edge – 1	0.7	Chlorophyll absorption post-maxima (reflectance minima 2). This point marks the change of maximum red-absorption to dramatic increase in red reflectance along the red edge. This has been found to be sensitive to stress levels in vegetation.

Red edge – 2	0.72	Critical point on the red edge where the “maximum change of slope reflectance spectra per unit change in wavelength” occurs. Sensitive to temporal changes in crop growth, stress, etc.
NIR	0.845	Centre of the “NIR shoulder”. Strongly correlated to chlorophyll.
NIR peak – 1	0.905	Peak of the NIR spectrum. Sensitive to stress or growth stages of some crops, where there is significant change in reflectance along the NIR shoulder [126]. Useful for calculating crop moisture sensitive index [127]
NIR peak – 2	0.920	Peak of the NIR spectrum.
NIR – Moisture Sensitive	0.975	Centre of moisture sensitive portion of NIR. Various measures of plant moisture can be made from this wavelength’s reflectance.

Similar analyses of other object classes in the study area derive distinctive reflectance behaviour properties, which were applied to simple band ratio. Simple band ratio, originally defined by Jordan (1969) [20] for extraction of LAI, identifies the sudden increase in reflectance from red to infrared wavelengths in vegetation. This logic was applied to object classes other than vegetation too, defining indices for classes that had similar distinctive increase in reflectance

After extensive analysis of the reflectance curves and the properties of classes, the indices tabulated in Table 4-2 form the input database of spectral indices for classification. The logic behind the indices was studied and applied to the APEX dataset as variations of bandwidths and centre wavelengths of the bands govern changes and reassessment of indices. Indices like NDWI, NDBI, etc. were formulated initially using multi-spectral datasets. The principles of the index were analyzed and applied to narrow band (APEX) data. All the indices reviewed from literature in Section 2.3 were investigated, applied and interpreted for their feasibility in the classification.

Table 4-2: Spectral indices for indices database as input for classification

Object Class	Index Formulated/Applied	APEX Band Combination (Wavelength in μm)
Artificial Turf	Band Ratio	95, 76 (0.8752 μm , 0.7716 μm)
Black Roof	Band Ratio	160, 149 (1.45 μm , 1.343 μm)
Buildings	NDBI	160, 145 (1.45 μm , 1.304 μm)
Clay Soil	Band Ratio	236, 225 (2.09 μm , 2.007 μm)
Mixed Coniferous Forest	Band Ratio	85, 53 (0.8167 μm , 0.6816 μm)

Mixed Deciduous Forest	MTVI1	81, 17, 52 ($0.7958 \mu m$, $0.5567 \mu m$, $0.6784 \mu m$)
Red Synthetic Ground	Band Ratio	197, 192 ($1.782 \mu m$, $1.74 \mu m$)
Stressed Grass	Band Ratio	234, 226 ($2.074 \mu m$, $2.015 \mu m$)
Vineyard	Modified NDVI (devised from spectral curve behavior in SWIR)	236, 225 ($2.09 \mu m$, $2.007 \mu m$)
Water	NDWI	183, 146 ($1.662 \mu m$, $1.314 \mu m$)
Roof	Band Ratio	142, 122 ($1.275 \mu m$, $1.082 \mu m$)
Basic Vegetation Index	MSAVI	85, 53 ($0.8167 \mu m$, $0.6816 \mu m$)

Every index, however, does not extract a unique class. One such example is illustrated in Figure 4-12, wherein the reflectance curves of Artificial Turf (white) and Roofs (Red) are shown. The Artificial Turf index (Table 4-2) is derived considering the 95th and 76th bands as keys for a band ratio index. These keys were identified from the increase in reflectance of this class within these bands. Note that in the indicated region (Figure 4-12), the Roofs class also shows similar increase in reflectance. In the index output, however, these classes show different values i.e. in the range of 132-154 and 78-93 for Artificial Turf and Roofs respectively (on a scale of 0 – 255).

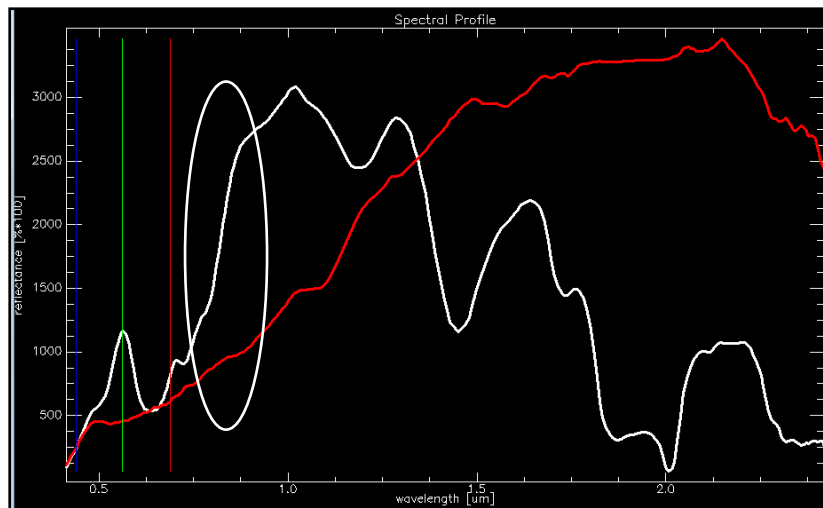


Figure 4-12: Spectral curve of Artificial Turf vs. Roofs

As illustrated in Figure 4-12, it is possible that a single index can extract more than one class. Therefore, the separation of the classes in the feature space is based on the classifier choice and the actual classification process, wherein signature vectors would differentiate the classes from the input indices database. Table 4-3 lists other classes identified in the indices used for classification.

Table 4-3: Depiction of index intended class and additional classes identified

Object Class Specific Index	Additional Class Identified through Index
Artificial Turf	Roof
Black Roof	Water
Buildings	Multiple Classes
Clay Soil	Artificial Turf, Vineyards
Mixed Coniferous Forest	-
Mixed Deciduous Forest	Grass
Red Synthetic Ground	Multiple Classes
Stressed Grass	Clay Soil, Vineyard
Vineyard	Clay Soil, Stressed Grass
Water	-
Roof	-
Basic Vegetation Index	All vegetation in the study area

4.5. Spatial Information through Textural Analysis

APEX Open Science Dataset is a high spectral resolution (285 bands) and fine spatial resolution (1.8m) source of information. The spectral characteristics of the data have been exploited while creating the spectral indices database through feature selection and extraction. However, the spatial domain of the dataset remains unexplored. Within a particular index, it is possible to use spatial statistics to differentiate object classes of similar spectral characteristic. For example, spatial analysis of spectral index output for Forests vs. Grass can distinguish between the two on the basis of its distributions. Texture analysis has been chosen for this research as a method of exploiting the spatial information of the classes.

Haralick *et al.*, 1973 [32] provides a detailed description of these Grey-Level Co-occurrence Matrix (GLCM) texture analysis. Texture analysis was done by selecting neighbourhoods and assessing the variation of grey levels in these regions for all the spectral indices, in search for optimal texture features for classification. These neighbourhoods translate into window sizes while application in tools that calculate these textures. A detailed processing of all the statistics was done for texture analysis (Eq. 4-4 – 4-6; Appendix – B). Eq. 4-4 – 4-6 illustrate the calculation of the textures that were added to the spectral indices database for further classification and analysis [32]:

$$Mean(\mu_i) = \sum_{i,j=0}^{N-1} i(P_{i,j}); Mean(\mu_j) = \sum_{i,j=0}^{N-1} j(P_{i,j}) \quad \text{Eq. (4-4)}$$

$$Entropy = \sum_{i,j=0}^{N-1} P_{i,j} (-\ln P_{i,j}) \quad \text{Eq. (4-5)}$$

$$Second\ Moment = \sum_{i,j=0}^{N-1} P_{i,j}^2 \quad \text{Eq. (4-6)}$$

In the equations 4-4 – 4-6:

- $P_{i,j}$ is the $(i,j)^{th}$ entry in a normalized gray tone spatial dependence matrix.
- N are the number of gray levels in the quantized image

Note that the textures do not always yield interpretable results. All GLCM textures were analyzed, but only the above 3 textures provided discernable results that could be added to the spectral indices input database.

Table 4-4: Spatial indices (texture analysis) added to input database of spectral indices

Source Spectral Index	Texture	Window Size (Neighborhood)
Black Roof	Entropy	3×3 window
Clay Soil	Mean	3×3 window
Mixed Coniferous Forest	Second Moment	3×3 window
MSAVI Vegetation Index	Second Moment	5×5 window
Roof	Mean	3×3 window

Texture analysis is performed on all the spectral indices and investigated. In all, five spatial indices (Table 4-4) were added to the spectral indices database, thereby formulating a combination of spectral and spatial indices for input to the classification process. Second Moment texture generates high results when there lie a few pixels with high magnitude, in the neighbourhood window. Considering this property of highlighting highly distributed data, the texture finds application in vegetation classes. When the input elements in the window are relatively equal, Entropy textures output high values. This principle makes the texture applicable in cases like continuous and consistent pixel values, i.e. Black Roof in the study. Considering a mean calculation within a neighbourhood window, Mean texture tends to highlight pixels of high value and increasing the separability of the classes. This texture finds applicability in cases of Roof and Clay Soil classes.

To understand the effect and applicability of each of these spatial indices, they are individually reduced from the indices database and the accuracy is assessed. The increase or decrease of accuracy would signify the influence of the texture feature. Results of this analysis are shown in the Chapter 5 (Table 5-2 – 5-3).

4.6. Entropy analysis and Defuzzification

The completion of the classification procedure requires adoption of methods to assess the accuracy of the procedure. Considering the fact that the classification approach remains the same for each of the inputs, the end result would be an interpretation of the influence of the input database for classification.

Based on various analysis and review, two approaches have been decided for assessing the classification outputs. Entropy calculation (as a measure of degree of uncertainty) and Accuracy assessment (as a measure of degree of correctness) are selected for the present research.

The outputs of the classification process are individual, grey-scale class soft outputs. The successful classification of an object class was assessed by a method of mean difference calculations (Figure 4-13). The illustration depicts a choice of random pixels in known class locations and calculating the difference. If the difference is significant, it implies that the class is separable after classification. If a certain class has been successfully classified, entropy measures and accuracy assessment are attempted to quantify their accuracy of identification. Generalizing, the particular class shows a better contrast in the output with reference to other classes.

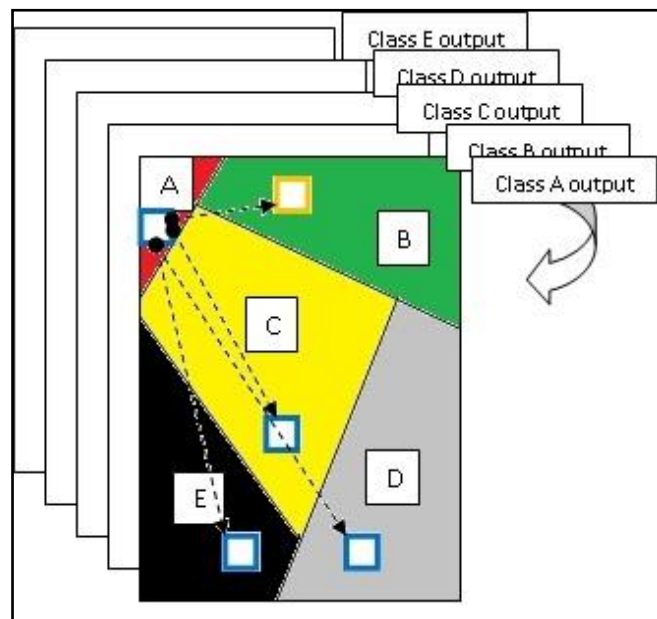


Figure 4-13: Illustration of class differentiation from soft outputs

Entropy calculations (Eq. (4-3) and Section 2.6) define the degree of certainty with which the classifier assigns a class label to a certain pixel. However, measures of entropy should be supported with accuracy assessment for acceptable interpretations [114]. The entropy measures

of the classes are established as an average of 50-75 membership vectors, depending on the spatial extent of the classes.

Defuzzification of the 20 soft outputs in all the cases is done by a simple maximum value approach. The algorithm reads the membership values along the pixel vector and assigns the class with the maximum membership to the pixel. The combination of 20 soft outputs, each corresponding to its respective class, is “hardened” to a single output, containing classification results that can be evaluated by traditional methods of accuracy assessment (user’s and producer’s accuracy), using a combination of ‘user-defined’ and randomly generated test sites.

5. RESULTS AND DISCUSSION

This chapter details the results obtained during the course of the present research and elaborates their possible interpretations. Section 5.1 discusses the determination of optimal PCs input. Section 5.2 provides an overview of the results of the classification approaches. Section 5.3, 5.4 and 5.5 depict the classification outputs and related discussions of all the approaches. The unclassified classes are discussed in the Appendix C – E.

5.1. Determination of Optimal PCs input database

In order to establish a baseline assessment of classification for the APEX data, traditional dimensionality reduction approaches were studied first. The most commonly used and accepted method is Principal Component Analysis (PCA). As discussed previously in Section 2.2, PCA has been used a pre-processing step to classification [36], wherein the algorithm transforms the data into orthogonal projections that maximize variance using linear transformations [12], [58]. In order to define an optimal baseline assessment, optimal number of Principal Components (PCs) has to be decided upon. This choice is based on three aspects:

- Amount of information contained in the principal components;
- Number of classes successfully identified in the classification output;
- Minimal entropy (degree of uncertainty).

With regard to the amount of information in the principal components, Figures 4-10 and 4-11 (Ch. 4) illustrate the amount of information gained with addition of each principal component. As it can clearly be observed, the amount of information gained beyond the 8th component becomes highly trivial. With a gain of 0.04%, adding dimensions becomes questionable. Therefore, 8 PCs were considered for further processing.

As depicted in the methodology (Ch. 4; Figure 4-1), the approach follows a dimensionality reduction and optimal determination of PCs using entropy for the baseline classification assessment. Each of the PCs is individually added to 1 PC, thereby making the inputs (1PC), (1PC, 2PC), (1PC, 2PC, 3PC)... (1PC, 2 PC ... 8PC). An optimal PCs input would show the maximum number of successful classes identified and comparatively minimal entropy. The corresponding accuracy of the optimal PCs will serve as the baseline for the present research for comparison and assessment purposes.

Figure 5-1 provides a graphical illustration of classes identified (X axis) with their corresponding entropy values (Y axis). Note that the classes are in the order of identification with respect to increasing PCs input. Therefore, for example, “Lawn Tennis Court” and “Buildings” classes were identified after adding 7 and 8 PCs respectively to the input principal components database. “Clay Soil” was successfully identified from the initial considered 3 PCs. An input of the first or first two PCs was not considered as the 2-dimensional signature vector could not distinguish most of the classes, resulting in uninterpretable outputs. Even in the absence of considering the maximum number of classified classes, the entropy values show significantly

higher values for classes like “Mixed Coniferous Forest (MCF)” while considering lesser PC inputs.

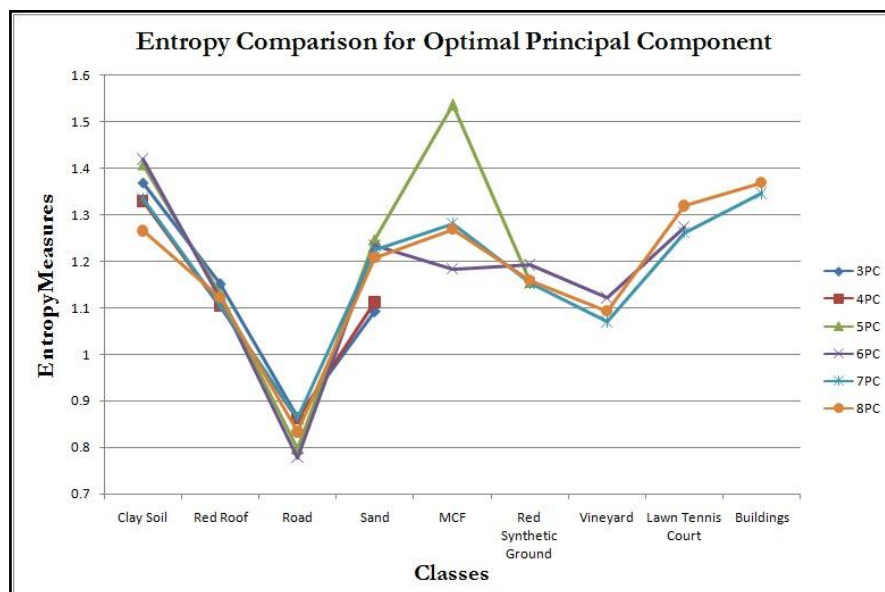


Figure 5-1: Graphical illustration of entropy of classes identified with respective to PCs

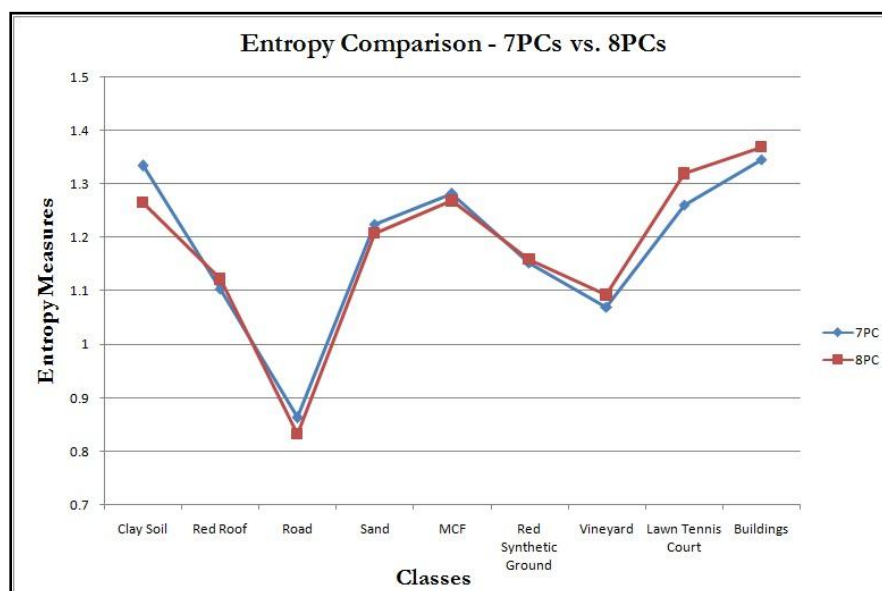


Figure 5-2: Entropy of classes with respective to 7 and 8 PCs

With reference to previously defined criteria for choice of baseline classification accuracy, maximum number of classes (9) were successfully classified (Figure 5-1) while considering an input of 7PCs and 8PCs. Figure 4-13 illustrates the determination of successful classification of a particular class. Considering the individual soft outputs and thresholds of membership values were used to analyze the conflicting classes. A comparative analysis of entropy values for 7PCs and 8PCs (Figure 5-2) was approached to determine the optimal baseline classification. Similar or lesser entropy can be associated with 7PCs input when compared to 8PCs (Figure 5-2). Therefore, the optimal PCs input is decided to be 7PCs as there is no significant variation in entropy measures with increasing dimensionality of the principal components input. Entropy

measures define the certainty with which a class label has been assigned to a pixel. A combination of amount of information in components, number of classes determined and entropy values is, therefore, used to determine the baseline classification. Also supporting this assessment is the defuzzified evaluation of 8PCs classification output, wherein an accuracy of 57.50% was obtained against 59.50% of 7PCs.

5.2. Entropy and Accuracy Assessment Comparison

In this section, an overview of the results is detailed, which are referred in the following sections. The classes that are denoted in red signify those classes that could not be identified in their respective soft outputs without conflict from other considered classes in the study. This indicates that pixels belonging to different classes were found to have membership values higher than the established class threshold. User's (UA) and Producer's Accuracy (PA) are also calculated from the defuzzified outputs of classification.

Table 5-1: PC and Indices input database – Entropy and Accuracy Assessment

Class No.	Class	PC Input Database (7 features)			Indices Input Database (12 features)		
		Entropy	UA	PA	Entropy	UA	PA
1	Artificial Turf		20	100	1.94	100	100
2	Black Roof		62.5	83.34		55.56	100
3	Building	1.35	100	50		100	42.86
4	Clay Soil	1.334	88.89	80	1.45	90	100
5	Grass		40	44.45		40	57.14
6	Lawn Tennis Court	1.26	70	100		40	100
7	Mixed Coniferous Forest	1.3	60	40	1.62	80	57.14
8	Mixed Deciduous Forest		80	29.63	1.6	90	50
9	Pasture		30	100	1.46	55.56	100
10	Railway		28.57	100		30	50
11	Red Roof	1.1	100	25		66.67	54.55
12	Red Synthetic Ground	1.15	60	85.71		60	100
13	Road	0.86	90	47.37		70	23.34
14	Roof		40	50	0.68	100	66.67
15	Sand	1.23	50	100		10	100
16	Stressed Grass		40	40	1.49	70	70
17	Synthetic Sports Surface		100	100		44.45	100
18	Vineyard	1.07	30	50	1.49	66.67	75
19	Water		100	90.9	2.06	100	90.91
20	Yellow Tartan		33.34	100	0.6	30	100
	Overall Classification Accuracy	59.50%			65%		

Table 5-1 describes comparative implications of PC inputs and Indices input (Section 4.4; Table 4-2) to the classifier for extracting specific class information. Besides the increase in overall

classification accuracy of the processes (65% while using indices compared to 59.50% for optimal principal components), note that 7 classes previously unclassified while using optimal principal component (PC) inputs were successfully classified. However, some classes like Lawn Tennis Court were not classified while using indices input database. Also, there are variations in classification accuracy for Vineyards, etc. wherein entropy results show an increase, while classification accuracy from the “hardened” results shows an improvement. The results are discussed subsequently in Section 5.3 (classification of PC inputs) and 5.4 (classification of indices inputs). Comparison with the baseline classification, accuracy measures and entropy is conducted with every combination of output. For all the classification output sets, entropy (Section 4.3; Eq. (4-3)) was calculated as an average of 50 membership vectors per class.

Table 5-2: Spectral-spatial indices – Entropy and Accuracy Assessment (1)

Class No.	Class	Indices and Textures Database (17 features)			Indices and Textures Database (without MSAVI Mean texture) (16 features)		
		Entropy	UA	PA	Entropy	UA	PA
1	Artificial Turf	1.146	80	80	1.274	100	100
2	Black Roof		37.5	75		12.5	100
3	Building	0.63	60	31.58	0.44	100	63.63
4	Clay Soil	1.212	80	100	1.2	100	100
5	Grass	1.004	60	85.71	1.25	90	90
6	Lawn Tennis Court	0.64	80	66.67	0.5	88.89	100
7	Mixed Coniferous Forest	0.956	100	71.43	1.34	100	83.33
8	Mixed Deciduous Forest	1.02	80	61.54	1.35	100	76.92
9	Pasture	0.966	71.43	83.34	1.25	44.44	100
10	Railway		10	33.34		25	100
11	Red Roof		20	100	0.46	100	91.67
12	Red Synthetic Ground	0.65	81.82	90	0.55	42.86	100
13	Road		50	15.625	0.44	88.89	24.24
14	Roof		30	27.27		71.43	75
15	Sand		20	33.34		14.29	100
16	Stressed Grass	1.126	80	80	1.3	87.5	100
17	Synthetic Sports Surface	0.65	50	100	0.55	87.5	100
18	Vineyard	0.94	80	88.89	1.1	90.91	83.34
19	Water	1.44	100	76.92	1.85	90	75
20	Yellow Tartan		10	100	0.5	33.33	100
	Overall Classification Accuracy	62.50%			80.50%		

At the outset, the classes identified through while considering spectral-spatial indices input are notably higher. Comparison with Table 5-1 infers information regarding classification thus discussed. All the classes, without exception, show a significant decrease in entropy values. The degree of uncertainty in determination of class labels to the pixels is lesser when spatial indices

(Section 4.5; Table 4-4) are added to spectral indices feature set to better describe the classes. Although the uncertainty is lesser; the accuracy assessed for the hardened output shows an overall classification of 62.50%. Significant improvement of classification was noted (Section 5-5) for sub-pixel classification and identification of vegetation classes, like Vineyard.

Further, the classification was assessed in terms of the features of the input spectral-spatial indices. The “Mean” texture derived from the MSAVI vegetation index (initially used to separate vegetation and non-vegetation classes) was omitted from the input feature set. An overall accuracy of 80.50% was achieved with better individual accuracies of classes and lesser degree of uncertainty of determination of class labels, when compared to PC and indices input to classification. This input feature set (16 features) of spectral-spatial indices best describes the classes in the study area.

Table 5-3: Spectral-spatial indices – Entropy and Accuracy Assessment (2)

Class No.	Class	Indices and Textures Database (without MSAVI Mean and Black Roof Entropy textures) (15 features)		
		Entropy	UA	PA
1	Artificial Turf	1.296	100	100
2	Black Roof		30	100
3	Building	0.399	100	70.59
4	Clay Soil	1.14	100	100
5	Grass	1.17	80	80
6	Lawn Tennis Court	0.46	75	100
7	Mixed Coniferous Forest	1.18	100	83.33
8	Mixed Deciduous Forest	1.2	90	81.82
9	Pasture	1.19	70	100
10	Railway		12.5	33.33
11	Red Roof	0.44	63.64	70
12	Red Synthetic Ground	0.52	75	85.71
13	Road	0.41	73.33	28.95
14	Roof		72.73	66.67
15	Sand		0	0
16	Stressed Grass	1.16	100	63.64
17	Synthetic Sports Surface	0.54	75	100
18	Vineyard	1.1	50	100
19	Water	1.138	100	83.33
20	Yellow Tartan	0.5	11.12	100
	Overall Classification Accuracy	72%		

The primary objective of using indices to reduce the dimensionality of the hyperspectral data and thereby improve the overall accuracy in comparison to PCA in this research stands

achieved. Further reducing the input feature set with omission of “Entropy” texture of Black Roof index and classifying the feature set of 15 indices; classification accuracy reduces to 72%.

Note that classes that remain unidentified when considering the Possibilistic c -Means sub-pixel classification approach yield accuracy measures after defuzzification. This is reasoned in relation to the method of defuzzification being a maximum membership value approach. The pixel is assigned the class label of the class having maximum value along the membership vector.

The subsequent sections detail and discuss the results of the classification process while considering the three inputs. Besides PC (Section 5.3) and indices inputs (Section 5.4), the results of the spectral-spatial indices (Section 5.5) that yielded the maximum accuracy of 80.50% will be discussed as the optimal combination of spectral and spatial features for dimensionality reduction and classification.

5.3. Classification using PCA based database

The estimation of optimal principal components ensures an appropriate input of PCA based input database. The measure of entropy has already been applied for obtaining the optimal input, while defuzzification will provide an assessment in terms of user’s, producer’s and overall classification accuracy. Pixels depicted in red are those that have a membership value higher than a threshold, i.e. 0.6 for most cases.

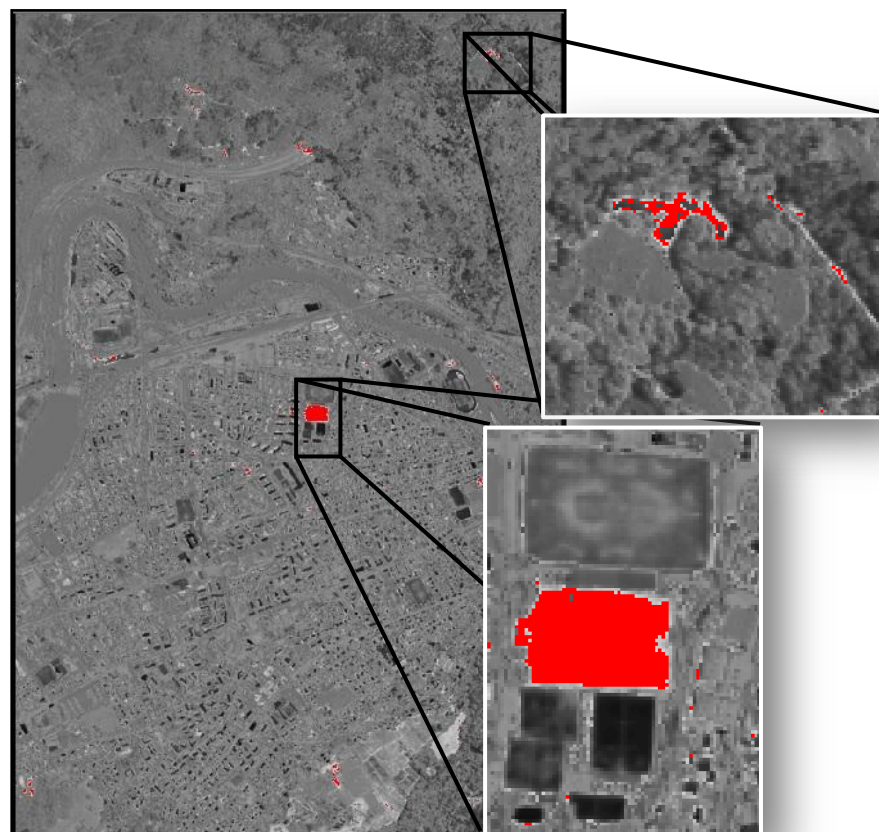


Figure 5-3: Optimal PC input-classification – Clay Soil

Successful classification with pixels gaining high membership values are shown over the grey-scale image of the output. “Clay Soil” class (Figure 5-3) is successfully identified while using the optimal principal components input. Indicated are the areas of identification of the class of interest, verified from ground truth knowledge.



Figure 5-4: Optimal PC input-classification – Red Roof

Successful classification of Red Roofs (Figure 5-4) in the study area was also achieved. Verification of conflict from other classes was checked above the threshold membership value of 0.6. If all pixels above the threshold belong to a single class, the class of interest is considered to have been successfully identified and classified. Ground truth knowledge of sites where the class is ‘present’ and ‘absent’ are noted and verified subsequently. These sites were used for calculation of entropy.

Roads are significantly distributed in the study area. Considering the urban nature of the study area, identification of roads occupies a substantial weightage in the classification procedure. Showing accuracies of 90% and 88.89% while considering PC (Table 5-1) and spectral-spatial inputs (Table 5-2) respectively, Figure 5-5 illustrates the classification results of the “Road” class while considering optimal principal components input.

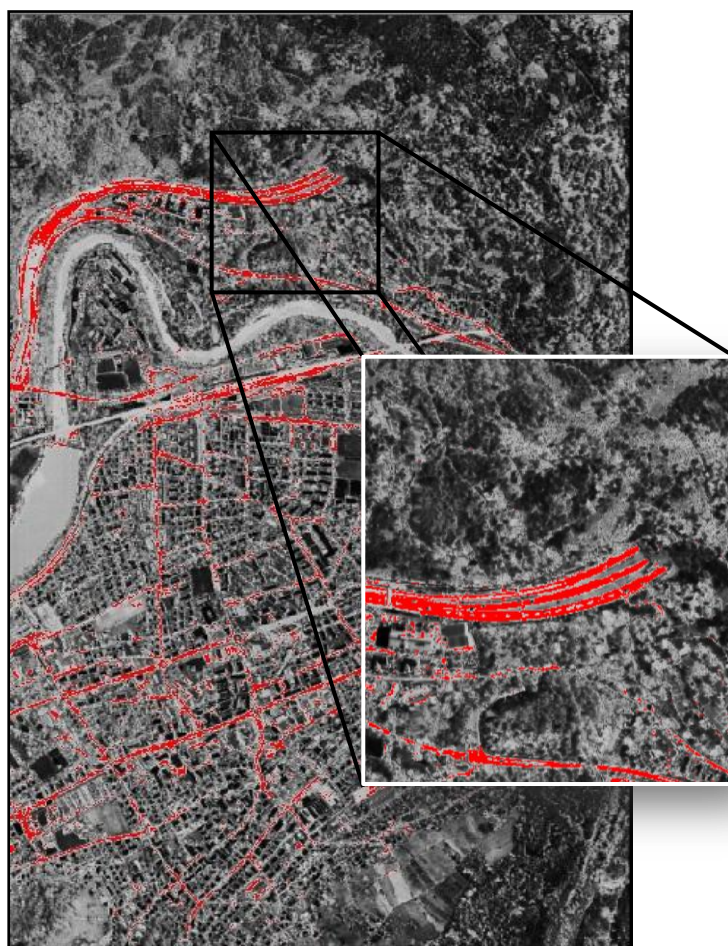


Figure 5-5: Optimal PC input-classification – Roads

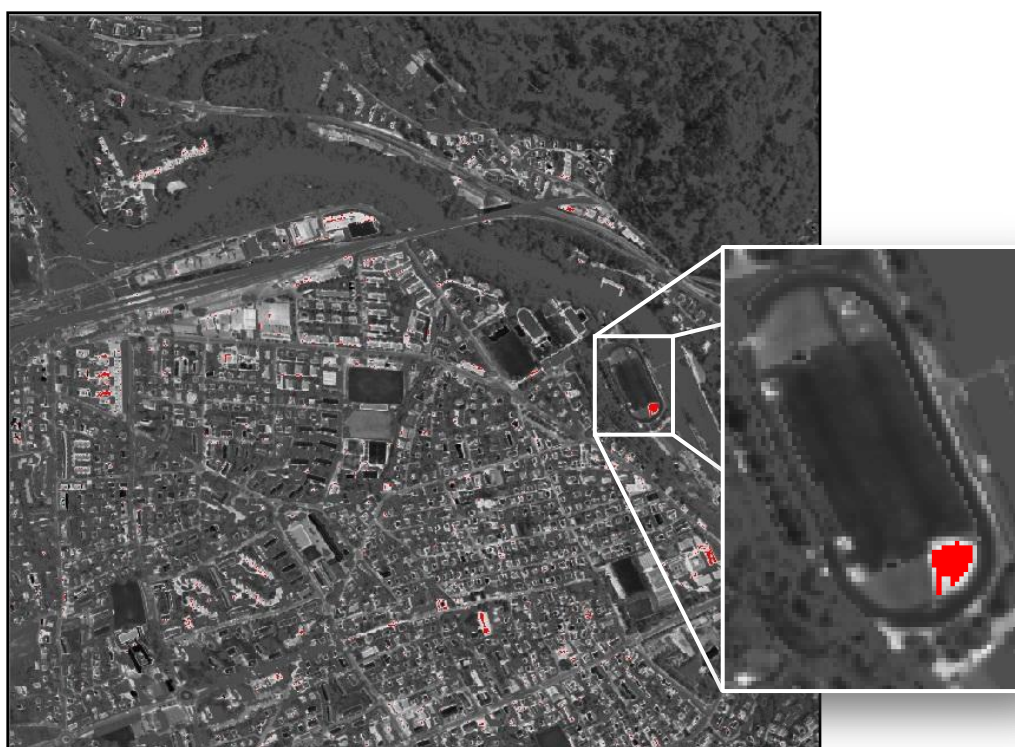


Figure 5-6: Optimal PC input-classification – Sand

Although, occupying a very small area with respect to the extent of the study area, the “Sand” class has been classified with a high membership value when using the principal components input (Figure 5-6).

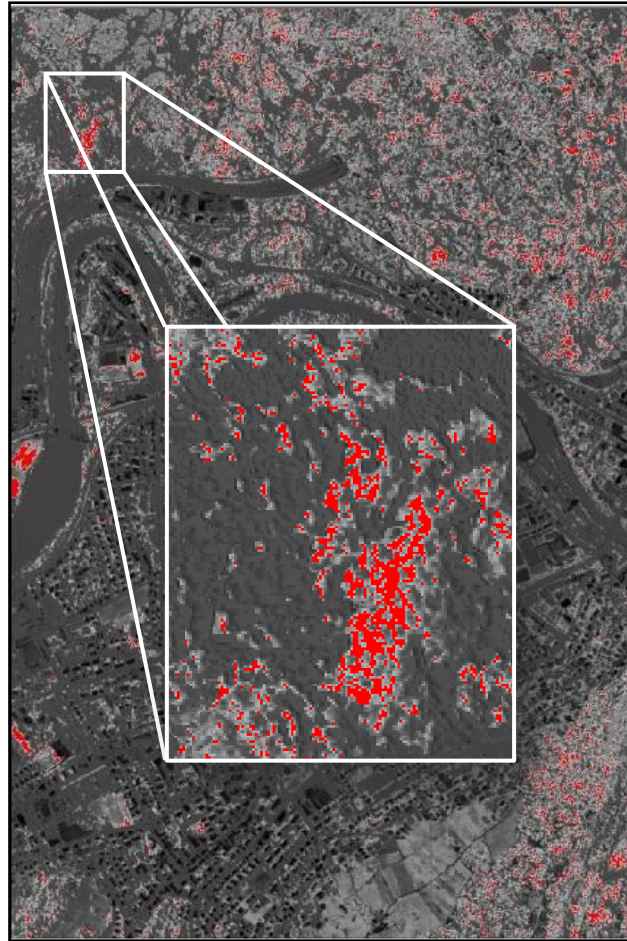


Figure 5-7: Optimal PC input-classification – Mixed Coniferous Forest

The study area of Baden, in this APEX dataset, is characterized by mixed forests around the urban portion. Coniferous, Mixed Coniferous, Deciduous and Mixed Deciduous Forests exist in the study area. Considering the overall distribution and the capability of hyperspectral data in differentiating vegetation of varying species, Mixed Coniferous (Figure 5-7) and Mixed Deciduous Forests were attempted for classification.

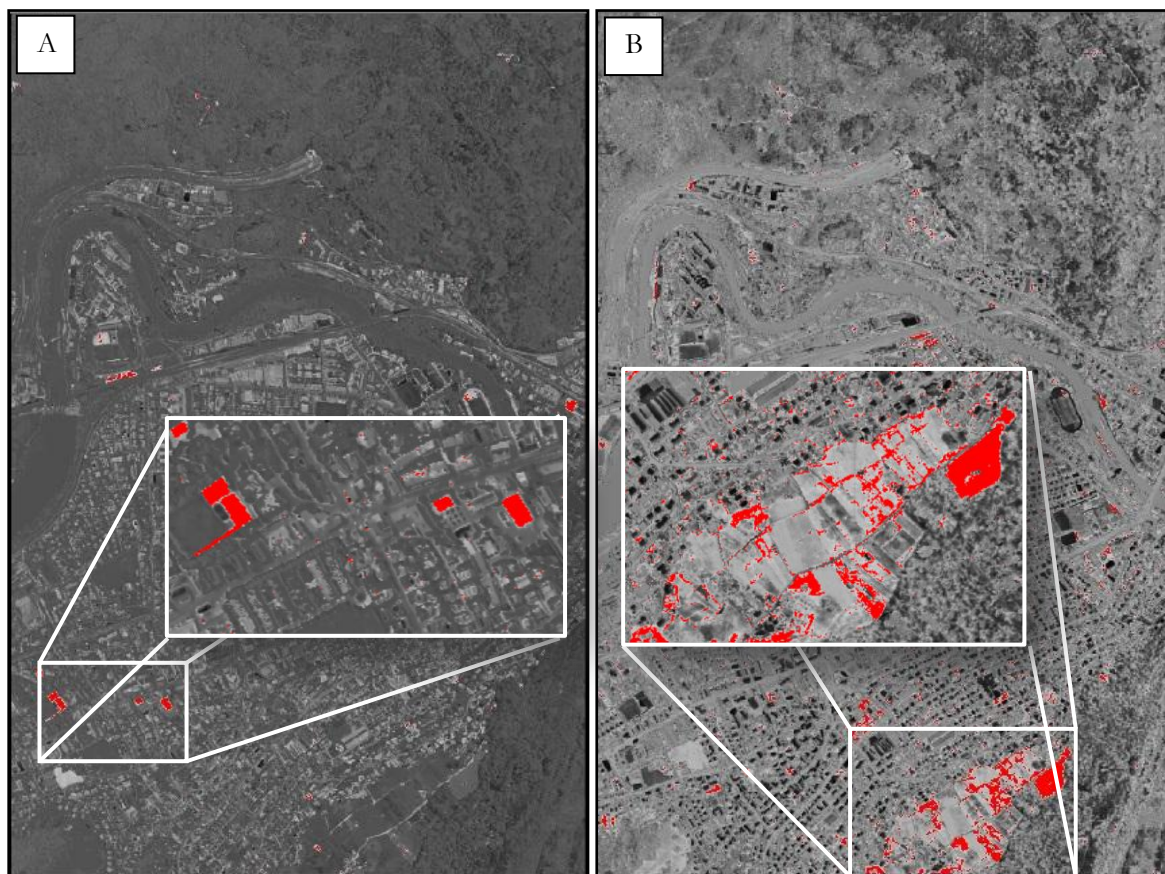


Figure 5-8: Optimal PC input-classification – Red Synthetic Ground (A); Vineyard (B)

The study area consists of 3 different kinds of sports surfaces. As their purposes vary, so do their characteristic material. This results in slight but observable variation in spectral reflectance responses (Figure 4-4). Of these, Red Synthetic Ground (Figure 5-8 (A)) has been classified while considering the PCA based approach.

Hyperspectral data, due to its contiguous spectra, has the potential to separate classes of vegetation. The study area consists of stressed grass, grass, vineyards, etc. Although accuracy assessment shows a low percentage of successful classification, the identification of vineyards has been successfully done. There is confusion while comparing the classification of Vineyard against Stressed Grass and Clay Soil classes, mainly due to the season of data acquisition. The APEX OSD was acquired in June 2011. Considering the life cycle of grapes, June is the time of fruit formation. Therefore, there is a significant amount of reflectance from the underlying soil and very small amount of grapevine-characteristic spectra. Even in this scenario, successful classification of vineyards (Figure 5-8 (B)) while using the PCM algorithm is achieved.

Although a conflict of classes between the classes Lawn Tennis Court and Buildings (Figure 5-9 (B)) occurred considering PCs until the 6PCs composite, the classes were separable beyond the 7PCs input. The spatial distribution of the Buildings class is very small, with one dominant site. All the other structures in the study area relate to either Red Roof or Roofs classes. Therefore, the localised nature of the class was identified in the 7PCs composite, along with the Lawn Tennis Courts (Figure 5-9 (A)).

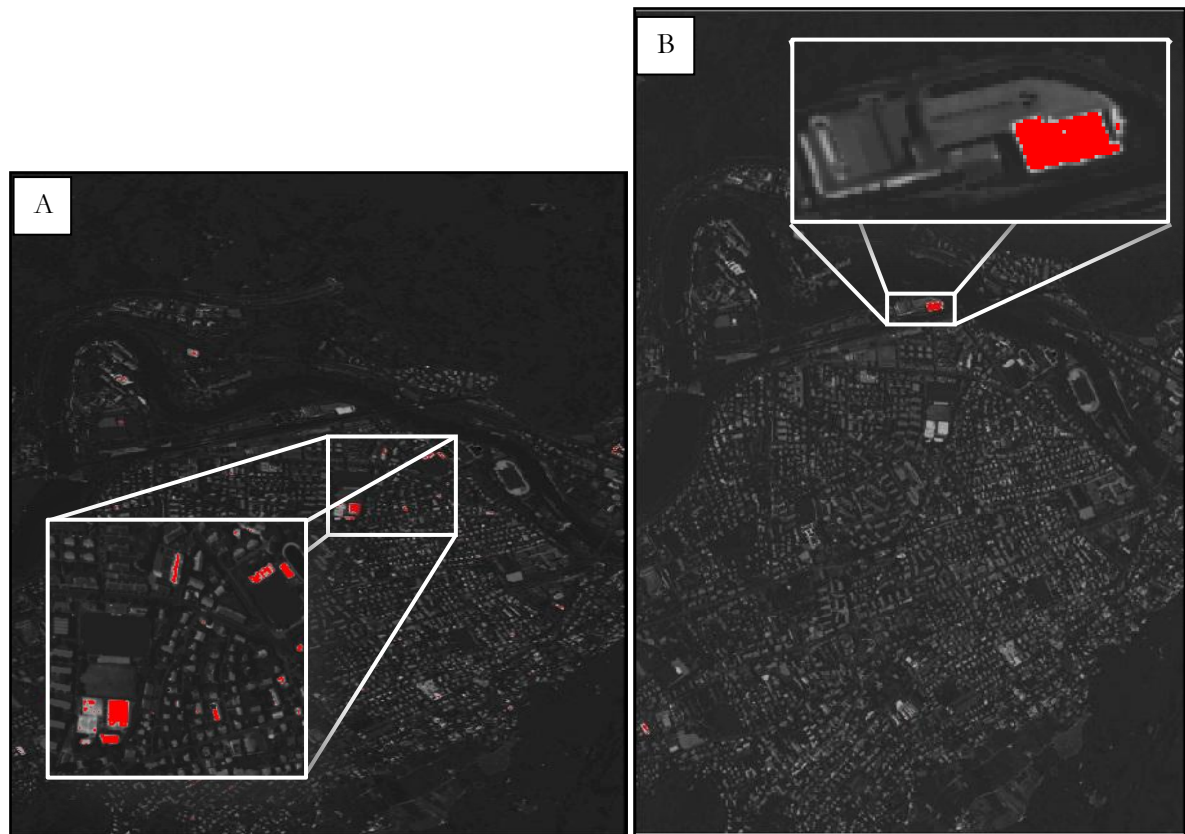
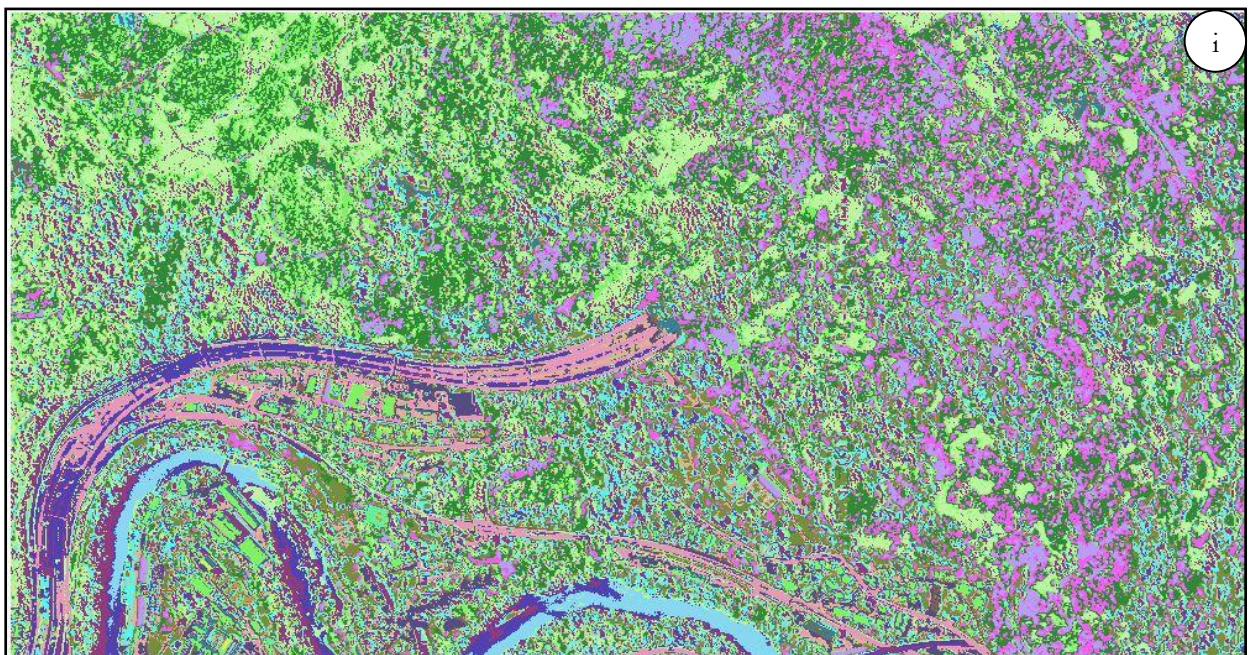


Figure 5-9: Optimal PC input-classification – Lawn Tennis Court (A); Buildings (B)

For the purpose of appropriate illustration, the hardened outputs of the individual approaches have been shown in images of portions (*i – iii*) of the study area. This provides a better understanding, rather than an overview of the output.



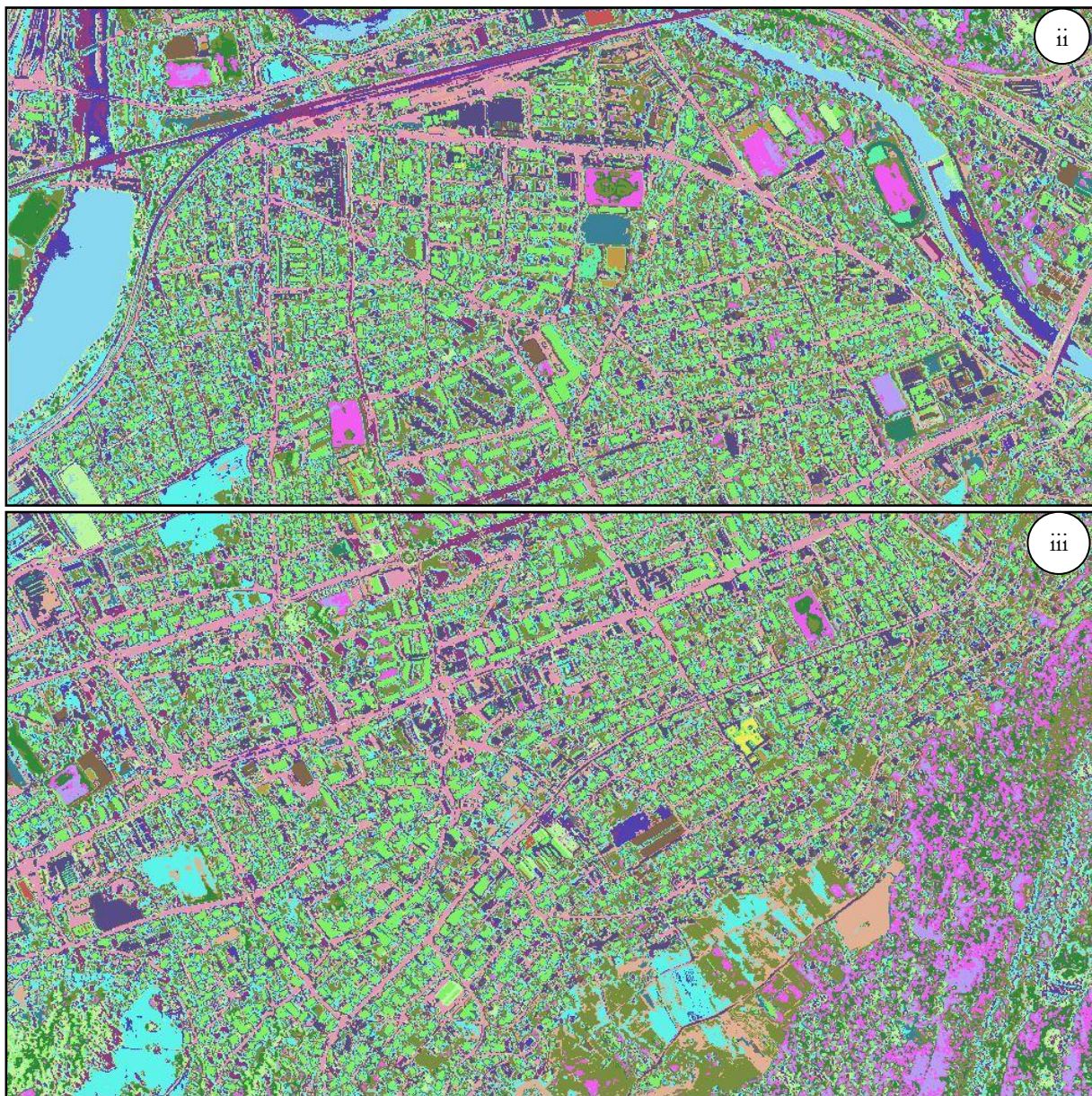


Figure 5-10: Defuzzified optimal PCs classification output (i – iii)



Due to the spatial extent of the study area, it is divided into 3 parts while depicting the defuzzified output (Figure 5-10) of the research work. Although the entropy provides a degree of uncertainty of class label being assigned to a pixel, it does not account for misclassified pixels. Therefore, a simple maximum value defuzzification algorithm is applied and accuracy measures (Tables 5-1, 5-2 & 5-3) are calculated from this defuzzified output.

5.4. Classification using Indices based database

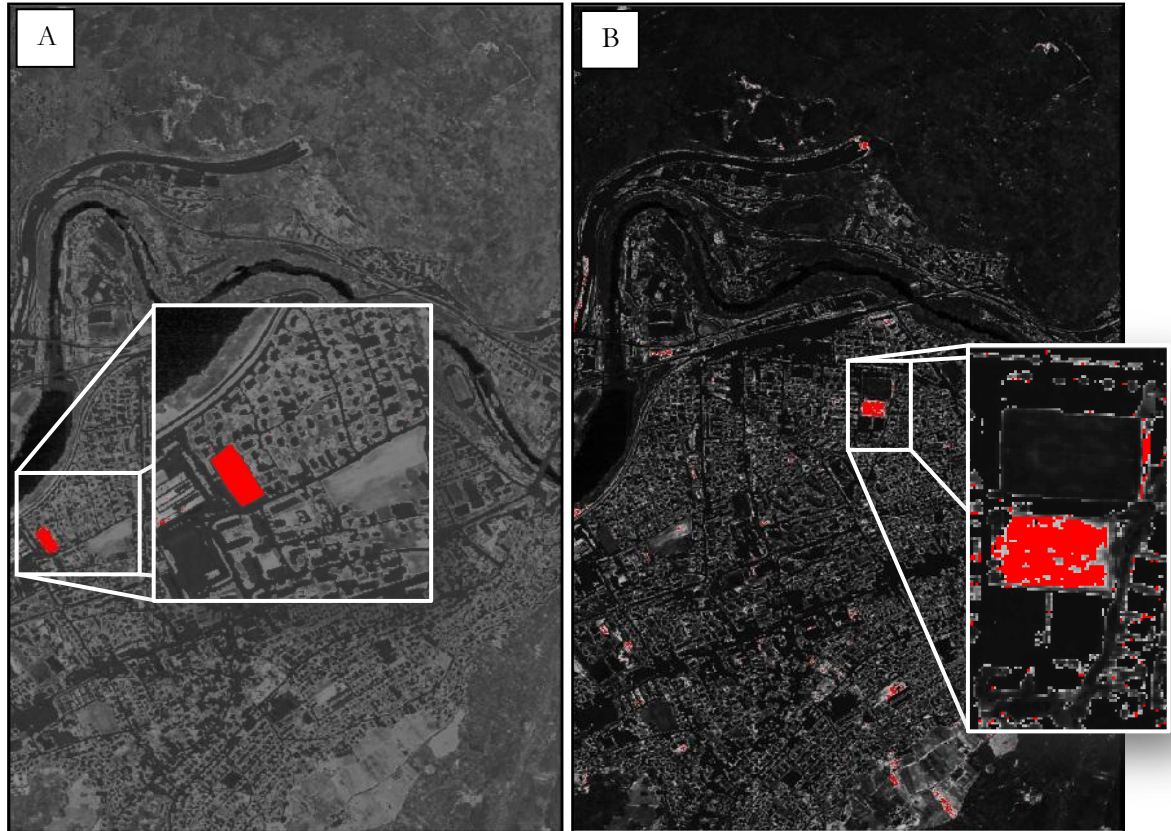


Figure 5-11: Spectral indices input-classification – Artificial Turf (A); Clay Soil (B)

As the baseline classification accuracy estimates have been established, an initial analysis for improvement of classification (Table 5-1) was done using spectral indices input. Considering the high spectral dimensionality of the input dataset (285 bands), an attempt is realised to exploit this through indices.

The classification results show an improvement in identification of 10 classes (as compared to 9 in the case of optimal PCs). However, an inference of identification of vegetation classes is made in this case. Considering the PCM classification outputs, the classes show a better identification of classes as compared to that of PCs input. Also supporting the assumption of indices better describing the classes is supported by the increase in accuracy measures of the subsequently hardened outputs. One such class is that of Clay Soil (Figure 5-11 (B)). The class shows a similar entropy result, considering the increase in accuracy measures. Previously, in PCs approach, unclassified class of Artificial Turf is accurately classified (Figure 5-11 (A)) while considering the indices input, having added the spectral index as an input feature (Table 4-2).

Identification of vegetation classes, utilizing their spectral characteristics was one of the main motivations for the present research. One such scenario of differentiating vegetation using their spectral responses was that of separating the two forest types in the study area. Mixed coniferous and mixed deciduous forests are characteristic of different leaf structures, and therefore, indices that were used for the purposes of LAI were used (Table 4-1, 4-3).

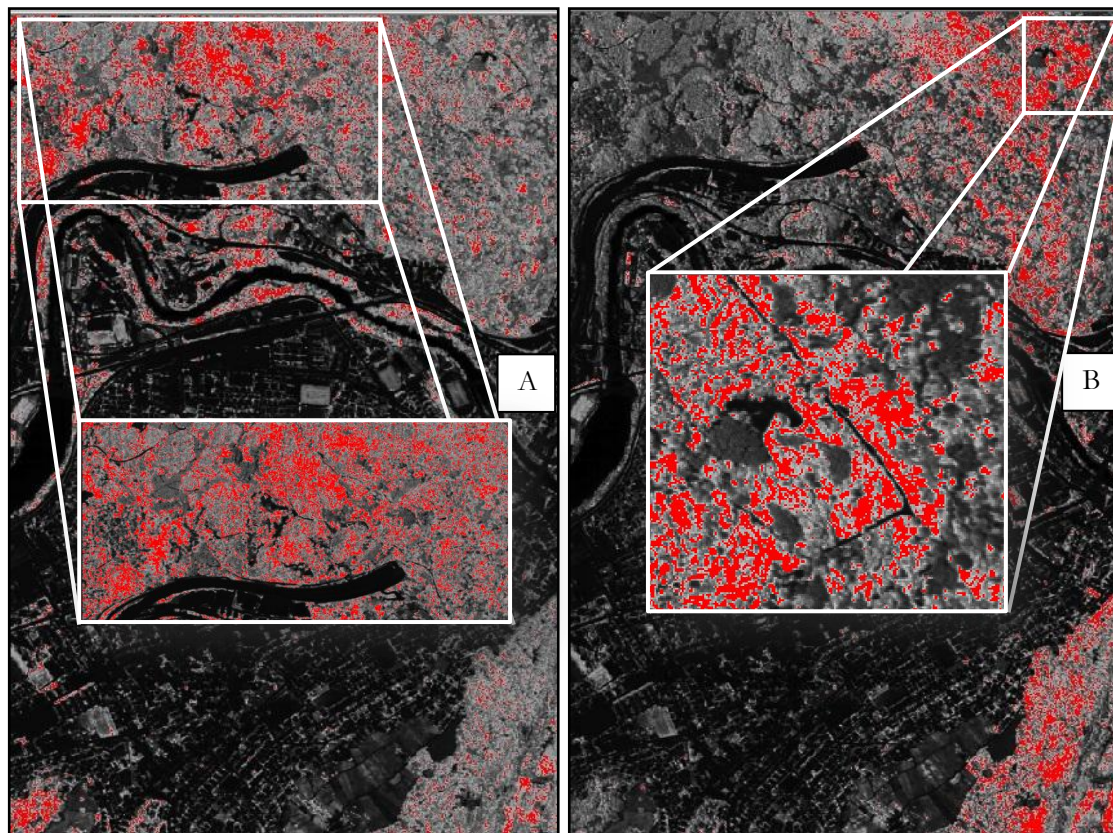


Figure 5-12: Spectral indices input-classification – Mixed Coniferous (A) and Deciduous (B) Forests

Mixed Coniferous (Figure 5-12 (A)) and Mixed Deciduous (Figure 5-12 (B)) Forests were distinctly separable from the classification outputs, with minor conflicts from classes like Grass. These were, however, dealt with while defuzzifying the soft classification outputs..

Although assumed to be of the same constituent grass, Pastures, as a class, was separately classified (Figure 5-13 (A)) from the dataset. The spectral curve in comparison to that of Grass (Figure 4-3) showed variations that were exploited through spectral indices.

Considering the extensive urban distribution in the study area of Baden, through the APEX OSD, the class of Roof was intended to be classified utilizing the advantages of band ratio of infrared bands (Table 4-3). The consequent result shows a very promising classification of roofs in the study area with very low entropy of 0.68 and accuracies of 100% (UA) and 66.67% (PA). Note that this class is not further classified while considering spatial indices and therefore, spectral indices stand as the optimal option for classification of roofs in the study area. Note that the combination of spectral index (Table 4-2) and spatial index of “Mean” texture over a

3X3 neighbourhood extracts roof information, without a further classification with an exception of a few pixels from the Water class (Appendix – E, Figure E-1).

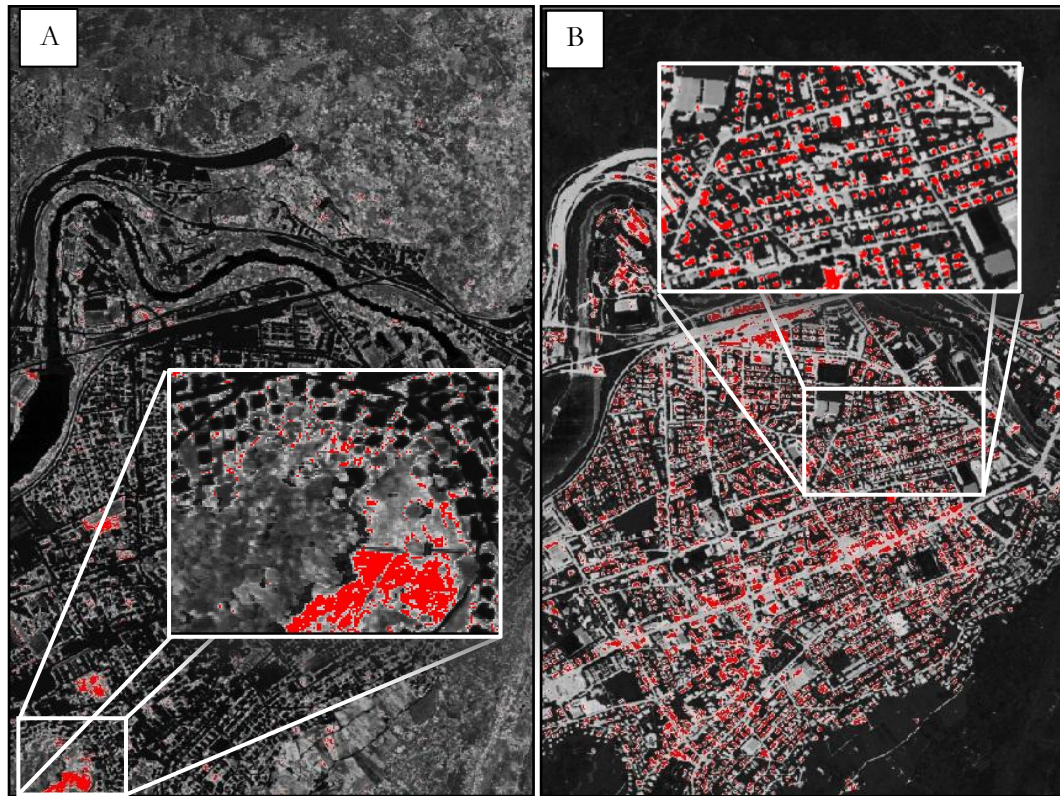


Figure 5-13: Spectral indices input-classification – Pasture (A); Roofs (B)

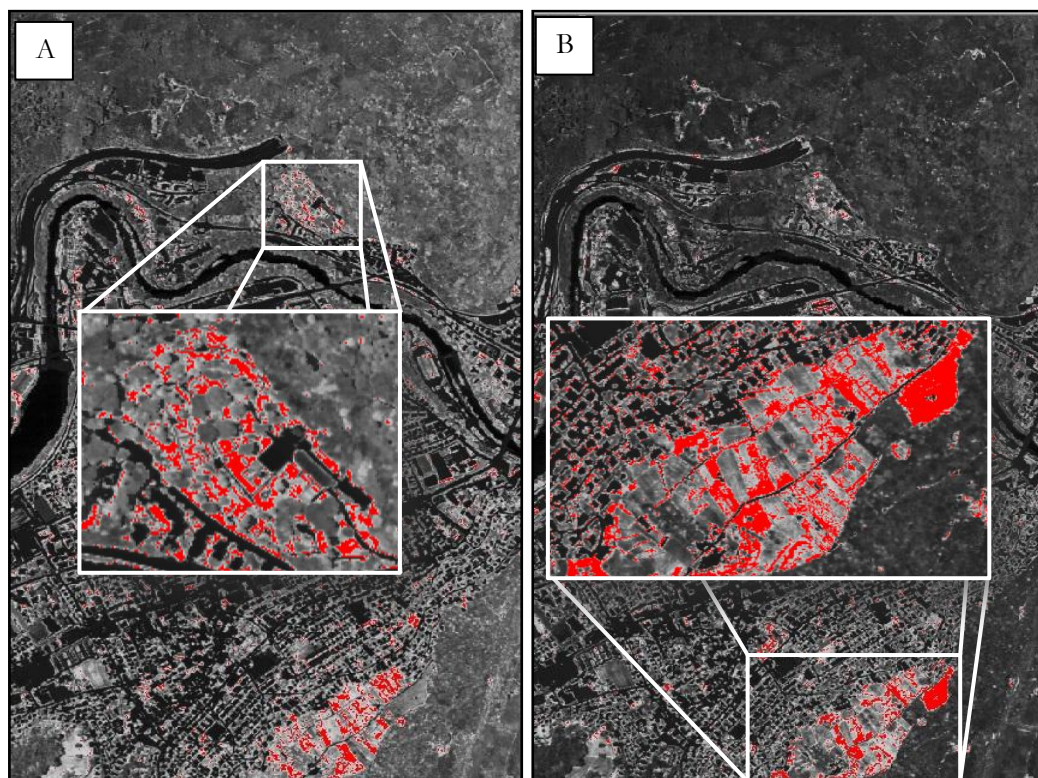


Figure 5-14: Spectral indices input-classification – Stressed Grass (A); Vineyard (B)

As previously discussed in the case of vineyard classification for optimal PCs input, there is an inherent confusion between stressed grass and vineyards due the season of data acquisition. Therefore, some pixels of both classes are classified in their respective outputs (Figure 5-14 (A), (B)). However, noting the significant amount of membership values assigned to the pixels of the class of interest, upon defuzzification, were able to deal with the mis-classification. This is supported by the significant increase in the classification accuracy measures of both classes (Table 5-1).

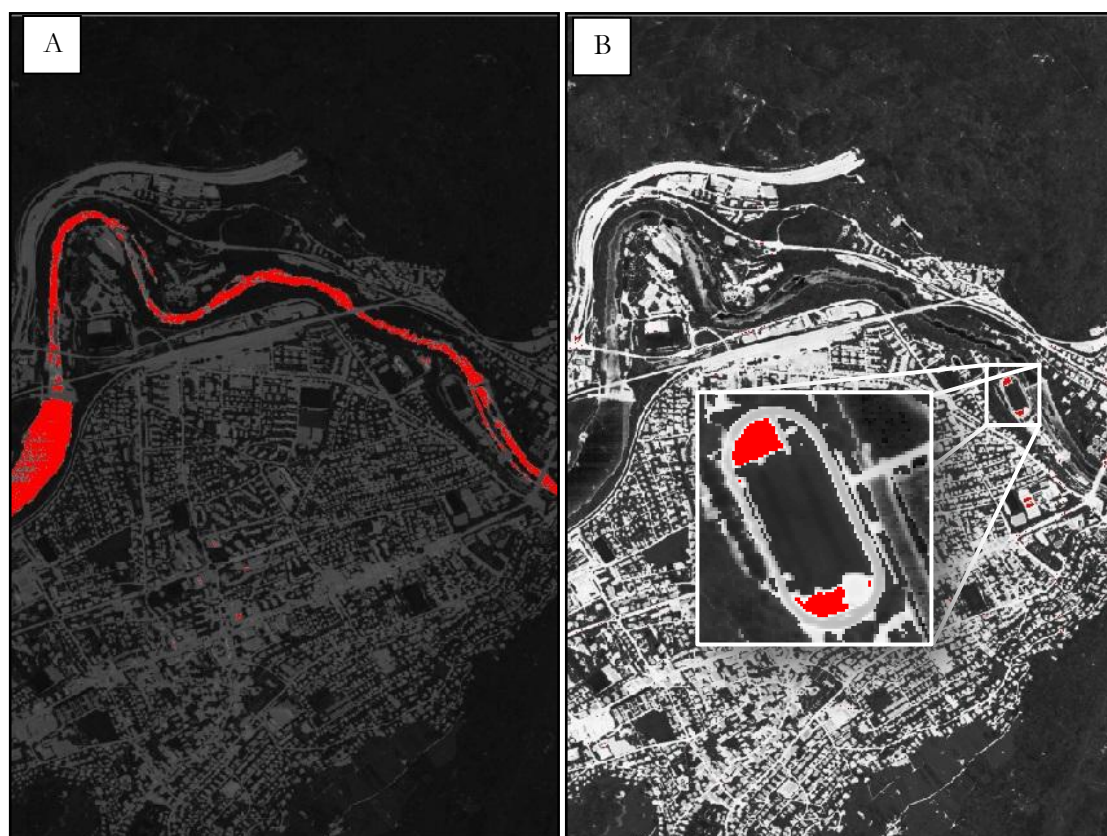


Figure 5-15: Spectral indices input-classification – Water (A); Yellow Tartan (B)

Supported by NDWI spectral index (Table 4-2) for water classification, the Water class has been successfully identified, although with a higher entropy (Table 5-1, 5-2) than while considering spectral-spatial indices. The overall classification accuracy is also better (Table 5-1, 5-2).



Figure 5-16: Defuzzified spectral indices input database classification output (i – iii)



The defuzzified output of the indices input classification is illustrated in the Figure 5-16, along with its associated legend (above). The defuzzified output allows for calculation of accuracies for classes that could not be identified without conflict in the soft outputs of the PCM classification. These classes showed conflict with other classes, but upon maximum value defuzzification were able to be identified, with varying degrees of accuracy.

5.5. Proposed Approach of Spectral and Spatial Indices database for Classification

Considering the improvements of classification while considering spectral indices (65%), when compared to the traditional dimensionality reduction approach of PCA (59.50%), the encouraging results assist in progress of the study to exploiting the spatial characteristics of the data. Individual class determination accuracies also improved, with specific emphasis on vegetation classes. APEX sensor acquires the data at a spatial resolution of 1.8 m. This allows for a possible application of neighbourhood characteristics for constructing spatial indices. Of the various types of spatial indices, texture analysis has been chosen for the present study.

Of the various combinations of spectral and spatial indices assessed, three acceptable combinations have been listed in Tables 5-2 and 5-3. Note that the final result of the present research is an input feature set of 16 indices, i.e. 12 spectral and 4 spatial indices. The classification accuracy of 80.50%, better than both PCs and spectral indices inputs, shows that knowledge-based dimensionality reduction approach, through feature selection, provides better identification of classes from a study area.

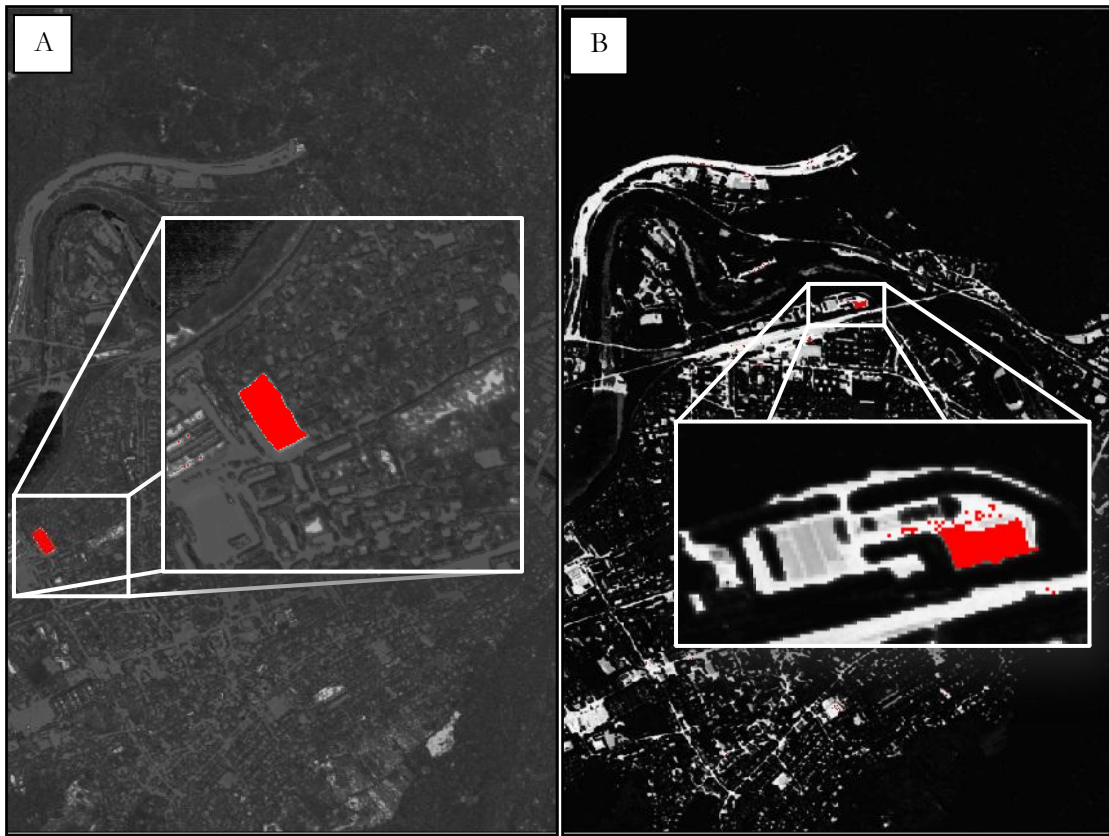


Figure 5-17: Spectral-Spatial indices classification – Artificial Turf (A); Building (B)

An improvement of classification is observed while considering spectral and spatial input database. Note that the entropy values of all the classes reduce (Table 5-2) when compared to previous approaches (Table 5-1). A significant improvement when compared to PCs input classification; Artificial Turf is accurately classified (Figure 5-17 (B)) while considering spectral and spectral-spatial inputs, but comparatively better classified in the latter. This is supported by the reduction in entropy values of the class.

Although determined with a lesser degree of uncertainty, the Building class shows high membership values, a characteristic of the soft output that is enhanced after defuzzification. Improvements in producer's accuracy of the class indicate accurate identification of the class labels assigned to the ground pixels.

Clay Soil (Figure 5-18 (A)) and Grass (Figure 5-18 (B)) are two classes that were successfully classified with lesser entropy measures. While Clay Soil (also classified from PCs and Spectral indices approaches) was classified with better UA and PA measures, Grass is identified without conflict from Mixed Deciduous Forest class as in previous cases (Figure 8-2 (A) and 8-8 (A)). The addition of spatial descriptors is considered responsible for differentiating similar spectral responses from these classes, as textures for grass and trees is significantly different. Classification improves to 90% from 40% (PCs and spectral indices inputs, Table 5-1).

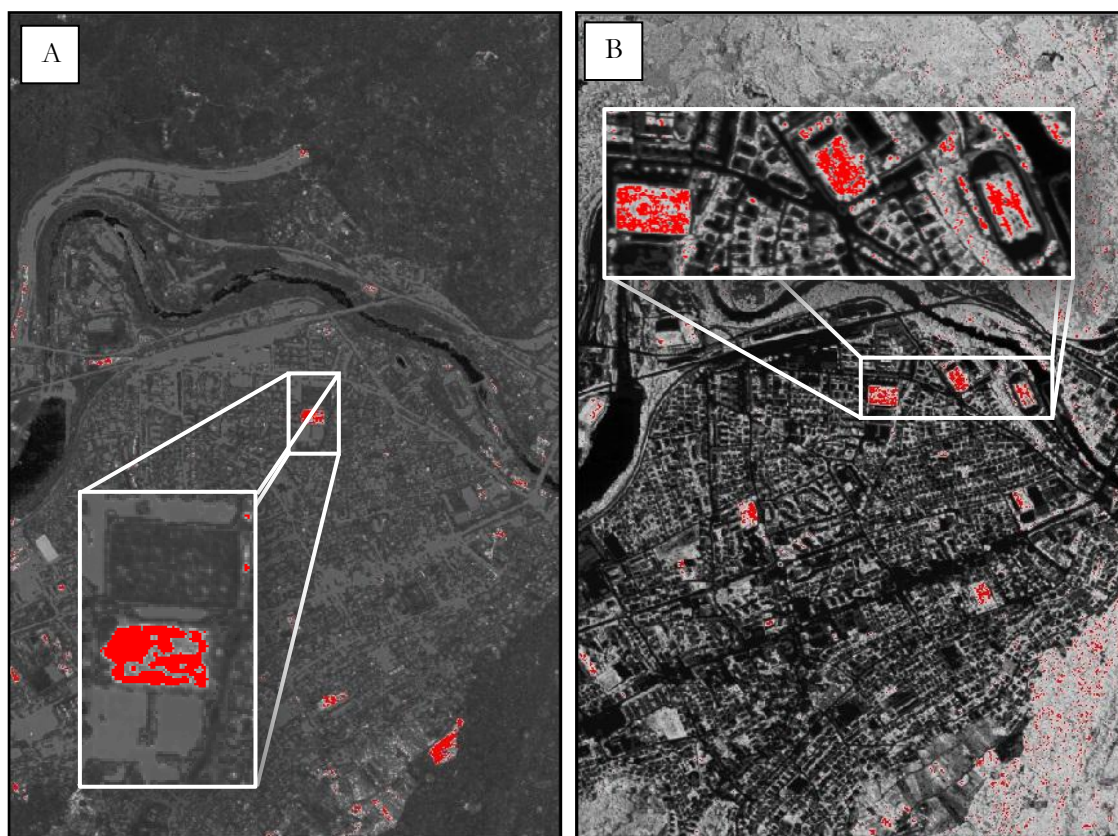


Figure 5-18: Spectral-Spatial indices database-classification – Clay Soil (A); Grass (B)

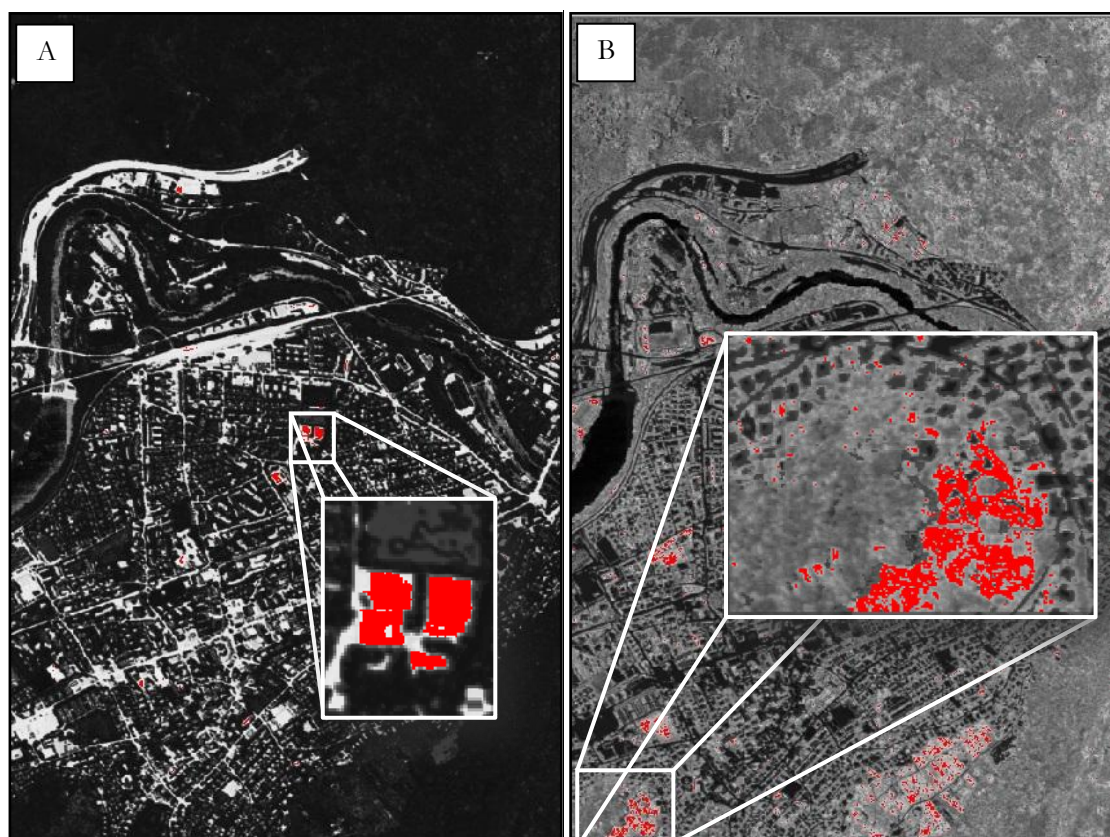


Figure 5-19: Spectral-Spatial indices classification – Lawn Tennis Court (A); Pasture (B)

As interpreted from the Figure 5-19 (B), Pasture class shows conflict of lower memberships near the threshold from classes like Vineyard. Note that although the entropy measures are lower (Table 5-1, 5-2), the accuracy measures are lower than PCs and Spectral Indices approaches. Also, the feature set input of 17 indices (Table 5-2) provides the best results for Pasture class. With a minimal entropy and better accuracy than other input feature sets, the class is said to be best classified with the presence of the vegetation deriving “Mean” texture of MSAVI spectral index.

Minimal entropy and maximum accuracy measures for classification of Lawn Tennis Courts (Figure 5-19 (A), Table 5-2) are obtained while describing the hyperspectral information through a dimensionality reduction approach of spectral and spatial indices. Through defuzzification, all the sites of this class are successfully identified and classified.

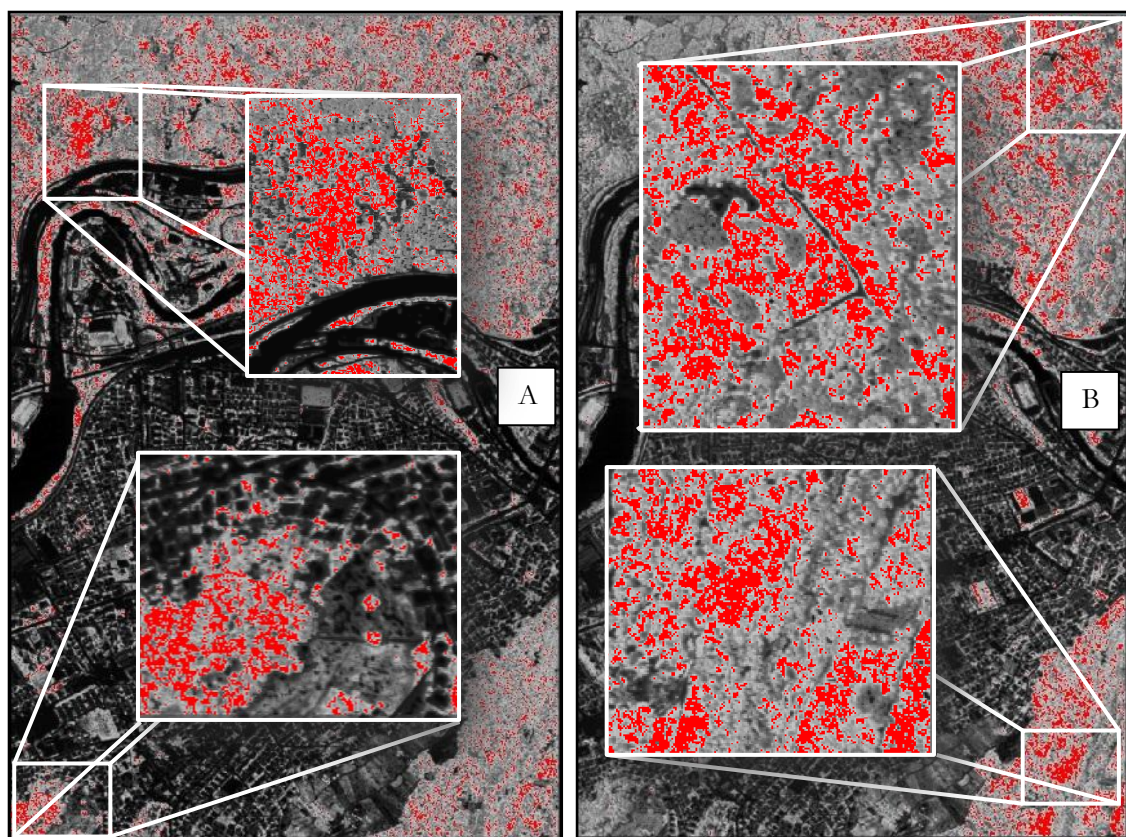


Figure 5-20: Spectral-Spatial indices classification – Mixed Coniferous (A); Deciduous (B) Forests

As previously discussed, differentiating species of vegetation was made possible with addition of spatial information descriptors. Through textures, the different tonal distributions of the two types of forests allowed definition of signature vectors that resulted in the eventual successful classification.

Figure 5-20 illustrates the successful identification of Mixed Coniferous (A) and Deciduous (B) forests. The class labels were assigned with entropy lesser than that of the spectral indices input, while the accuracy measures were better while compared to previous approaches (Table 5-2).

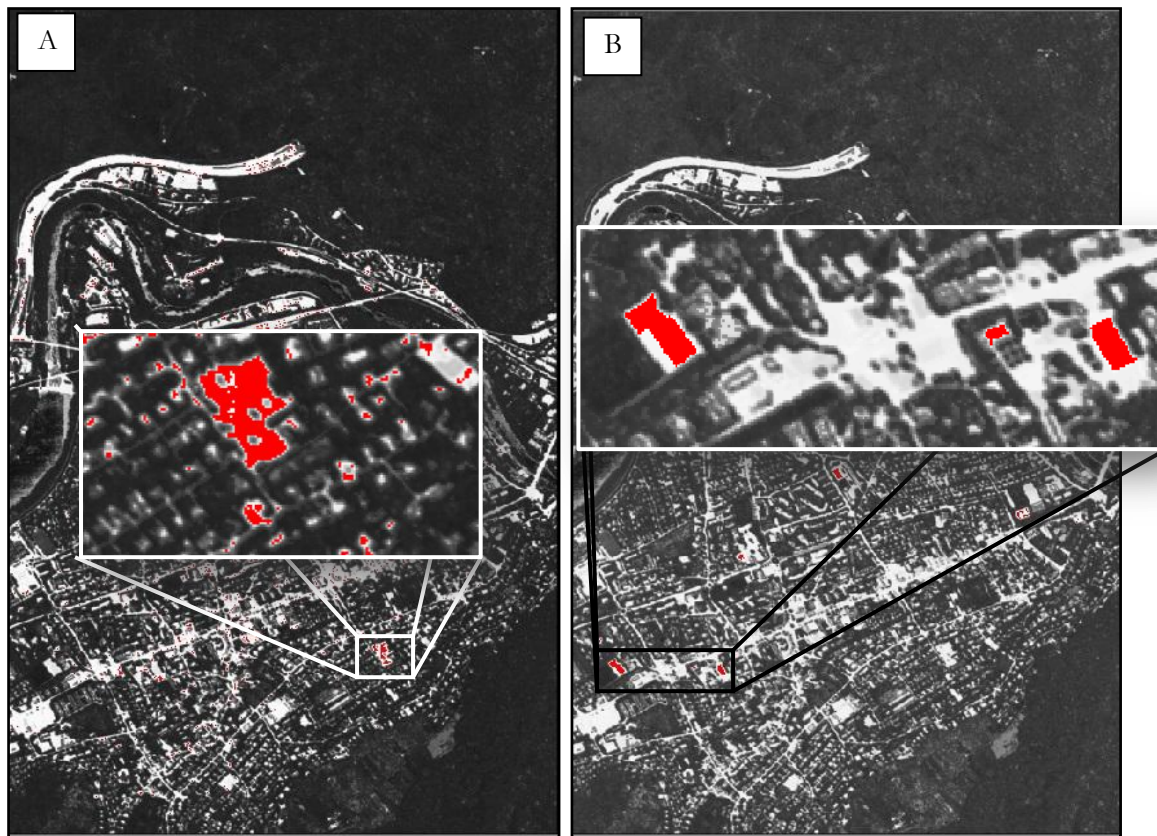


Figure 5-21: Spectral-Spatial indices classification – Red Roof (A); Red Synthetic Ground (B)

The classes illustrated in Figure 5-21 (A, B) are identified with lesser entropy in the spectral-spatial indices approach. Defuzzification of the classification outputs produces encouraging results, however, with the exception of Red Synthetic Ground being classified with 81.82% (UA) accuracy while considering 17 input feature sets.

The Road class (Figure 5-22 (A)) is classified with an accuracy of 88.89% (UA) as compared to similar measures while considering PCs input. The entropy, however, is significantly lower. Synthetic Sports Surface is yet another class that was not identified through the PCs and Spectral Indices approaches. This class is classified while considering the spectral-spatial indices input (16 features) with a minimal entropy of 0.55 at an accuracy of 87.5%. The spectral-spatial indices composite of 16 layers renders the successful classification of this class possible, after defuzzification of soft outputs.

As previously discussed, there lies a degree of conflict of membership values for some of the classes. One such class combination is that of Stressed Grass and Vineyard (Figure 5-23). Considering Figure 5-23 (A), the stressed grass sites show high membership value, while the pixels with membership value near the considered threshold membership of 0.6 tend to lie in the sites of Vineyard class. Defuzzification procedure successfully eliminates conflict of classes of interest.

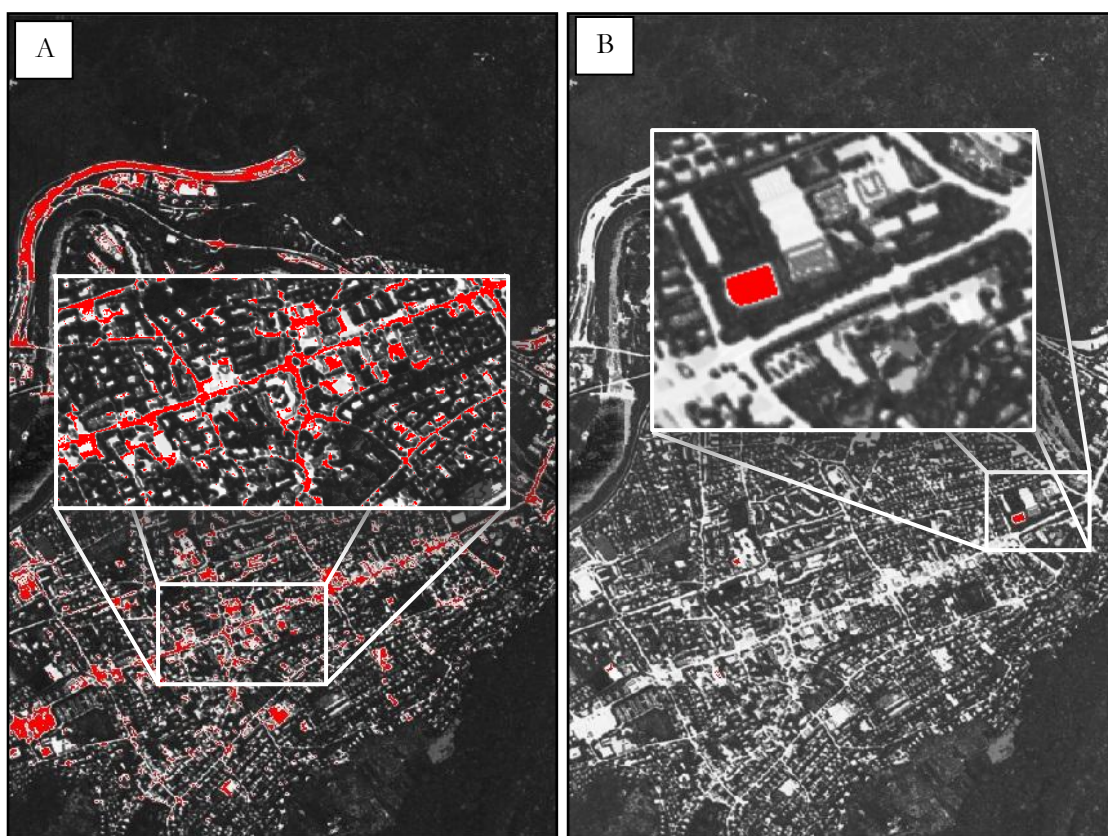


Figure 5-22: Spectral-Spatial indices classification – Road (A); Synthetic Sports Surface (B)

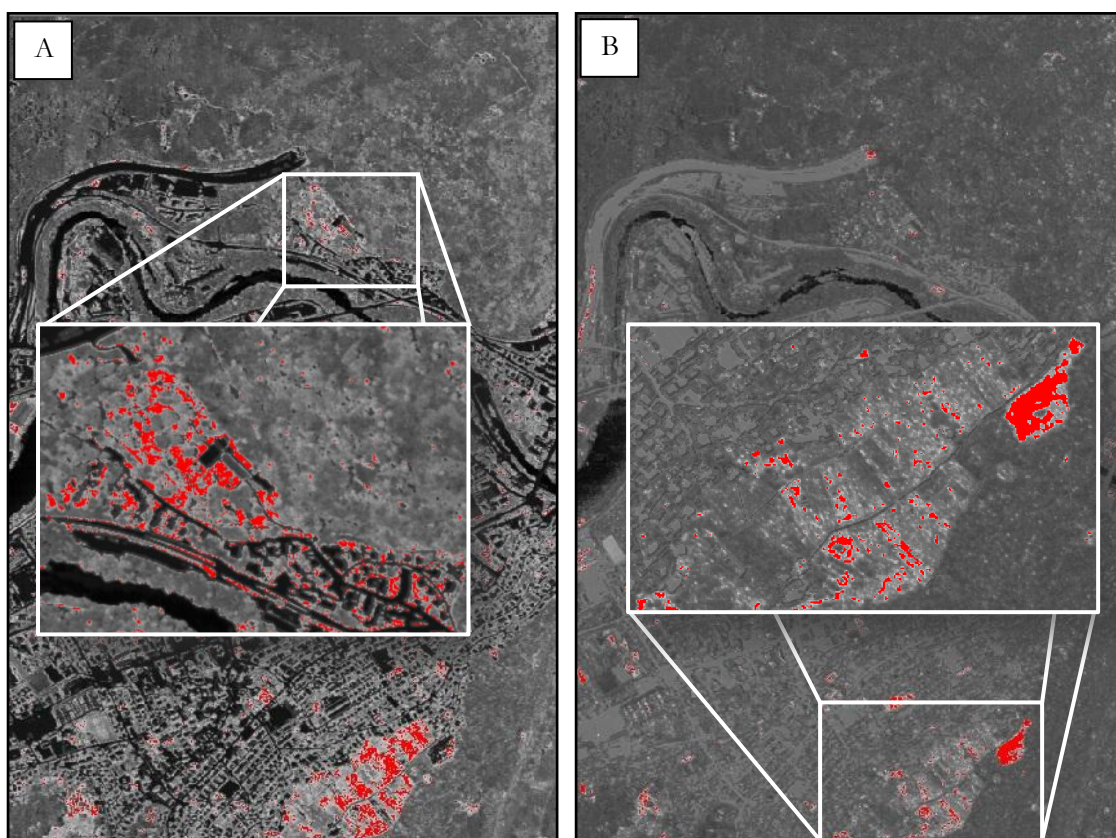


Figure 5-23: Spectral-Spatial indices classification – Stressed Grass (A); Vineyards (B)

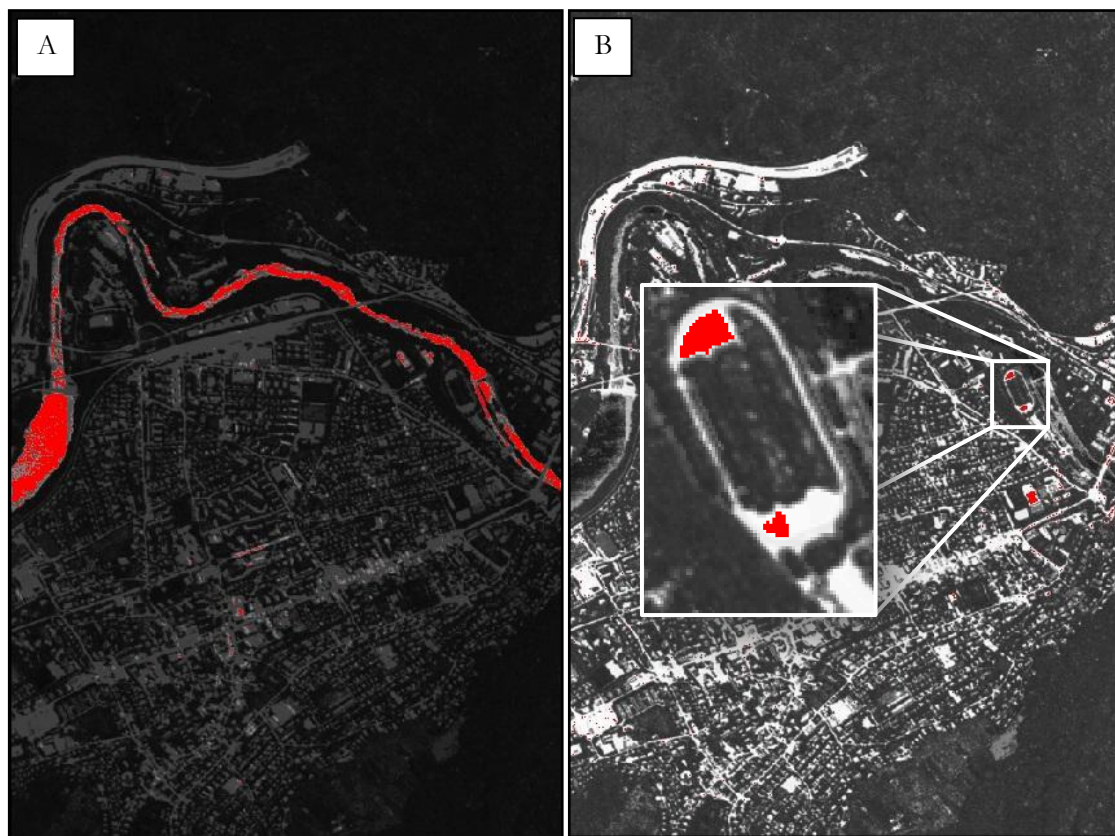
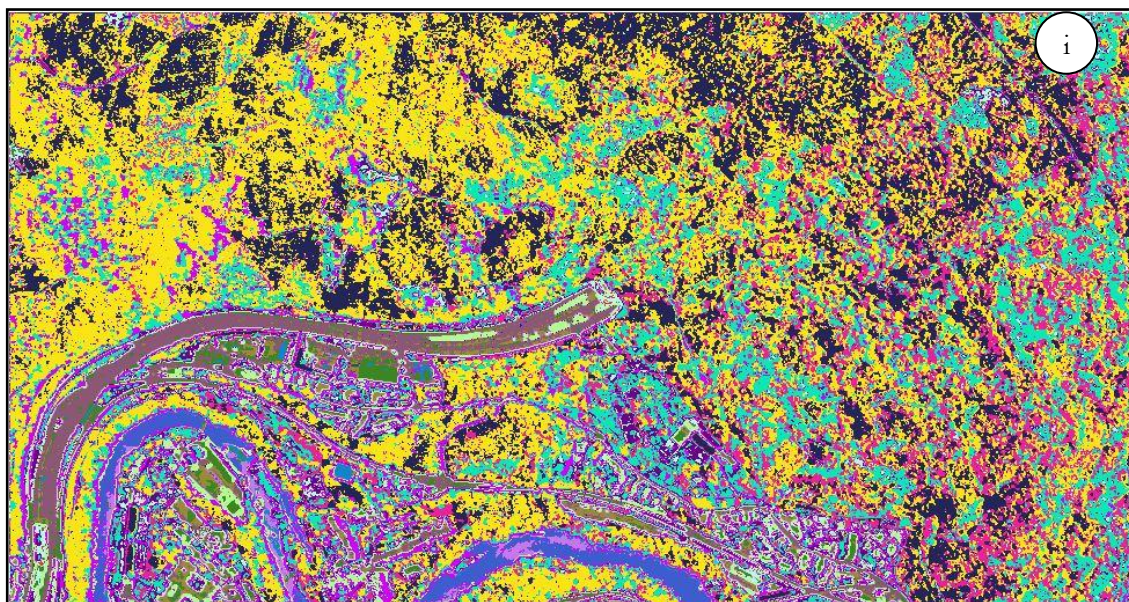


Figure 5-24: Spectral-Spatial indices classification – Water (A); Yellow Tartan (B)

The final classes of analysis are those of Water and Yellow Tartan. The Water class has been classified in Spectral Indices approach while considering the NDWI feature in the input dataset. The class is identified with lower entropy compared to Indices input database. Yellow Tartan, like some of the other classes in the study occupies a very small spatial extent. Due to this reason and characteristics of signature vector, their classification occurs with conflict from some of the other classes. However, considering the defuzzification results, it can be inferred that their classification accuracies are comparatively lower than other classes (Table 5-2).



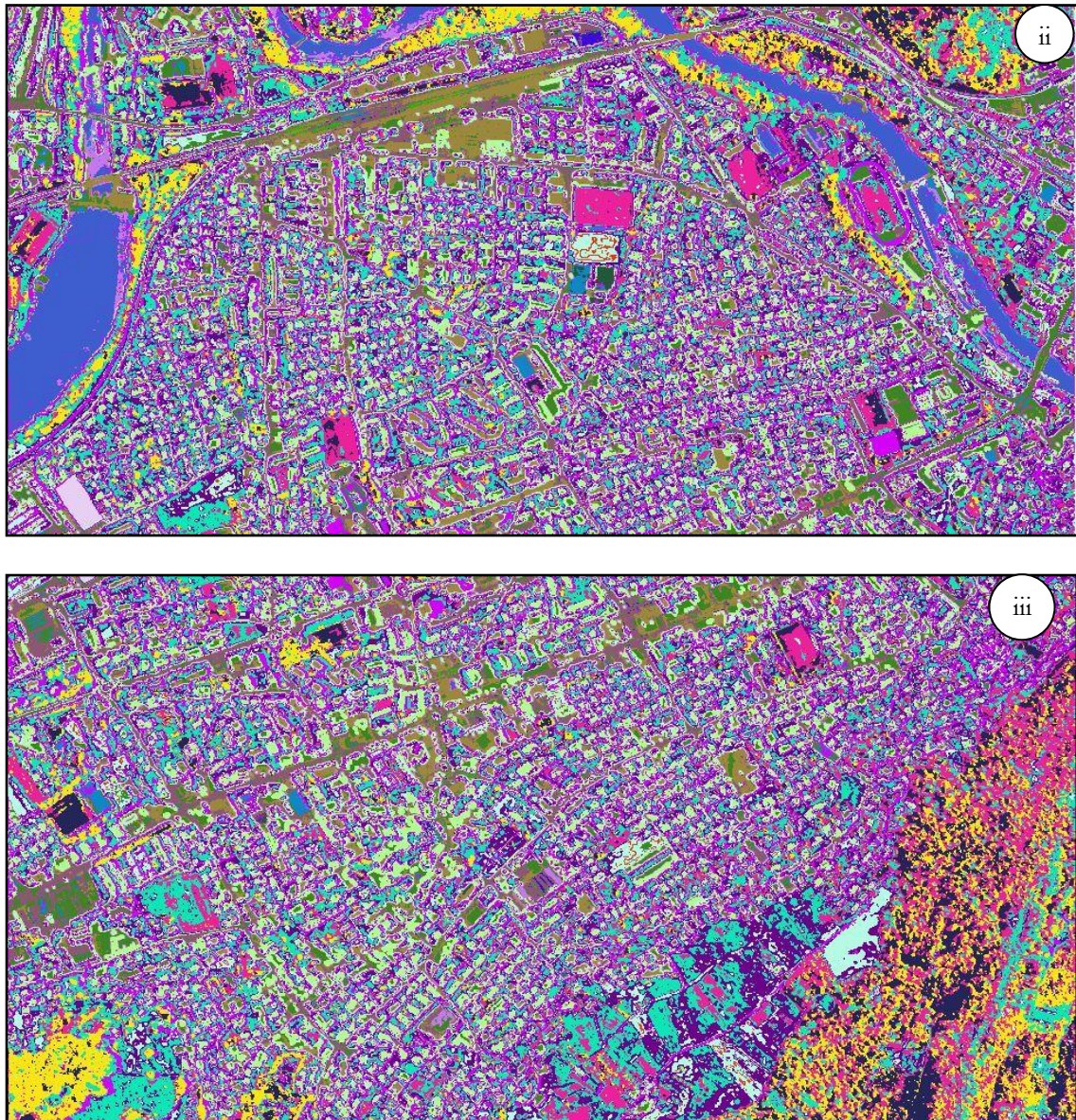


Figure 5-25: Defuzzified spectral-spatial indices input database classification output (i – iii)

6. CONCLUSIONS AND RECOMMENDATIONS

Summarizing the research results, a direct inference can be drawn in regard to the impacts on classification accuracy. Considering that the classification process remains the same, variations in the input and dimensionality reduction approaches are a key to understanding the applicability of the proposed approach in this research work. The research deals with an initial establishment of baseline measures for the purpose of comparison, wherein a traditional dimensionality reduction approach of PCA is considered. Possibilistic c – Means algorithm is used to derive the initial classification results. With an overall classification accuracy of 59.50%, the baseline classification established a reference for the subsequent methodology. In an attempt to exploit the characteristics of the airborne hyperspectral dataset, spectral indices are constructed from literature review based analysis and knowledge of spectral response curve behaviour. Indices were formulated specific to the APEX dataset and band ratio combinations were used for distinctive class behaviour.

The formulated indices were tabulated (Table 4-3) and discussed in detail (Section 4.4). Distinctive properties that allowed formulation of these indices were detailed and “keys” from the spectral curves were identified. Texture analysis (Table 4-4) from neighbourhood operations of GLCM, as spatial descriptors; added spatial information to the spectral indices input feature set.

Results proved that the addition of these spatial descriptors to the spectral indices feature set enhances the classification of the classes. They depicted a reduction in measures of uncertainty and improvement of overall and individual classification accuracies from the initial PCA based dimensionality reduction approach to knowledge-based feature selection and classification approach. A classification accuracy of 80.50% with indices based input database to dimensionality reduction achieves the objectives set to be achieved. The extensive study of spectral curves and their properties facilitated formulation of indices from the APEX dataset. Indices were formulated specific to the dataset, highlighting the applicability of the approach through the results. Also, using the principles of previous studies [13]–[15], [19]–[21], [25], [28], [79], indices were constructed from the spectral curve.

Research Question: Which object classes require formulation of indices in terms of airborne hyperspectral data?

Hyperspectral spectrometers collect information in many, very contiguous bands, allowing a detailed analysis of the target class/ground. This characteristic of the data creates a problem or “curse” of dimensionality. Famously known as the Hughes phenomenon, the dimensionality problem reduces the accuracy of class identification due to inadequacy of training samples.

Object classes with distinctive spectral characteristics require the formulation of indices. Considering the nature of the APEX data, airborne and resolutions, object classes of great detail, like roofs can be identified. Most of the class based indices have been uniquely formulated, either considering different bands or specificity to the dataset. Due attention was paid to the indices of

the vegetation classes, as the improvement in classification and separability of these classes, compared to PCA based approaches, was one of the primary motivation of this study. Enhancing the spectral characteristics of these object classes, spatial indices were chosen on the basis of their neighbourhood operations and overall texture analysis.

Research Question: Which bands are relevant for the definition of indices?

The relevance of bands and their choice served two purposes in this study. Firstly, it described the object class in lesser dimensionality, as a transformation of 2 or more bands. Secondly, it assisted in dimensionality reduction, as out of 285 (APEX) bands, the object class is defined in terms of one index output. This reduction is considered knowledge based, as the choice of bands requires an understanding of spectral curves and their associated properties.

The choice of bands relevant for the definition of indices was assisted by prior understanding of the spectral curves (Table 4-1). Vegetation reflectance spectra and understanding assists in choice of specific “keys” that identify properties that differentiate the type of vegetation. Similar analysis is done for other classes, but identification of keys depends on unique properties/behavior of the classes’ curves.

Research Question: Which characteristics would be selected as spatial indices of the object classes?

The various spectral indices (Table 4-3) are supplemented by the spatial indices (Table 4-4) in describing the information of the APEX dataset in lesser dimensions. As the results proved, the addition of these indices indeed improves the classification.

Spatial information is of formidable weightage in the present study. This is due the high spatial resolution of 1.8m, associated with the APEX data. Utilizing this information through neighborhood operations using GLCM textures was the considered approach in the present study. The choice of textures depends on separability of the classes. Interpretation of texture analysis was done in order to judge their applicability to effectively add meaningful information to the input feature set, and is considered case specific. Mean, Entropy and Second Moment (Section 4.5), amongst other GLCM approaches, were chosen as appropriate spatial descriptors. For instance, the two forest types, not distinguished from spectral indices input, were separable after the addition of the spatial descriptor, Second Moment texture.

Previous studies [98] have proven that consideration of all textures collectively does not improve the accuracy and thus, of the analyzed textures (Section 4.5; Appendix-2), the optimal choice was made on the basis of interpretation of the texture analysis and the separability of classes. Therefore, the above mentioned measures (Table 4.4) are considered as the spatial indices for this research.

Research Question: Which classifier is appropriate for the baseline classification, and subsequent classifications, and why?

The choice of the classifier for the baseline classification, and the overall classification approach was governed by the characteristics of the data. The classification process is used for evaluation of the input feature set, therefore decided on the characteristics of the dataset and number of classes chosen.

Considering the mixed pixels problem largely associated with land use land cover classification, the intended classifier is expected to accommodate for possibility of more than one class in a single pixel, thus focusing on sub-pixel classification approaches. Of the various algorithms for the same, Possibilistic c -Means was chosen. The objective function of the PCM algorithm removes the constraint of membership values adding up to 1, thereby extracting the class values from the strength of their signature vectors. Through this algorithm, the membership values of classes that are present in the pixel are maximized and other classes subsequently minimized. Although the membership values in the membership vector do not add up to 1, the possibility of the class in the pixel is evaluated against probability in cases of other fuzzy algorithms. This property of PCM has a major advantage. It is possible that the 'user' cannot exhaustively identify all the classes in the study area. Considering an urban area dataset like that of APEX OSD, where a unique mix of vegetation and urban classes are present, all the existing classes are not possible to be identified. While considering constrained objective functions (like FCM, etc.), unidentified classes are misclassified into the class that has the maximum probability of belonging. This can be avoided, and unidentified classes remain unclassified and do not affect the classification process while considering PCM.

Research Question: What is a suitable method to combine data from multiple bands in a single index?

As discussed, indices serve a dual purpose in this research, dimensionality reduction and class identification. Identification of relevant bands has also been discussed. A suitable method to combine these bands would be the appropriate choice of bands and index. The properties and applications of the indices were studied and used to accommodate for different properties. For example, indices formulated for LAI assist in the discrimination of the two forest types that have significantly different leaf structures. Considering the multiple bands, from the overall feature set effectively reduces the dimensionality with regard to identification of a specific class.

Recommendations for Future Research:

The results of this present research have supported the motivation of using spectral and spatial indices to reduce the dimensionality of the dataset and improve the classification. An established database of formulated indices was developed from spectral curve understanding and neighborhood operations.

Some recommendations for future research would be:

- The present research has been successfully completed using pixel based classification techniques. Further research can be performed with Object Oriented classification approaches. While signature vectors mark the classification input for pixel based classification approaches, various segmentation approaches could be used to create segments for classification. Object based image analysis accounts for both spectral and spatial properties of the object classes.
- Classes like Sand, Black Roof, etc. were not classified in any of the approaches. This has been attributed to a comparatively smaller spatial distribution of these classes and inadequate information added to these classes through the indices. The information through signature vectors was not sufficient to differentiate these classes from the remaining, therefore an improvement for these classes' identification could be scope for future research. These classes, in other study areas, might be of some significance. Formulating indices suitable for these classes could be the way forward.
- Optimal choice of hyperspectral bands is a research domain in itself. For the specified indices, an automated procedure to calculate the band combinations for indices could be attempted. An optimal choice of bands would yield the highest accuracy amongst all computed combinations of bands for a specific index. Supporting literature for a similar process of optimal agricultural crop characteristics estimation is available, wherein evaluation for optimal choice of hyperspectral bands has been done using a reference of field collected biophysical variables [125].

REFERENCES

- [1] T. M. Lillesand, R. W. Kiefer, and J. W. Chipman, *Remote Sensing and Image Interpretation*, 5th ed. Sanjeev Offset Printers, Delhi: John Wiley and Sons (Asia) Pte. Ltd., Singapore.
- [2] S.-E. Qian and G. Chen, "A new nonlinear dimensionality reduction method with application to hyperspectral image analysis," in *International Geoscience and Remote Sensing Symposium, 2007*, 2007, pp. 270–273.
- [3] M. Govender, K. Chetty, and H. Bulcock, "A review of hyperspectral remote sensing and its application in vegetation and water resource studies," *Water SA*, vol. 33, no. 2, 2007.
- [4] P. M. Mather and M. Koch, *Computer Processing of Remotely-Sensed Images: An Introduction*, 4th ed. Singapore: Wiley-Blackwell.
- [5] "MINEO Consortium: Final Report - Section 6," May 2003.
- [6] S. A. H. Scottish Government, "Assessing the Extent and Severity of Erosion on the Upland Organic Soils of Scotland using Earth Observation: A GIFTSS Implementation Test: Final Report," Scottish Government, St. Andrew's House, Regent Road, Edinburgh EH1 3DG Tel:0131 556 8400 ceu@scotland.gsi.gov.uk, Report, Nov. 2009.
- [7] C. R. da Silva, J. A. S. Centeno, and S. R. Aranha, "Reduction of the dimensionality of hyperspectral data for the classification of agricultural scenes," presented at the 13th FIG Symposium on Deformation Measurement and Analysis, 2008.
- [8] I. T. Jolliffe, *Principal component analysis*. New York: Springer, 2002.
- [9] A. A. Green, M. Berman, P. Switzer, and M. D. Craig, "A transformation for ordering multispectral data in terms of image quality with implications for noise removal," *IEEE Transactions on Geoscience and Remote Sensing*, vol. 26, no. 1, pp. 65–74, 1988.
- [10] G. Hughes, "On the mean accuracy of statistical pattern recognizers," *IEEE Transactions on Information Theory*, vol. 14, no. 1, pp. 55–63, 1968.
- [11] J. C. Harsanyi and C.-I. Chang, "Hyperspectral image classification and dimensionality reduction: an orthogonal subspace projection approach," *IEEE Transactions on Geoscience and Remote Sensing*, vol. 32, no. 4, pp. 779–785, 1994.
- [12] A. Plaza, P. Martinez, J. Plaza, and R. Perez, "Dimensionality reduction and classification of hyperspectral image data using sequences of extended morphological transformations," *IEEE Transactions on Geoscience and Remote Sensing*, vol. 43, no. 3, pp. 466–479, Mar. 2005.
- [13] P. . Zarco-Tejada, J. . Miller, A. Morales, A. Berjón, and J. Agüera, "Hyperspectral indices and model simulation for chlorophyll estimation in open-canopy tree crops," *Remote Sensing of Environment*, vol. 90, no. 4, pp. 463–476, Apr. 2004.

- [14] P. . Zarco-Tejada, A. Berjon, R. Lopezlozano, J. Miller, P. Martin, V. Cachorro, M. Gonzalez, and A. Defrutos, "Assessing vineyard condition with hyperspectral indices: Leaf and canopy reflectance simulation in a row-structured discontinuous canopy," *Remote Sensing of Environment*, vol. 99, no. 3, pp. 271–287, Nov. 2005.
- [15] D. Haboudane, "Hyperspectral vegetation indices and novel algorithms for predicting green LAI of crop canopies: Modeling and validation in the context of precision agriculture," *Remote Sensing of Environment*, vol. 90, no. 3, pp. 337–352, Apr. 2004.
- [16] P. Lin, Q. Qin, H. Dong, and Q. Meng, "Hyperspectral vegetation indices for crop chlorophyll estimation: Assessment, modeling and validation," presented at the International Geoscience and Remote Sensing Symposium (IGARSS), 2012, pp. 4841–4844.
- [17] M. A. Cho, I. Sobhan, A. K. Skidmore, and J. de Leeuw, "Discriminating species using hyperspectral indices at leaf and canopy scales," in *Proceedings of ISPRS Congress*, Beijing, 2008, pp. 369–376.
- [18] G. R. Liu, C. K. Liang, T. H. Kuo, and T. H. Lin, "Comparison of the NDVI, ARVI and AFRI Vegetation Index, Along with Their Relations with the AOD Using SPOT 4 Vegetation Data.," *Terrestrial, Atmospheric and Oceanic Sciences*, vol. 15, no. 1, Mar. 2004.
- [19] J. Rouse, R. Haas, J. Schell, and D. Deering, "Monitoring vegetation systems in the Great Plains with ERTS," in *NASA Goddard Space Flight Center 3d ERTS-1 Symposium*, 1974, pp. 309–317.
- [20] C. F. Jordan, "Derivation of Leaf-Area Index from Quality of Light on the Forest Floor," *Ecology*, vol. 50, no. 4, pp. 663–666, Jul. 1969.
- [21] A. R. Huete, "A soil-adjusted vegetation index (SAVI)," *Remote Sensing of Environment*, vol. 25, no. 3, pp. 295–309, 1988.
- [22] G. A. Carter, W. G. Cibula, and T. R. Dell, "Spectral reflectance characteristics and digital imagery of a pine needle blight in the southeastern United States," *Can. J. For. Res.*, vol. 26, no. 3, pp. 402–407, Mar. 1996.
- [23] J. E. Vogelmann, B. N. Rock, and D. M. Moss, "Red edge spectral measurements from sugar maple leaves," *International Journal of Remote Sensing*, vol. 14, no. 8, pp. 1563–1575, 1993.
- [24] A. A. Gitelson and M. N. Merzlyak, "Remote estimation of chlorophyll content in higher plant leaves," *International Journal of Remote Sensing*, vol. 18, no. 12, pp. 2691–2697, Aug. 1997.
- [25] N. H. Broge and E. Leblanc, "Comparing prediction power and stability of broadband and hyperspectral vegetation indices for estimation of green leaf area index and canopy chlorophyll density," *Remote Sensing of Environment*, vol. 76, no. 2, pp. 156–172, 2001.
- [26] C. S. T. Daughtry, C. L. Walthall, M. S. Kim, E. B. De Colstoun, and J. E. McMurtrey Iii, "Estimating corn leaf chlorophyll concentration from leaf and canopy reflectance," *Remote Sensing of Environment*, vol. 74, no. 2, pp. 229–239, 2000.
- [27] B. Gao, "NDWI—A normalized difference water index for remote sensing of vegetation liquid water from space," *Remote Sensing of Environment*, vol. 58, no. 3, pp. 257–266, Dec. 1996.

- [28] Y. Zha, J. Gao, and S. Ni, "Use of normalized difference built-up index in automatically mapping urban areas from TM imagery," *International Journal of Remote Sensing*, vol. 24, no. 3, pp. 583–594, Jan. 2003.
- [29] R. W. Sidjak and R. D. Wheate, "Glacier mapping of the Illecillewaet icefield, British Columbia, Canada, using Landsat TM and digital elevation data," *International Journal of Remote Sensing*, vol. 20, no. 2, pp. 273–284, 1999.
- [30] P. S. Thenkabail, I. Mariotto, M. K. Gumma, E. M. Middleton, D. R. Landis, and K. F. Huemmrich, "Selection of Hyperspectral Narrowbands (HNBS) and Composition of Hyperspectral Twoband Vegetation Indices (HVIs) for Biophysical Characterization and Discrimination of Crop Types Using Field Reflectance and Hyperion/EO-1 Data," *IEEE Journal of Selected Topics in Applied Earth Observations and Remote Sensing*, vol. 6, no. 2, pp. 427–439, Apr. 2013.
- [31] D. Wong, "Spatial Indices of Segregation," *Urban Studies*, vol. 30, no. 3, pp. 559–572, Apr. 1993.
- [32] R. M. Haralick, K. Shanmugam, and I. Dinstein, "Textural Features for Image Classification," *IEEE Transactions on Systems, Man and Cybernetics*, vol. SMC-3, no. 6, pp. 610–621, 1973.
- [33] J. E. Estes, E. J. Hajic, and L. R. Tinney, "Fundamentals of image analysis: Analysis of visible and thermal infrared data," *Manual of Remote Sensing*, vol. 1, pp. 987–1124, 1983.
- [34] M. Herold, X. Liu, and K. C. Clarke, "Spatial metrics and image texture for mapping urban land use," *Photogrammetric Engineering and Remote Sensing*, vol. 69, no. 9, pp. 991–1002, 2003.
- [35] B. Datt, T. R. McVicar, T. G. Van Niel, D. L. B. Jupp, and J. S. Pearlman, "Preprocessing eo-1 hyperion hyperspectral data to support the application of agricultural indexes," *IEEE Transactions on Geoscience and Remote Sensing*, vol. 41, no. 6, pp. 1246–1259, Jun. 2003.
- [36] C. Rodarmel and J. Shan, "Principal component analysis for hyperspectral image classification," *Surveying and Land Information Science*, vol. 62, no. 2, pp. 115–122, 2002.
- [37] K. Barott, J. Smith, E. Dinsdale, M. Hatay, S. Sandin, and F. Rohwer, "Hyperspectral and Physiological Analyses of Coral-Algal Interactions," *PLoS ONE*, vol. 4, no. 11, p. e8043, Nov. 2009.
- [38] G. Vane and A. F. Goetz, "Terrestrial imaging spectroscopy," *Remote Sensing of Environment*, vol. 24, no. 1, pp. 1–29, 1988.
- [39] A. F. H. Goetz, G. Vane, J. E. Solomon, and B. N. Rock, "Imaging Spectrometry for Earth Remote Sensing," *Science*, vol. 228, no. 4704, pp. 1147–1153, Jun. 1985.
- [40] G. Vane, "First Results From The Airborne Visible/Infrared Imaging Spectrometer (AVIRIS)," in *Proc. SPIE, Imaging Spectroscopy II*, San Diego, CA, 1987, vol. 0834, pp. 166–175.
- [41] T. G. Chrien, R. O. Green, and M. L. Eastwood, "Accuracy of the spectral and radiometric laboratory calibration of the Airborne Visible/Infrared Imaging Spectrometer," in *Proc. SPIE, Imaging Spectroscopy of the Terrestrial Environment*, Orlando, FL, 1990, vol. 1298, pp. 37–49.

- [42] S. K. Babey and C. D. Anger, "Compact airborne spectrographic imager (CASI): a progress review," in *Proc. SPIE, Imaging Spectrometry of the Terrestrial Environment*, Orlando, FL, 1993, vol. 1937, pp. 152–163.
- [43] S.-H. Chang, M. J. Westfield, F. Lehmann, D. Oertel, and R. Richter, "79-channel airborne imaging spectrometer," in *Proc. SPIE, Imaging Spectrometry of the Terrestrial Environment*, Orlando, FL, 1993, vol. 1937, pp. 164–172.
- [44] K. I. Itten, F. Dell'Endice, A. Hueni, M. Kneubühler, D. Schläpfer, D. Odermatt, F. Seidel, S. Huber, J. Schopfer, T. Kellenberger, Y. Bühler, P. D'Odorico, J. Nieke, E. Alberti, and K. Meuleman, "APEX - the Hyperspectral ESA Airborne Prism Experiment," *Sensors*, vol. 8, no. 10, pp. 6235–6259, Oct. 2008.
- [45] M. Jehle, A. Hueni, A. Damm, P. D'Odorico, J. Weyermann, M. Kneubühler, D. Schläpfer, M. E. Schaepman, and K. Meuleman, "APEX-current status, performance and validation concept," in *Sensors*, 2010, pp. 533–537.
- [46] F. A. Kruse, J. W. Boardman, and J. F. Huntington, "Comparison of airborne hyperspectral data and eo-1 hyperion for mineral mapping," *IEEE Transactions on Geoscience and Remote Sensing*, vol. 41, no. 6, pp. 1388–1400, Jun. 2003.
- [47] C. Kratt, M. F. Coolbaugh, B. Peppin, and C. Sladek, "Identification of a New Blind Geothermal System with Hyperspectral Remote Sensing and Shallow Temperature Measurements at Columbus Salt Marsh, Esmeralda County, Nevada," presented at the Geothermal Resources Council Annual Meeting, Reno, Nevada, 2009, pp. 481–485.
- [48] M. Herold and D. A. Roberts, "Mapping Asphalt Road Conditions with Hyperspectral Remote Sensing," in *5th International Symposium Remote Sensing of Urban Areas (URS 2005)*, Tempe, AZ, 2005.
- [49] Y. Zhang, J. M. Chen, J. R. Miller, and T. L. Noland, "Leaf chlorophyll content retrieval from airborne hyperspectral remote sensing imagery," *Remote Sensing of Environment*, vol. 112, no. 7, pp. 3234–3247, Jul. 2008.
- [50] S. Jacquemoud and F. Baret, "PROSPECT: A model of leaf optical properties spectra," *Remote Sensing of Environment*, vol. 34, no. 2, pp. 75–91, 1990.
- [51] S. Lu, Y. Shimizu, J. Ishii, I. Washitani, and K. Omasa, "Identification of invasive vegetation using hyperspectral imagery in the shore of the Kinu River, Japan," *Journal of Agricultural Meteorology*, vol. 67, no. 2, pp. 85–88, 2011.
- [52] N. M. Knox, A. K. Skidmore, H. M. A. van der Werff, T. A. Groen, W. F. de Boer, H. H. T. Prins, E. Kohi, and M. Peel, "Differentiation of plant age in grasses using remote sensing," *International Journal of Applied Earth Observation and Geoinformation*, vol. 24, pp. 54–62, Oct. 2013.
- [53] A. Nakazawa, J.-H. Kim, T. Mitani, S. Odagawa, T. Takeda, C. Kobayashi, and O. Kashimura, "A study on detecting the poppy field using hyperspectral remote sensing techniques," presented at the International Geoscience and Remote Sensing Symposium (IGARSS), 2012, pp. 4829–4832.
- [54] United Nations Office on Drugs and Crime (UNODC), "Afghanistan Opium Survey, 2011," United Nations, 2011.

- [55] J. Pontius, M. Martin, L. Plourde, and R. Hallett, "Ash decline assessment in emerald ash borer-infested regions: A test of tree-level, hyperspectral technologies," *Remote Sensing of Environment*, vol. 112, no. 5, pp. 2665–2676, May 2008.
- [56] J. M. Van Campenhout, "On the peaking of the Hughes mean recognition accuracy: the resolution of an apparent paradox," *IEEE Transactions on Systems, Man and Cybernetics*, vol. 8, no. 5, pp. 390–395, 1978.
- [57] S. Kaewpijit, J. Le-Moigne, and T. El-Ghazawi, "Automatic reduction of hyperspectral imagery using wavelet spectral analysis," *IEEE Transactions on Geoscience and Remote Sensing*, vol. 41, no. 4, pp. 863–871, 2003.
- [58] R. H. Yuhas, A. F. H. Goetz, and J. W. Boardman, "Discrimination among semi-arid landscape endmembers using the spectral angle mapper (SAM) algorithm," in *Summaries of the Third annual JPL Airborne Geoscience workshop*, Pasadena, California, 1992, vol. 1, pp. 147–149.
- [59] A. R. Gillespie, M. O. Smith, J. B. Adams, S. C. Willis, A. F. Fischer III, and D. E. Sabol, "Interpretation of residual images: Spectral Mixture Analysis of AVIRIS images, Owen Valley, California," in *Proc. 2nd AVIRIS Workshop*, 1990, pp. 243–270.
- [60] S. T. Roweis and L. K. Saul, "Nonlinear Dimensionality Reduction by Locally Linear Embedding," *Science*, vol. 290, no. 5500, pp. 2323–2326, Dec. 2000.
- [61] L. K. Saul and S. T. Roweis, "Think Globally, Fit Locally: Unsupervised Learning of Low Dimensional Manifolds," *Journal of Machine Learning Research*, vol. 4, pp. 119–155, Dec. 2003.
- [62] M. Belkin and P. Niyogi, "Laplacian Eigenmaps for Dimensionality Reduction and Data Representation," *Neural Computation*, vol. 15, no. 6, pp. 1373–1396, Jun. 2003.
- [63] A. Jain and D. Zongker, "Feature selection: Evaluation, application, and small sample performance," *IEEE Transactions on Pattern Analysis and Machine Intelligence*, vol. 19, no. 2, pp. 153–158, 1997.
- [64] A. K. Jain and B. Chandrasekaran, "39 Dimensionality and sample size considerations in pattern recognition practice," in *Handbook of Statistics*, vol. Volume 2, P.R. Krishnaiah and L.N. Kanal, Ed. Elsevier, 1982, pp. 835–855.
- [65] A. K. Jain, R. P. W. Duin, and J. Mao, "Statistical pattern recognition: A review," *IEEE Transactions on Pattern Analysis and Machine Intelligence*, vol. 22, no. 1, pp. 4–37, 2000.
- [66] R. Kohavi and G. H. John, "Wrappers for feature subset selection," *Artificial Intelligence*, vol. 97, no. 1, pp. 273–324, 1997.
- [67] K. Khoshelham and S. O. Elberink, "Role of Dimensionality Reduction in Segment-Based Classification of Damaged Building Roofs in Airborne Laser Scanning Data," presented at the 4th GEOBIA, Rio de Janeiro, Brazil, 2012.
- [68] A. G. Janeczek and W. N. Gansterer, "A comparison of classification accuracy achieved with wrappers, filters and PCA," in *Workshop on New Challenges for Feature Selection in Data Mining and Knowledge Discovery*, 2008.

- [69] J. R. Jensen, "Biophysical remote sensing," *Annals of the Association of American Geographers*, vol. 73, no. 1, pp. 111–132, 1983.
- [70] P. R. Wolf and B. A. Dewitt, *Elements of Photogrammetry: with applications in GIS*. Boston: McGraw-Hill, 2000.
- [71] R. D. Jackson and A. R. Huete, "Interpreting vegetation indices," *Preventive Veterinary Medicine*, vol. 11, no. 3, pp. 185–200, 1991.
- [72] S. W. Todd and R. M. Hoffer, "Responses of spectral indices to variations in vegetation cover and soil background," *Photogrammetric Engineering and Remote Sensing*, vol. 64, pp. 915–922, 1998.
- [73] J.-L. Roujean and F.-M. Breon, "Estimating PAR absorbed by vegetation from bidirectional reflectance measurements," *Remote Sensing of Environment*, vol. 51, no. 3, pp. 375–384, 1995.
- [74] J. D. Barnes, L. Balaguer, E. Manrique, S. Elvira, and A. W. Davison, "A reappraisal of the use of DMSO for the extraction and determination of chlorophylls *a* and *b* in lichens and higher plants," *Environmental and Experimental Botany*, vol. 32, no. 2, pp. 85–100, 1992.
- [75] J. A. Gamon, J. Penuelas, and C. B. Field, "A narrow-waveband spectral index that tracks diurnal changes in photosynthetic efficiency," *Remote Sensing of Environment*, vol. 41, no. 1, pp. 35–44, 1992.
- [76] J. Peñuelas, J. A. Gamon, A. L. Fredeen, J. Merino, and C. B. Field, "Reflectance indices associated with physiological changes in nitrogen-and water-limited sunflower leaves," *Remote Sensing of Environment*, vol. 48, no. 2, pp. 135–146, 1994.
- [77] H. K. Lichtenthaler, M. Lang, M. Sowinska, F. Heisel, and J. A. Miede, "Detection of vegetation stress via a new high resolution fluorescence imaging system," *Journal of Plant Physiology*, vol. 148, no. 5, pp. 599–612, 1996.
- [78] J. Peñuelas, I. Filella, P. Lloret, F. Muñoz, and M. Vilajeliu, "Reflectance assessment of mite effects on apple trees," *International Journal of Remote Sensing*, vol. 16, no. 14, pp. 2727–2733, 1995.
- [79] J. Qi, A. Chehbouni, A. R. Huete, Y. H. Kerr, and S. Sorooshian, "A modified soil adjusted vegetation index," *Remote Sensing of Environment*, vol. 48, no. 2, pp. 119–126, 1994.
- [80] C. D. Elvidge and Z. Chen, "Comparison of broad-band and narrow-band red and near-infrared vegetation indices," *Remote Sensing of Environment*, vol. 54, no. 1, pp. 38–48, 1995.
- [81] C. J. Tucker, "Red and photographic infrared linear combinations for monitoring vegetation," *Remote Sensing of Environment*, vol. 8, no. 2, pp. 127–150, May 1979.
- [82] A. J. Richardson and C. L. Weigand, "Distinguishing Vegetation from Soil Background Information," *Photogrammetric Engineering and Remote Sensing*, vol. 43, no. 12, pp. 1541–1552, Dec. 1977.
- [83] F. Baret, G. Guyot, and D. J. Major, "TSAVI: A Vegetation Index Which Minimizes Soil Brightness Effects On LAI And APAR Estimation," in *Geoscience and Remote Sensing Symposium, 1989. IGARSS'89. 12th Canadian Symposium on Remote Sensing, 1989 International*, 1989, vol. 3, pp. 1355–1358.

- [84] M. S. Kim, "The Use of Narrow Spectral Bands for Improving Remote Sensing Estimation of Fractionally Absorbed Photosynthetically Active Radiation (fAPAR)," Masters, Department of Geography, University of Maryland, College Park, MD, 1994.
- [85] W. Verhoef, "Light scattering by leaf layers with application to canopy reflectance modeling: The SAIL model," *Remote Sensing of Environment*, vol. 16, no. 2, pp. 125–141, Oct. 1984.
- [86] P. J. Zarco-Tejada, J. R. Miller, T. L. Noland, G. H. Mohammed, and P. H. Sampson, "Scaling-up and model inversion methods with narrowband optical indices for chlorophyll content estimation in closed forest canopies with hyperspectral data," *IEEE Transactions on Geoscience and Remote Sensing*, vol. 39, no. 7, pp. 1491–1507, 2001.
- [87] A. Hall, D. W. Lamb, B. Holzapfel, and J. Louis, "Optical remote sensing applications in viticulture - a review," *Australian Journal of Grape and Wine Research*, vol. 8, no. 1, pp. 36–47, 2002.
- [88] D. Haboudane, J. R. Miller, N. Tremblay, P. J. Zarco-Tejada, and L. Dextraze, "Integrated narrow-band vegetation indices for prediction of crop chlorophyll content for application to precision agriculture," *Remote Sensing of Environment*, vol. 81, no. 2, pp. 416–426, Aug. 2002.
- [89] G. Rondeaux, M. Steven, and F. Baret, "Optimization of soil-adjusted vegetation indices," *Remote Sensing of Environment*, vol. 55, no. 2, pp. 95–107, 1996.
- [90] G. A. Carter, "Ratios of leaf reflectances in narrow wavebands as indicators of plant stress," *International Journal of Remote Sensing*, vol. 15, no. 3, pp. 697–703, 1994.
- [91] J. M. Chen, "Evaluation of vegetation indices and a modified simple ratio for boreal applications," *Canadian Journal of Remote Sensing*, vol. 22, no. 3, pp. 229–242, 1996.
- [92] A. A. Gitelson, Y. Zur, O. B. Chivkunova, and M. N. Merzlyak, "Assessing carotenoid content in plant leaves with reflectance spectroscopy," *Photochem. Photobiol.*, vol. 75, no. 3, pp. 272–281, Mar. 2002.
- [93] M. A. Cho and A. K. Skidmore, "Hyperspectral predictors for monitoring biomass production in Mediterranean mountain grasslands: Majella National Park, Italy," *International Journal of Remote Sensing*, vol. 30, no. 2, pp. 499–515, Jan. 2009.
- [94] M. M. Verstraete and B. Pinty, "Designing optimal spectral indexes for remote sensing applications," *IEEE Transactions on Geoscience and Remote Sensing*, vol. 34, no. 5, pp. 1254–1265, 1996.
- [95] F. Jiang, S. Liu, H. Yuan, and Q. Zhang, "Measuring urban sprawl in Beijing with geo-spatial indices," *Journal of Geographical Sciences*, vol. 17, no. 4, pp. 469–478, Oct. 2007.
- [96] S. Berberoglu and P. J. Curran, "Merging Spectral and Textural Information for Classifying Remotely Sensed Images," in *Remote Sensing Image Analysis: Including The Spatial Domain*, S. M. D. Jong and F. D. V. der Meer, Eds. Springer Netherlands, 2004, pp. 113–136.
- [97] J. R. Jensen, *Introductory Digital Image Processing: A Remote Sensing Perspective.*, 2nd ed. Prentice Hall, 1996.

- [98] D. A. Clausi, "An analysis of co-occurrence texture statistics as a function of grey level quantization," *Canadian Journal of Remote Sensing*, vol. 28, no. 1, pp. 45–62, 2002.
- [99] F. Wang, "Fuzzy supervised classification of remote sensing images," *IEEE Transactions on Geoscience and Remote Sensing*, vol. 28, no. 2, pp. 194–201, 1990.
- [100] G. M. Foody, N. A. Campbell, N. M. Trodd, and T. F. Wood, "Derivation and applications of probabilistic measures of class membership from the maximum-likelihood classification," *Photogrammetric Engineering and Remote Sensing*, vol. 58, no. 9, pp. 1335–1341, 1992.
- [101] G. M. Foody, "Sub-Pixel Methods in Remote Sensing," in *Remote Sensing Image Analysis: Including The Spatial Domain*, S. M. D. Jong and F. D. V. der Meer, Eds. Springer Netherlands, 2004, pp. 37–49.
- [102] J. R. G. Townshend, "Land cover," *International Journal of Remote Sensing*, vol. 13, no. 6–7, pp. 1319–1328, 1992.
- [103] J. R. Eastman and R. M. Laney, "Bayesian soft classification for sub-pixel analysis: A critical evaluation," *Photogrammetric Engineering and Remote Sensing*, vol. 68, no. 11, pp. 1149–1154, Nov. 2002.
- [104] J. J. Settle and N. A. Drake, "Linear mixing and the estimation of ground cover proportions," *International Journal of Remote Sensing*, vol. 14, no. 6, pp. 1159–1177, 1993.
- [105] R. Krishnapuram and J. M. Keller, "A possibilistic approach to clustering," *IEEE Transactions on Fuzzy Systems*, vol. 1, no. 2, pp. 98–110, 1993.
- [106] A. Kumar and V. K. Dadhwal, "Entropy-based fuzzy classification parameter optimization using uncertainty variation across spatial resolution," *Journal of the Indian Society of Remote Sensing*, vol. 38, no. 2, pp. 179–192, 2010.
- [107] R. Krishnapuram and J. M. Keller, "The possibilistic c-means algorithm: insights and recommendations," *IEEE Transactions on Fuzzy Systems*, vol. 4, no. 3, pp. 385–393, 1996.
- [108] G. M. Foody, "Estimation of sub-pixel land cover composition in the presence of untrained classes," *Computers & Geosciences*, vol. 26, no. 4, pp. 469–478, May 2000.
- [109] L. Bastin, "Comparison of fuzzy c-means classification, linear mixture modelling and MLC probabilities as tools for unmixing coarse pixels," *International Journal of Remote Sensing*, vol. 18, no. 17, pp. 3629–3648, Nov. 1997.
- [110] H. Dehghan and H. Ghassemian, "Measurement of uncertainty by the entropy: application to the classification of MSS data," *International Journal of Remote Sensing*, vol. 27, no. 18, pp. 4005–4014, Sep. 2006.
- [111] G. M. Foody and P. M. Atkinson, Eds., *Uncertainty in Remote Sensing and GIS*. John Wiley & Sons, Ltd, 2002.
- [112] F. Maselli, C. Conese, and L. Petkov, "Use of probability entropy for the estimation and graphical representation of the accuracy of maximum likelihood classifications," *ISPRS Journal of Photogrammetry and Remote Sensing*, vol. 49, no. 2, pp. 13–20, 1994.

- [113] E. Binaghi, P. A. Brivio, P. Ghezzi, and A. Rampini, "A fuzzy set-based accuracy assessment of soft classification," *Pattern Recognition Letters*, vol. 20, no. 9, pp. 935–948, 1999.
- [114] G. M. Foody, "Cross-entropy for the evaluation of the accuracy of a fuzzy land cover classification with fuzzy ground data," *ISPRS Journal of Photogrammetry and Remote Sensing*, vol. 50, no. 5, pp. 2–12, 1995.
- [115] D. Schlapfer, M. Schaepman, S. Bojinski, and A. Borner, "Calibration and validation concept for the airborne prism experiment (APEX)," *Canadian Journal of Remote Sensing*, vol. 26, no. 5, pp. 455–465, 2000.
- [116] A. Hueni, J. Biesemans, K. Meuleman, F. Dell'Endice, D. Schlapfer, D. Odermatt, M. Kneubuehler, S. Adriaensen, S. Kempenaers, J. Nieke, and K. I. Itten, "Structure, Components, and Interfaces of the Airborne Prism Experiment (APEX) Processing and Archiving Facility," *IEEE Transactions on Geoscience and Remote Sensing*, vol. 47, no. 1, pp. 29–43, Jan. 2009.
- [117] J. Nieke, K. I. Itten, W. Debruyne, and APEX Team, "The Airborne Imaging Spectrometer APEX: From Concept to Realization," in *4th EARSeL Workshop on Imaging Spectroscopy*, Warsaw, 2005, pp. 73–80.
- [118] C. Popp, D. Brunner, A. Damm, M. Van Roozendaal, C. Fayt, and B. Buchmann, "High-resolution NO₂ remote sensing from the Airborne Prism EXperiment (APEX) imaging spectrometer," *Atmospheric Measurement Techniques*, vol. 5, no. 9, pp. 2211–2225, 2012.
- [119] "APEX Open Science Data Set Leaflet." European Space Agency, 26-Jun-2011.
- [120] "APEX." [Online]. Available: <http://www.apex-esa.org/>. [Accessed: 19-Dec-2013].
- [121] A. Hueni, J. Nieke, J. Schopfer, M. Kneubühler, and K. I. Itten, "The spectral database SPECCHIO for improved long-term usability and data sharing," *Computers & Geosciences*, vol. 35, no. 3, pp. 557–565, Mar. 2009.
- [122] "SwissTopo Web Portal." [Online]. Available: <http://map.geo.admin.ch/?topic=ech&lang=en&X=257116.37&Y=664823.41&zoom=6&bgLayer=ch.swisstopo.swissimage>. [Accessed: 03-Mar-2014].
- [123] M. A. Cho and A. K. Skidmore, "A new technique for extracting the red edge position from hyperspectral data: The linear extrapolation method," *Remote Sensing of Environment*, vol. 101, no. 2, pp. 181–193, Mar. 2006.
- [124] J. C. Bezdek, R. Ehrlich, and W. Full, "FCM: The fuzzy c-means clustering algorithm," *Computers & Geosciences*, vol. 10, no. 2–3, pp. 191–203, 1984.
- [125] P. S. Thenkabail, R. B. Smith, and E. De Pauw, "Evaluation of narrowband and broadband vegetation indices for determining optimal hyperspectral wavebands for agricultural crop characterization," *Photogrammetric Engineering and Remote Sensing*, vol. 68, no. 6, pp. 607–622, 2002.
- [126] P. S. Thenkabail, R. B. Smith, and E. De Pauw, "Hyperspectral Vegetation Indices and Their Relationships with Agricultural Crop Characteristics," *Remote Sensing of Environment*, vol. 71, no. 2, pp. 158–182, Feb. 2000.

- [127] J. Peñuelas, I. Filella, C. Biel, L. Serrano, and R. Savé, “The reflectance at the 950–970 nm region as an indicator of plant water status,” *International Journal of Remote Sensing*, vol. 14, no. 10, pp. 1887–1905, 1993.

APPENDIX – A

APEX Sensor Parameters, OSD Detailed Description and Known Issues

Besides the information presented in Table 8-1, detailed information about the APEX sensor, its development and calibration, and other related information can be obtained in Itten *et al.*, 2008 [44]. Detailed calibration and validation concepts information are available in Schl pfer *et al.*, 2000 [115]. The structure, components and interfaces of the APEX data archiving facilities was described by Hueni *et al.*, 2009 [116]. The performance of the sensor, besides other aspects, was illustrated by Jehle *et al.*, 2010 [45].

The performance of the APEX system is very important in understanding its data acquisition method. The details are listed in the Table 8-1.

Table A-1: APEX Selected Performances. Source - [45]

APEX Performance		
Spectral Performance	<i>VNIR</i>	<i>SWIR</i>
Spectral Range	380.5 – 971.7 nm	941.2 – 2501.5 nm
Spectral Bands	Up to 334, def. 114	198
Spectral Sampling Interval	0.55 – 8 nm	5 – 10 nm
Spectral Resolution (FWHM)	0.6 – 6.3 nm	6.2 – 11 nm
Spatial Performance		
Spatial Pixels (across track)	1000	
FOV	28°	
IFOV	0.028° (~0.5 mrad)	
Spatial Sampling Interval (across track)	1.75 m @ 3500 m AGL	
Sensor Characteristics	<i>VNIR</i>	<i>SWIR</i>
Type	CCD	CMOS
Dynamic Range	14 bit	13 bit
Pixel Size	22.5 μm ± 22.5 μm	30 μm ± 30 μm
Smile	Average < 0.35 pixel	
Keystone (Frown)	Average < 0.35 pixel	
Co-registration	Average < 0.55 pixel	
Other Information		
Data Capacity	500 GB on SSD	
Data Transfer	Spectral frames: 30 MB/s, HK data: 20 kB/s	
Data Rate for default config.	0.4 GB/km (1250 km max.)	

APEX data is made available on the website after a series of pre-processing. The pre-processing performed with the RAW data, to make it available as a Level1 processed data, from the APEX sensor are [45], [119]:

- Dark Current Correction using linear dark current modelling per flight line.
- Radiometric correction.
- Bad Pixel replacement by spatial linear interpolation.
- Wire pixel replacement by spatial linear interpolation.
- Negative radiances, typically appearing in water vapour absorption bands, have been set to zero.
- Spatial mis-registration (frown) correction by linear resampling to common across track angles.
- Spatial co-registration of the VNIR and SWIR detector.
- Destriping.

The APEX system is experimental, therefore, some known issues prevail in the data even after pre-processing [119]:

- Residual along track striping;
- Residual across track striping;
- Interpolated wires;
- Image crispness;
- Radiometric artefacts;
- Saturated pixels;
- Directional effects;
- Low SWIR HCRF; detailed descriptions and information can be found in the APEX OSD Leaflet [119] and the official APEX website [120].

APPENDIX – B

Texture analysis

In this section, the additional textures calculated and analyzed during texture analysis are given and discussed. These textures were not considered due to inconclusive results obtained. The output of these textures created incoherent data, when applied on spectral indices. As the key criterion for using a texture as a spatial descriptor was that it could assist in extracting classes, the below statistics were not considered. These statistical measures of tonal distribution are also called GLCM (Grey Level Co-occurrence Matrix) [32].

$$Variance(\sigma_i^2) = \sum_{i,j=0}^{N-1} P_{i,j} (i - \mu_i)^2; Variance(\sigma_j^2) = \sum_{i,j=0}^{N-1} P_{i,j} (j - \mu_j)^2$$

Variance is a measure of the degree of dispersion of the values in the window, with respect to the mean and can be considered similar to Entropy measures.

$$Homogeneity = \sum_{i,j=0}^{N-1} \frac{P_{i,j}}{1 + (i - j)^2}$$

Homogeneity is a measure of the similarity in the pixel values in the neighbourhood window.

$$Contrast = \sum_{i,j=0}^{N-1} P_{i,j} (i - j)^2$$

An obvious converse of Homogeneity, Contrast is a measure of the local variation in an image or neighbourhood window.

$$Dissimilarity = \sum_{i,j=0}^{N-1} P_{i,j} |i - j|$$

Similar to Contrast, Dissimilarity outputs high values when contrast is high.

$$Correlation = \sum_{i,j=0}^{N-1} P_{i,j} \left[\frac{(i - \mu_i)(j - \mu_j)}{\sqrt{(\sigma_i^2)(\sigma_j^2)}} \right]$$

Correlation measures the linear dependency of grey levels of neighbouring pixels.

APPENDIX – C

Principal Component Analysis and Additional Classification Outputs

The input of 7PCs, optimally decided upon, yielded outputs of corresponding classes. The process of PCM classification led to the successful identification of some classes (Section 5.3), and the remaining are discussed here. The Figures depict the concerned class and its corresponding conflicting classes to understand the mis-classification.

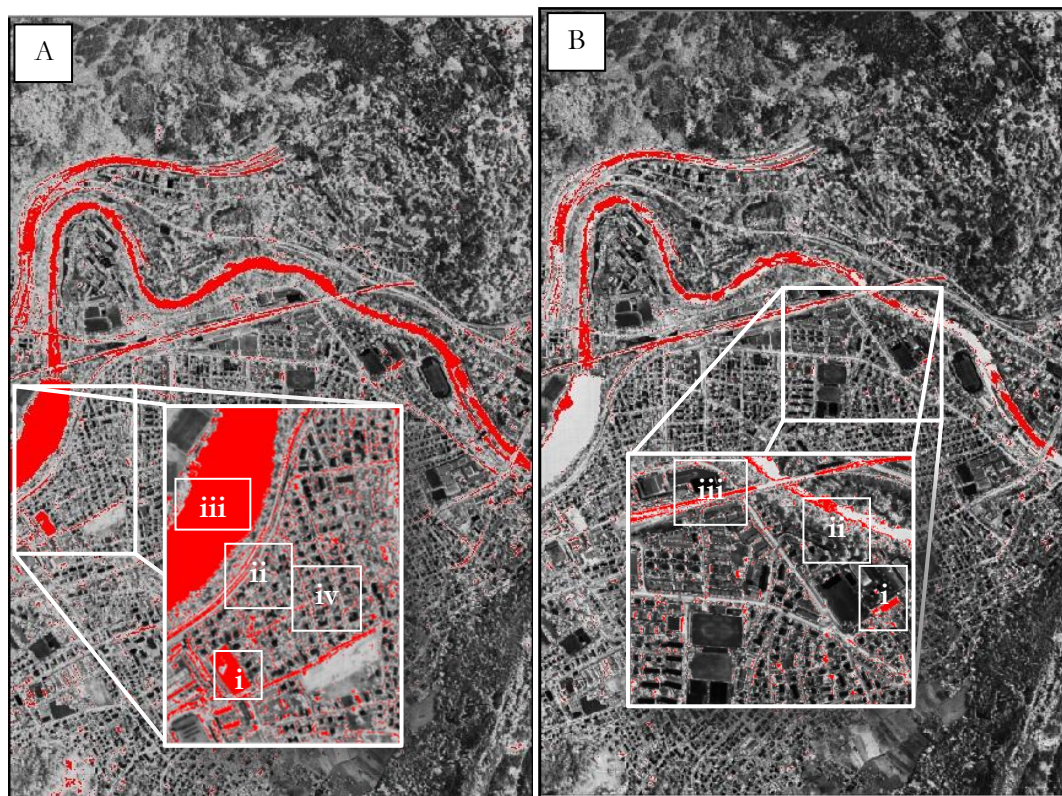


Figure C-1: Optimal PC input-classification – Artificial Turf (A); Black Roof (B)

The sole purpose of these results are to illustrate that the classification approach using PCM algorithm has failed to separate these classes while considering the PCA dimensionality reduction approach. Although these classes are not classified in their soft outputs, defuzzification allows for quantification of the approach. Figure C-1 (A) discusses the conflict of classes Artificial Turf (i), Railway (ii), Water (iii) and Roads (iv). Artificial Turf conflicts with the mentioned classes. Through analysis, it can be inferred that the 7PCs input is insufficient in defining a distinctive signature vector for these classes. The classification relies on the definition of adequate signature from the PCs input, for all the classes. Some classes like Sand, Black Roof, etc. occupy a very small spatial area, in comparison to the study area. Their distribution could be a factor in the misclassification of pixels belonging to these classes. Similarly, Fig. C-1 (B) illustrates a conflict between Black Roof (i), Water (ii) and Railway (iii) classes.

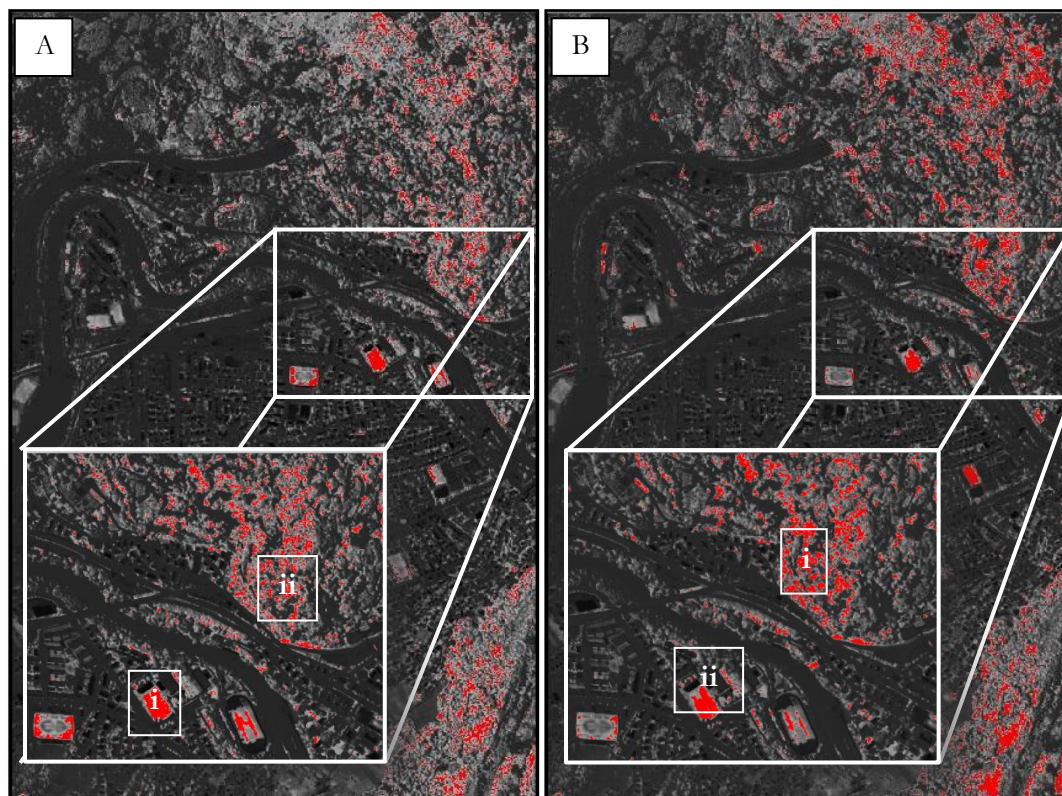


Figure C-2: Optimal PC input-classification – Grass (A); Mixed Deciduous Forest (B)

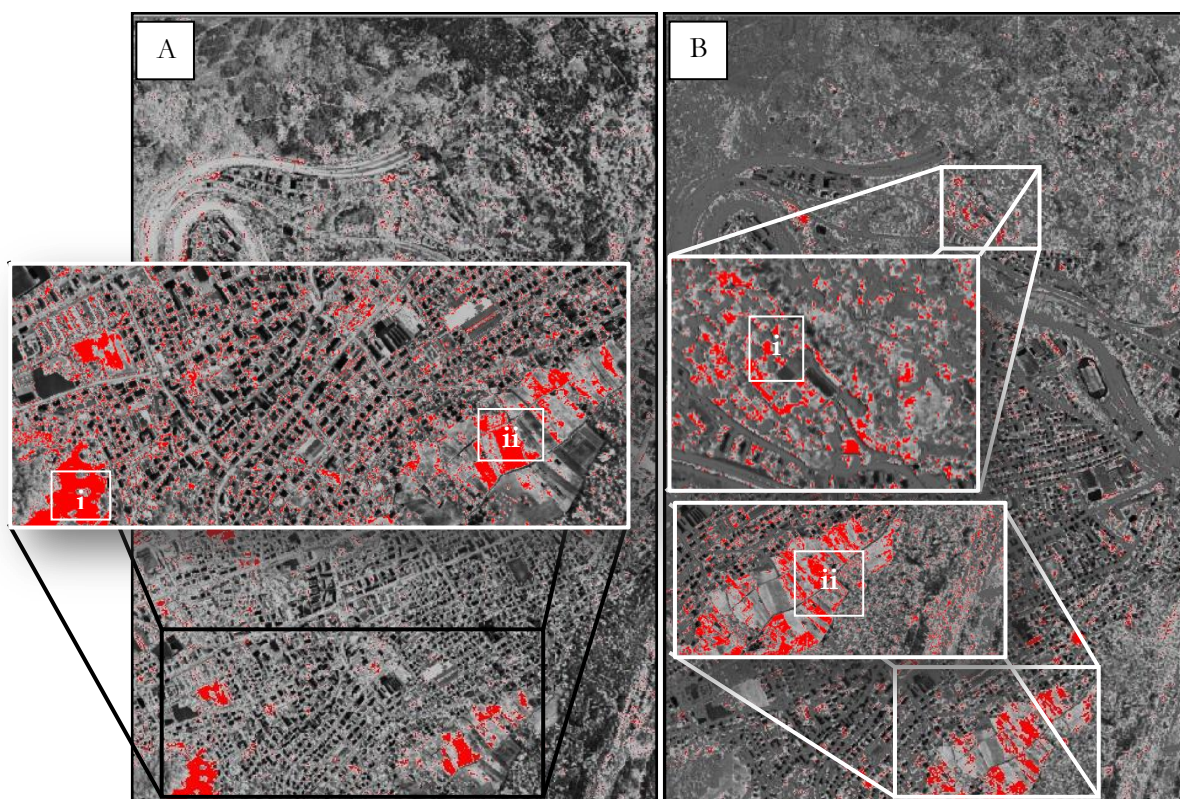


Figure C-3: Optimal PC input-classification – Pasture (A); Stressed Grass (B)

Both classes, Mixed Deciduous Forest and Grass, show similar spectral behaviour (Figure 4-2, 4-3), although the reflectance values are different. This implies that the classes cannot be

separately classified solely on the basis of spectral information. This inference is adequately supported by the classification accuracy results of Grass (Table 5-1). As indicated in Figure C-2 (A – Grass (i), Mixed Coniferous Forest (ii) and B – vice versa), both classes are identified in their respective PCM classification outputs.

Figure C-3 (A & B) is yet another illustration of spectral information being insufficient to differentiate between vegetation classes. As discussed previously and understood from their spectral curves (Figure 4-3), vegetation classes show similar properties in similar spectral ranges. When a simple dimensionality reduction approach is followed, the subsequent classification relies completely on spectral information, and therefore misclassification of these classes occurs. Figure C-3 A (Pastures (i) and Vineyards (ii)) and B (Stressed Grass (i) and Vineyard (ii)) depict the misclassification of these classes in the study area. The discussed classes of Stressed Grass and Pastures show low accuracy assessment values (UA – 30% and 40% respectively; Table 5-1), quantifying this misclassification.

The conflict of classification for Railway class (Figure C-4 – (i)) persists through all the approaches, indicating at the requirement of a different approach for classification. While considering the PCA approach, the class conflicts with Roads (ii) and Water (iii). As recommended, a different approach might be used to classify the Railway class.

Considering the urban nature of the study area, adequate numbers of roofs are encountered. Of the many, through ground truth consultation and verification, 3 types were considered for this study area i.e. Black Roof, Red Roof (Figure C-4 – B (ii)) and Roofs (Figure C-4 – B (i)).

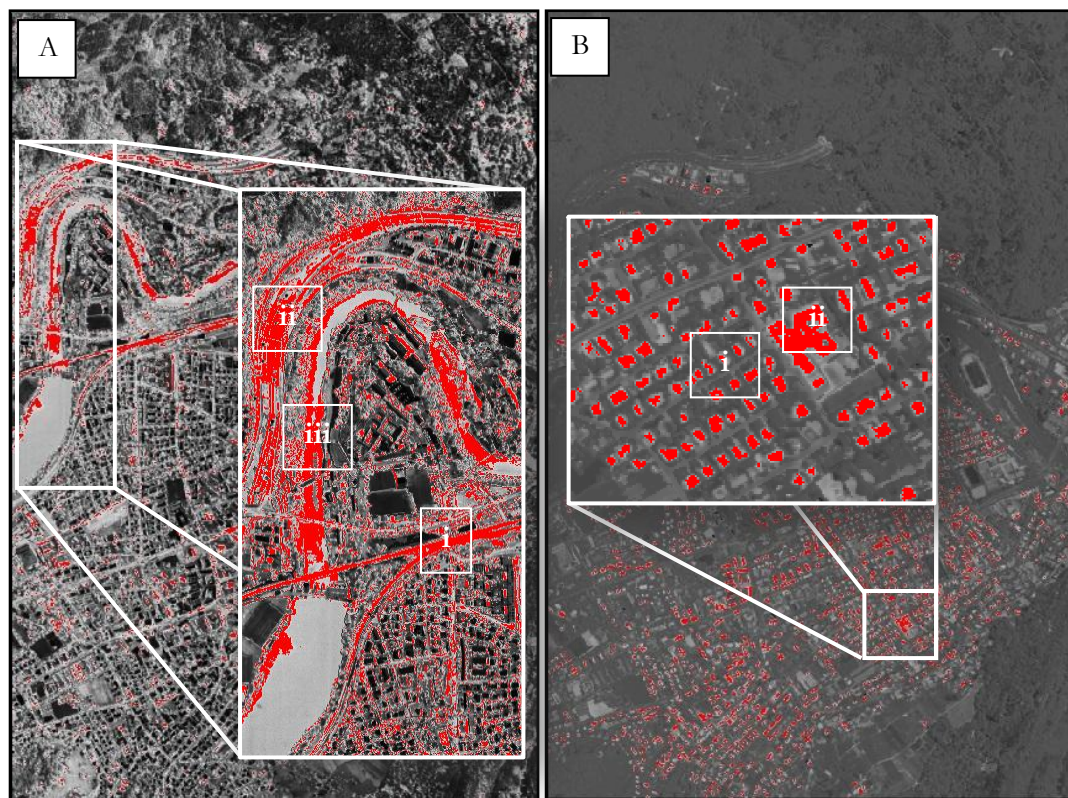


Figure C-4: Optimal PC input-classification – Railway (A); Roof (B)

Figure C-4 (B) illustrates the misclassification of Roof class, against Red Roofs. Red Roofs were accurately classified with a high UA (Table 5-1), while the conflicting class of Roofs' misclassification is quantified at a low 40% (UA).

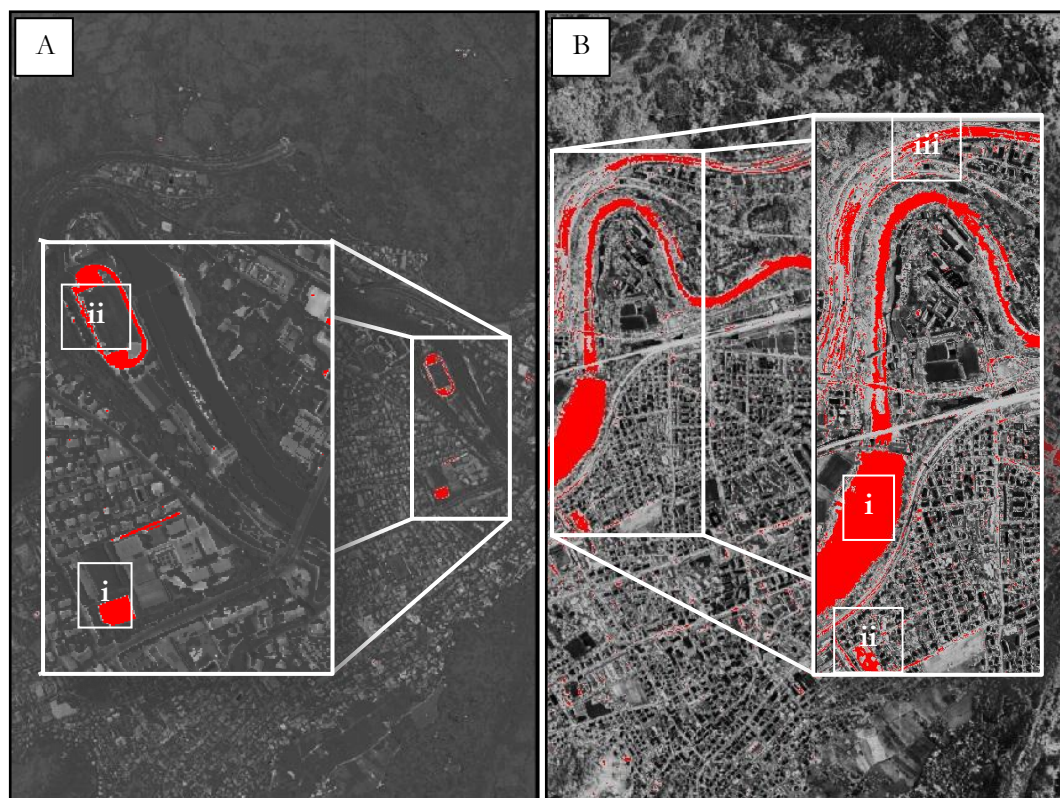


Figure C-5: Optimal PC input-classification – Synthetic Sports Surface (A); Water (B)

The classifier algorithm fails to differentiate between the classes Synthetic Sports Surface (i) and Yellow Tartan (ii), illustrated in Figure C-5 (A) while considering the soft classification approach. Defuzzification in this research is based on a simple, maximum value principle, and therefore, resultant output shows a high accuracy of this class's identification.

As shown previously in Figure C-1 (A & B) and C-4 (A), Water class conflicts with classification of multiple classes. The same case follows while considering the Water class output. However, like in the previous case of Synthetic Sports Surface, defuzzification results in high classification accuracy (UA) for this class the pixel carry the highest membership values, while locations of the conflicting classes have a lesser membership value.

Low classification accuracies characterize the Yellow Tartan class throughout the research, irrespective of the approach followed. This has been attributed to low spatial distribution of the class and inadequacy of indices (spectral or spatial) in describing the properties of the class. As illustrated, pixels of conflicting classes carry a membership value higher than the threshold, thereby describing misclassification in Figure C-6 (Yellow Tartan (i) and Synthetic Sports Surface (ii)).

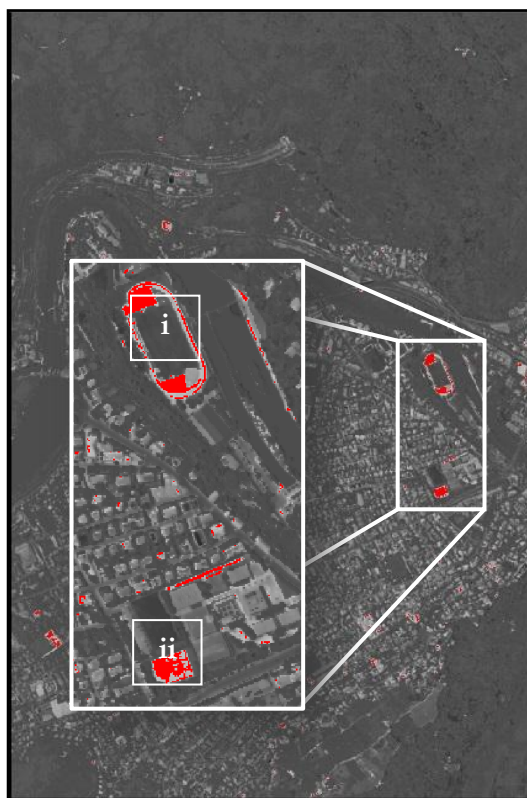


Figure C-6: Optimal PC input-classification – Yellow Tartan

APPENDIX – D

Additional Spectral Indices input database Classification Results

As the cases of misclassification while considering the PCs input was discussed in Appendix – C, here we discuss the dimensionality reduction approach of using spectral indices. The classification achieved was at a better accuracy of 65% (compared to 59.50% for optimal PCs input). The input database of features in this approach was of spectral indices corresponding to classes, hoping to best describe class information through these. Although an improvement was achieved and usage of spectral indices as input features was justified, a few classes still remained unclassified through PCM soft classification.

Classification accuracy for Black Roof (Figure D-1 (A)) reduces from the PCs input approach (Table 5-1, 5-2). The conflict of the classes above the threshold of membership values shows that Roads, Building and Sand classes conflict with the successful identification of Black Roof class. Similar conflict of class identification occurs in the case of Building (Figure D-1 (B-(i))) with Roads (Figure D-1 (B-(ii))).

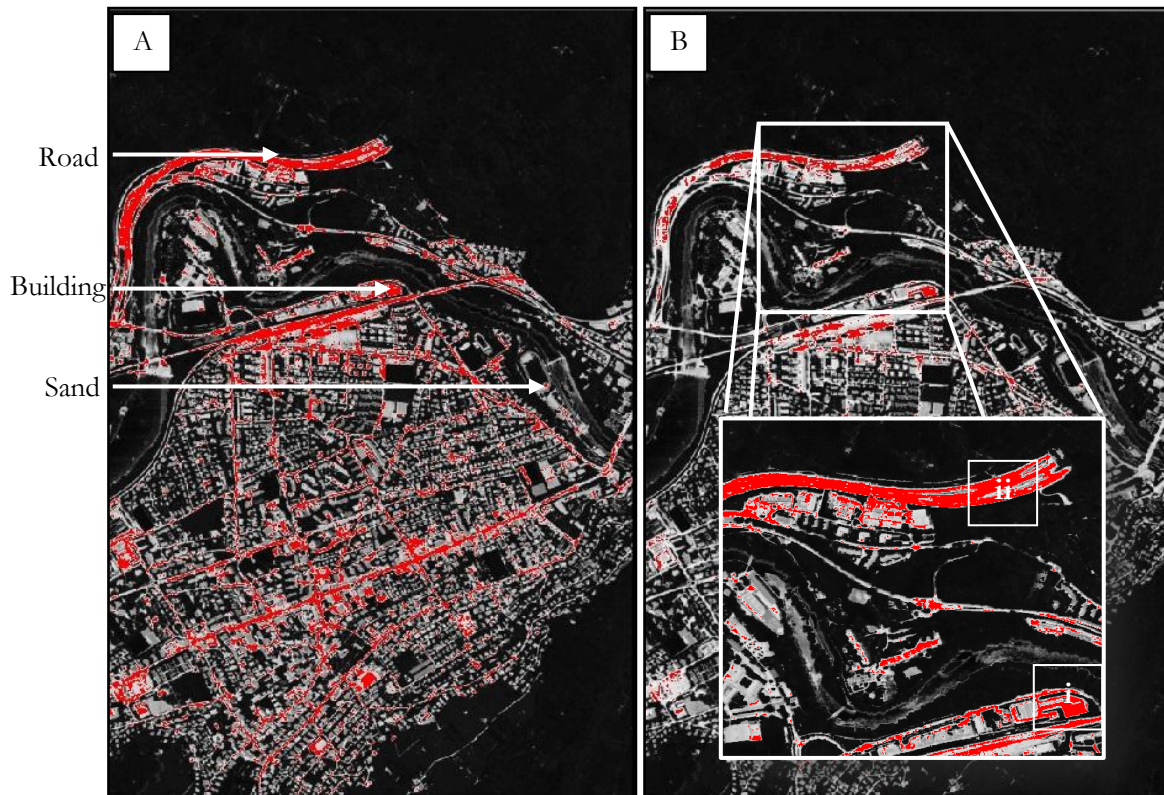


Figure D-1: Spectral indices input-classification – Black Roof (A); Buildings (B)

Conflict of classification of Grass (Figure D-2 (A (i))) persists with Mixed Deciduous Forests. Application of indices successfully classifies the two forest types in the study area (Figure 5-12), but the spectral information alone is not sufficient to differentiate Grass (evidence of similar spectral curve behaviour (Figure 4-2, 4-3)).

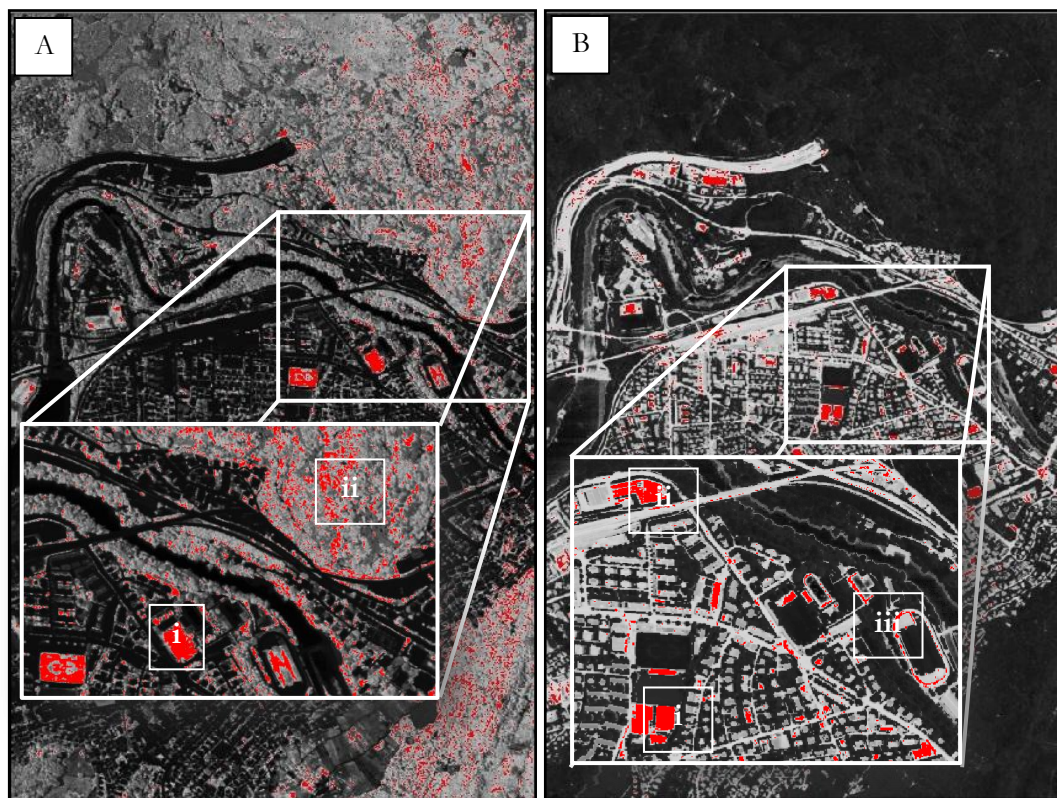


Figure D-2: Spectral indices input-classification – Grass (A); Lawn Tennis Court (B)

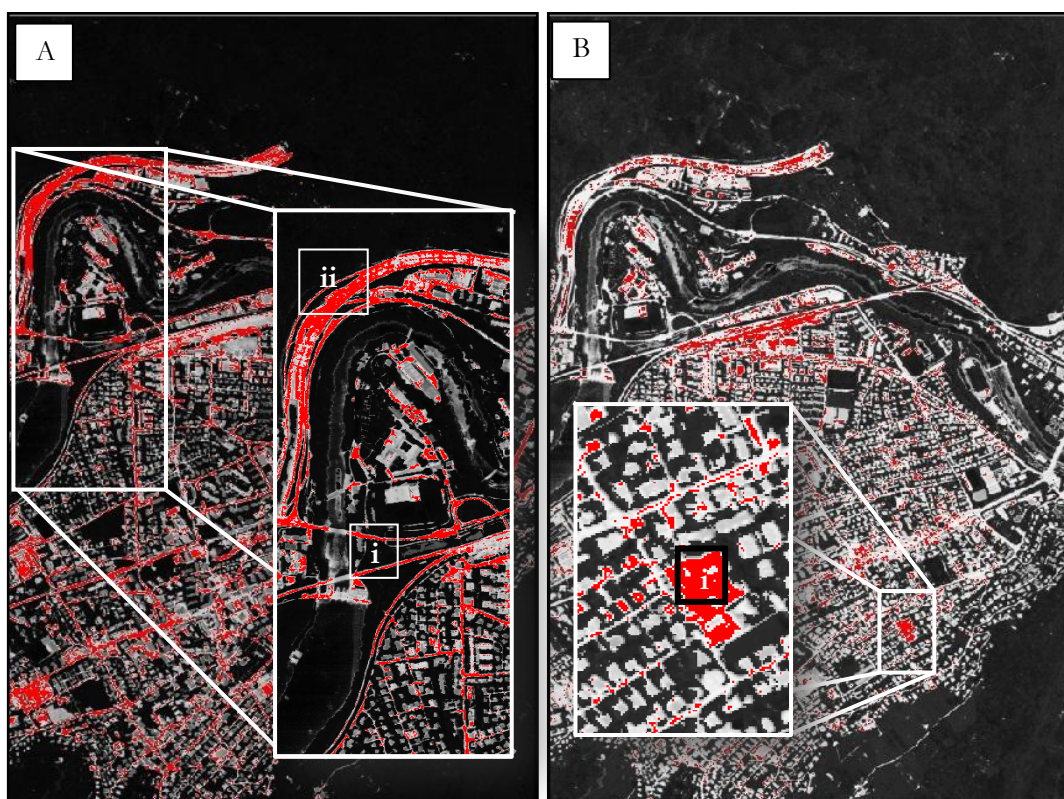


Figure D-3: Spectral indices input-classification – Railway (A); Red Roof (B)

Illustrated in Figure D-2 (B), Lawn Tennis Court (i) indicates a conflict of identification with Building class (ii) and Synthetic Sports Surface (iii). Similar spectral properties of these classes

illustrate a conflict even in the PCA dimensionality reduction approach. It is due to this conflict that the classes remain unclassified up until the 7-8PCs input feature database (Figure 5-1). Illustrated here is yet another example of spectral information being insufficient to separate these classes.

Similar spectral response curve behaviour of the sports surfaces in the study area create adequate amount of confusion in the classification approach. Note that between the bands considered as keys for Red Synthetic Ground (Table 4-2) index, these surfaces show similar spectral behaviour. Illustrated in Figure D-4 (A), these classes are misclassified while considering the spectral indices input for the classification. Figure 4-4 depicts the spectral curves of these classes. Similar conflict of class identification was also seen between Roads (Figure D-4 (B-(i))) and Railway (Figure D-4 (B-(ii))) classes. Both classes in Figure D-4 are however considered identified after defuzzification of the classification results with respectable accuracy measures (Figure 5-1).

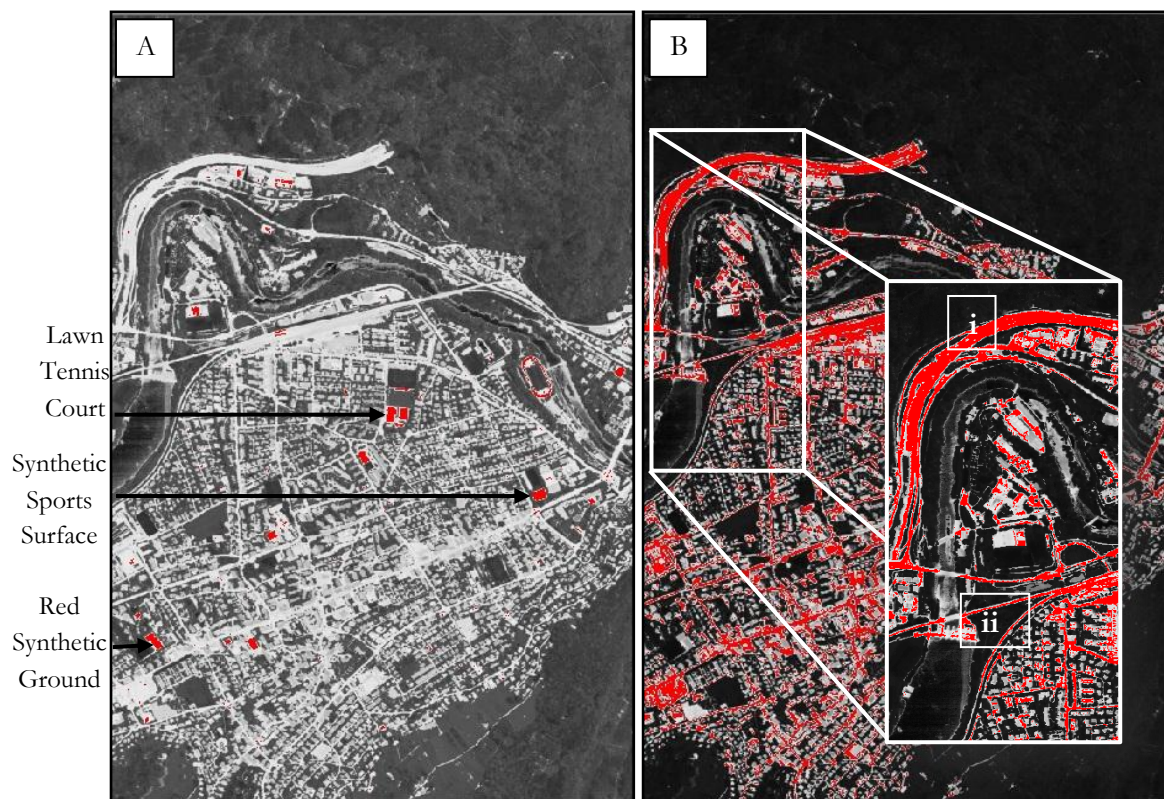


Figure D-4: Spectral indices input-classification – Red Synthetic Ground (A); Road (B)

Sand is yet another class whose misclassification has been attributed to similar spectral properties with other classes and lesser spatial distribution. Considering that the class has only a few pixels, information for training the classifier remains inadequate. This class might be some significance in other study areas, and applicability of an indices based approach could be researched in that situation. A similar understanding as that of Figure D-4 (A) is reiterated for Figure D-5 (B).

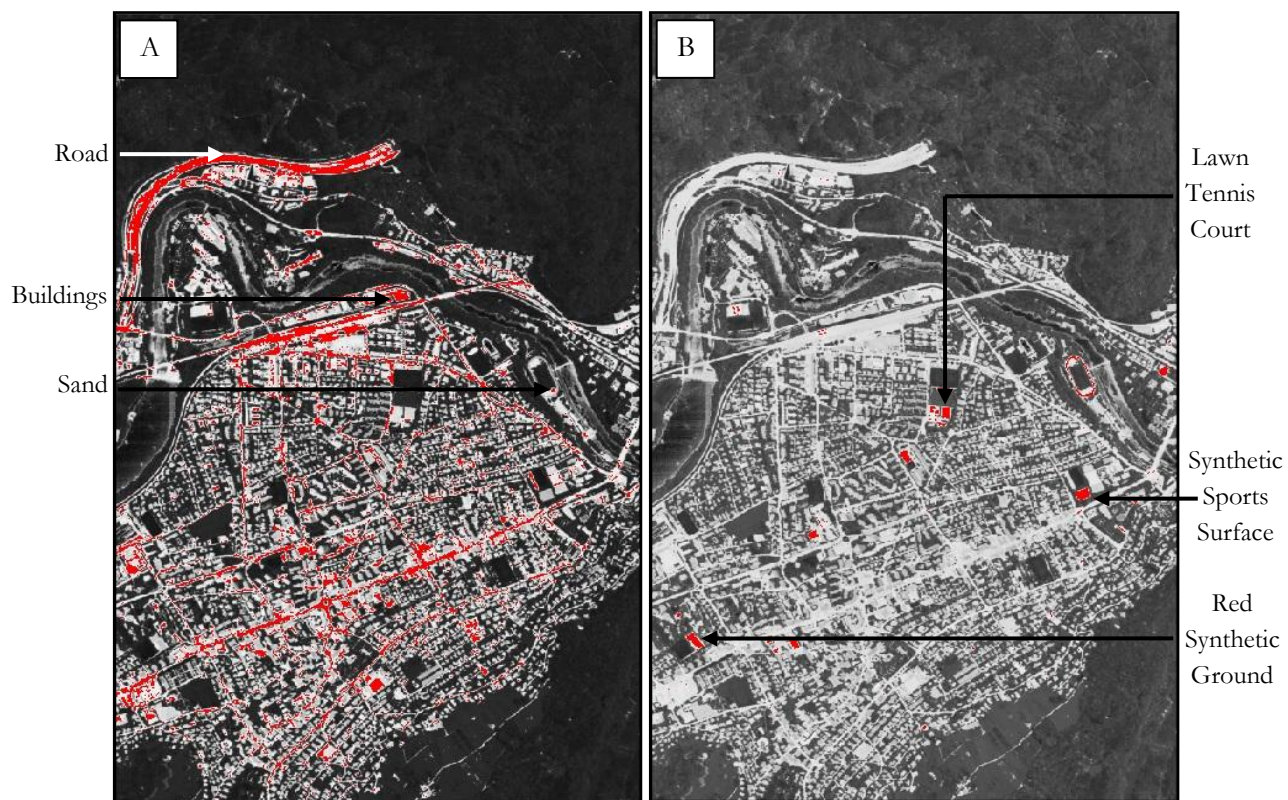


Figure D-5: Spectral indices input-classification – Sand (A); Synthetic Sports Surface (B)

APPENDIX – E

Additional Spectral-Spatial Indices input database Classification Results

The classification using spectral and spatial indices for exploiting the airborne hyperspectral data is the primary motivation of this research. Through the process, a specific combination of indices stands out. Roofs occupy a significant portion of any urban study site, and the present study area of Baden is no different. Extraction of this class deserves a dedicated description. Figure E-1 illustrates the end output of a simple Band Ratio (spectral) (Table 4-2) and Mean (spatial) (Table 4-4) index combination that yields the result of highly specific identification of Roofs. This index was later used as a feature to the classification.

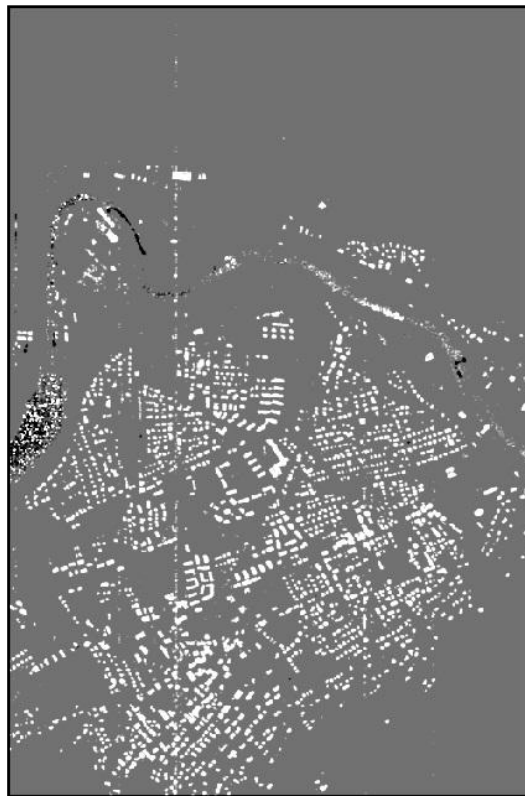


Figure E-1: Spectral-spatial index for “Roofs” class

The additional results of the spectral-spatial input database classification are discussed. It is to be noted that this approach dimensionality reduction greatly improves the classification. Understanding the dimensionality reduction approach and the end classification result is vital in establishing the applicability of spectral and spatial indices.

The classes in the Figures E-2 and E-3 were considered to be unclassified through any of the applied approaches. Dimensionality reduction through indices could be a major research area, and these classes could be the scope for future research. Black Roof, Railway, Roofs and Sand remain unclassified.

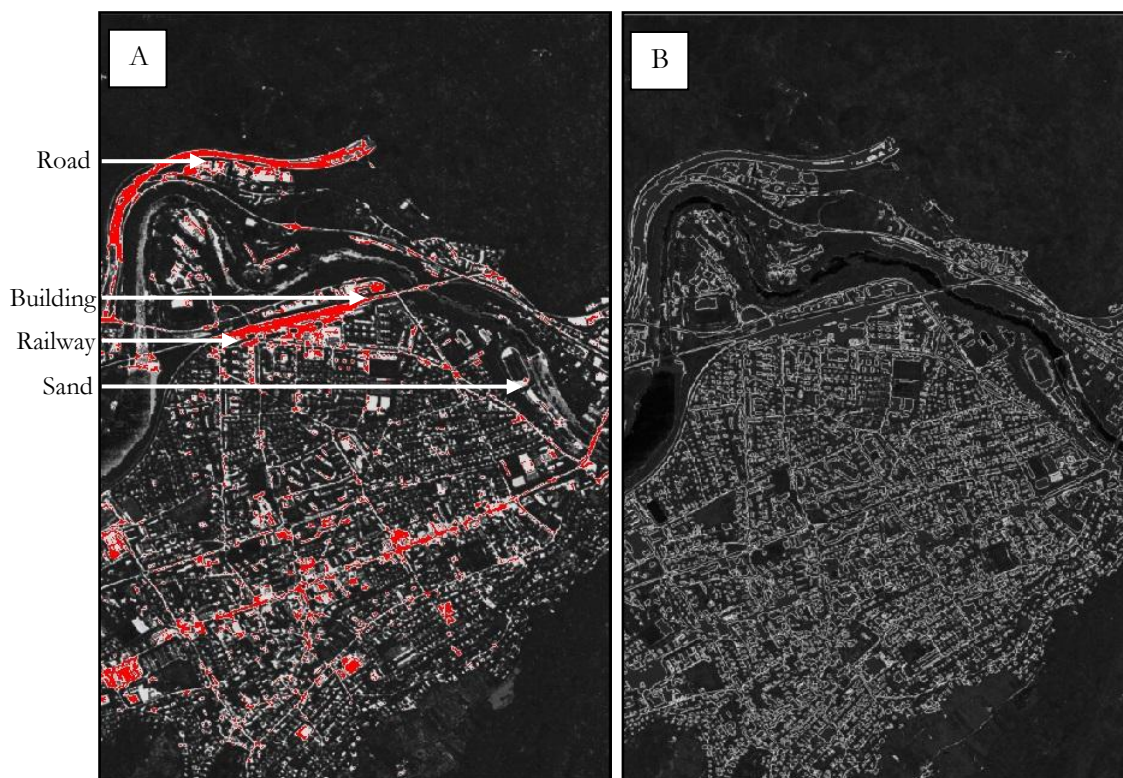


Figure E-2: Spectral-Spatial indices database-classification – Black Roof (A); Railway (B)

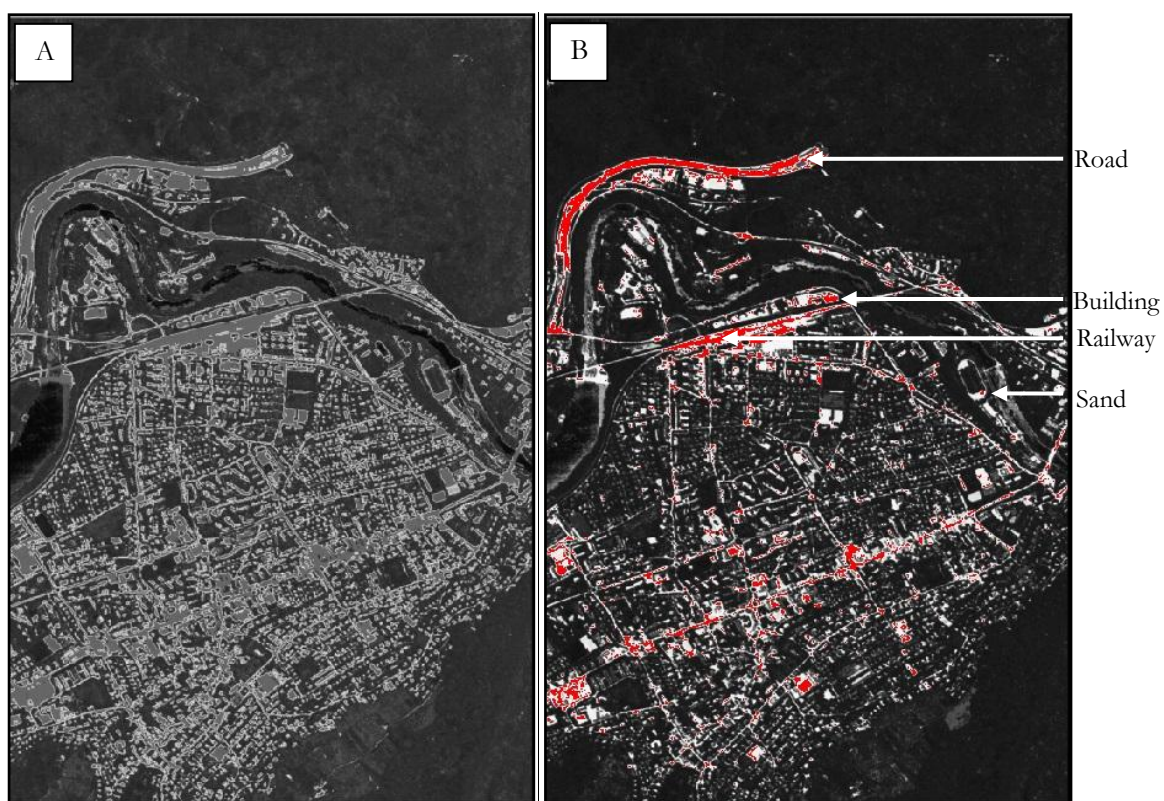


Figure E-3: Spectral-Spatial indices database-classification – Roofs (A); Sand (B)

The classes Railway and Roofs produce no interpretable outcome to the classification while Sand and Black Roof conflict with the indicated classes.

APPENDIX – F

Publications

1. A. Kallepalli, A. Kumar and K. Khoshelham, *Entropy based Determination of Optimal Principal Components of Airborne Prism EXperiment (APEX) imaging spectrometer data*. (Draft Prepared; To be submitted in a peer reviewed Journal)
2. A. Kallepalli, A. Kumar and K. Khoshelham, *Spectral and Spatial Indices based identification of Specific Class from Airborne Prism EXperiment (APEX) OSD*. (Draft Prepared; To be submitted in a peer reviewed Journal)